Stony Brook University

The Centriolar Distal Appendage Proteins CEP164 and Chibby1 Coordinate Multiple Steps in the Formation and Maintenance of Airway Multicilia

A Dissertation Presented

by

Saul Sylvan Siller

to

The Graduate School

in Partial Fulfillment of the

Requirements

for the Degree of

Doctor of Philosophy

in

Molecular and Cellular Pharmacology

Stony Brook University

May 2017

Stony Brook University

The Graduate School

Saul Sylvan Siller

We, the dissertation committee for the above candidate for the

Doctor of Philosophy degree, hereby recommend

acceptance of this dissertation.

Ken-Ichi Takemaru, Ph.D. – Dissertation Advisor
Associate Professor, Department of Pharmacological Sciences

Holly Colognato, Ph.D. – Chairperson of Defense
Associate Professor, Department of Pharmacological Sciences

Michael A. Frohman, M.D., Ph.D.
Distinguished Professor, Department of Pharmacological Sciences

Jiang Chen, M.D.
Associate Professor, Department of Pathology

This dissertation is accepted by the Graduate School

Charles Taber
Dean of the Graduate School

Abstract of the Dissertation

The Centriolar Distal Appendage Proteins CEP164 and Chibby1 Coordinate Multiple Steps in the Formation and Maintenance of Airway Multicilia

by

Saul Sylvan Siller

Doctor of Philosophy

in

Molecular and Cellular Pharmacology

Stony Brook University

2017

Multicilia are microtubule-based cellular projections that provide the motive force to propel mucus and debris out of our airways, cerebrospinal fluid in our nervous system, and the ovum in the female reproductive tract. Dysfunctional multicilia have been linked to genetic disorders, such as primary ciliary dyskinesia and cystic fibrosis, and been implicated in the pathologenesis of chronic respiratory diseases, including emphysema, chronic obstructive pulmonary disorder, and asthma. While multicilia play an absolutely essential role in human health, very little is known about how multicilia form and function. However, work from primary cilia, which are responsible for cellular signaling, as well as mutation analysis from human patients, has shown that a structure at the base of cilia termed the transition fiber (or distal appendage) is important. Therefore, to gain greater insight into the function of the transition fiber, I utilized two unique mouse knockout models where expression of the two transition fiber proteins Chibby1 and CEP164 was lost. I

employed various imaging modalities, including super-resolution and electron microscopy, tissue histology, and primary cell culture techniques to interrogate the function of Chibby1 and CEP164 in different stages of multicilia formation. Interestingly, I report that Chibby1 regulates intraflagellar transport, a process responsible for building and maintaining ciliary axonemes. Additionally, my work has determined that CEP164 is necessary for mammalian development and multiciliogenesis through the generation and characterization of a novel mouse model. I extend the role of CEP164 in basal body docking and ciliary vesicle formation to multicilia formation; however, I also reveal intriguing differences in CEP164 function in primary and multiciliogenesis. In particular, CEP164 limits the types of cellular membranes and associated membrane proteins that compose multicilia. These findings provide increased understanding into the physiological functions of the transition fiber and shed light on how proteins localizing to this critical structure function to build multicilia.

Table of Contents

List of Figures

List of Abbreviations

ALI	Air-liquid interface
MEF	Mouse embryonic fibroblast
SDS	Sodium deocyl sulfate
TBS-T	Tris-buffered saline with 0.1% Tween-20
HRP	Horseradish peroxidase
WLL	White light laser
PFA	Paraformaldehyde
SEM	Scanning electron microscopy
hCby1	Human Chibby1
3D-SIM	Three-dimensional structured illumination microscopy
IF	Immunofluorescence
GPCR	G-protein coupled receptor
A-tub	Acetylated α-tubulin
G-tub	γ-tubulin
EUCOMM	European Conditional Mouse Mutagenesis
PCR	Polymerase chain reaction
Flp	Flippase
OCT	Optimal Cutting Temperature
WT	Wild type
SVZ	Subventricular zone
INPP5E	Inositol polyphosphate-5-phosphatase E
DMP	Dimethyl pimelimidate
PCM	Pericentriolar matrix
MTOC	Microtubule organizing center
NPHP	Nephronophthisis
MKS	Meckel-Gruber syndrome
IFT	Intraflagellar transport
BBS	Bardet-Biedl syndrome
Hh	Hedgehog
SUFU	Suppressor of fused
PCP	Planar cell polarity
ECM	Extracellular matrix
PKD	Polycystic kidney disease
PCD	Primary ciliary dyskinesia
EM	Electron microscopy
CF	Cystic fibrosis
COPD	Chronic obstructive pulmonary disorder
GEF	Guanine nucleotide exchange factor
GAP	GTPase-activating protein
EHD	Eps15 homology domain
Arl	Arf-like
Arf	ADP-ribosylation factor
SILAC	Stable isotope labeling by amino acid in cell culture
TTBK2	Tau tubulin kinase 2

Cby1	Chibby1
CEP164	Centrosomal protein of 164 kilodaltons
TEM	Transmission electron microscopy
SIM	Structured illumination microscopy
FAM92A	Family with sequence similarity 92, member A
FAM92B	Family with sequence similarity 92, member B
KD	Knockdown
KO	Knockout
RNA	Ribonucleic acid
siRNA	Small-interfering RNA
P. aeruginosa	*Pseudomonas aeruginosa*
D. melanogaster	*Drosophila melanogaster*
X. laevis	*Xenopus laevis*
C. reinhardtii	*Chlamydomonas reinhardtii*
T. thermophila	*Tetrahymena thermophila*
T. cruzi	*Trypanosoma cruzi*
T. brucei	*Trypanosoma brucei*
IACUC	Institutional Animal Care and Use Committee
PEI	Polyethylenimine
MTEC	Mouse tracheal epithelial cell
P/S	Penicillin/streptomycin
FBS	Fetal bovine serum
BSA	Bovine serum albumin
HBSS	Hank’s balanced salt solution
DMEM	Dulbecco’s Modified Eagle’s Medium
PBS	Phosphate-buffered saline, pH 7.4
RA	Retinoic acid
EGF	Epidermal growth factor
BPE	Bovine pituitary extract

Acknowledgments

First and foremost, I would like to thank my mentor, Dr. Ken Takemaru. There are no words to truly codify my appreciation for his enduring support, mentorship, patience, and counsel. I have learned and grown more than I could have ever dreamt under your mentorship. Most importantly, thank you for treating me as a scientific partner, providing me the space and environment to grow and develop, and for never seeming to say no to my ideas, thoughts, and desires. I will cherish the lessons learned and that I continue to learn from you throughout my life. I also would like to thank Dr. Feng-Qian Li. I have learned so much scientifically and personally from you and value our conversations about science and otherwise. It is quite special and humbling to have trained with two world-class scientists, and I am honored and privileged to have learned and be learning as much as I have from both of you.

I would also like to thank the past and present members, including Dr. Michael Burke, Dr. Ben Cyge, Dr. Xingwang Chen, Dr. Dex-Ann Brown-Grant, Michael Wong, and June Yang of the Takemar/Li labs for their support, advice, mentorship, and friendship. When I first started, Ben and Xing were always there to answer any question I had, for which I will always be grateful. Thank you also to my rotation student Jinelle Wint and my high school students Sara Caulfield, Vishal Nyayapathi, and Alia Rizvon from whom I have learned more than I could have ever expected.

I also must thank all of those who contributed to this project, including Susan van Horn in the Microscopy Core facility, the Research Histology Core facility, Drs. Himanshu Sharma and Holly Colognato for the SVZ data, Dr. Bernadette Holdener for help with embryo dissections and imaging, Drs. Shuai Li and Wipawee Winuthayanon from

Washington State University for assistance with the fallopian tube data, and Dr. Michael Holtzman from Washington University in St. Louis for the FOXJ1-Cre mice. In particular, I want to acknowledge Himanshu for his advice, thoughts, and being an amazing friend. I would like to additionally thank Dr. Steve Brody from Washington University in St. Louis for his help with MTEC generation as well as for never saying no and always happily responding to any e-mail I sent him.

I additionally would like to thank my committee members, Drs. Holly Colognato, Michael Frohman, and Jiang Chen for their advice and support. Their willingness to talk and meet with me was absolutely invaluable. To my clinical advisor, Dr. Hussein Foda, I am grateful for your time and insight, which have allowed me to maintain contact within the clinical world during the Ph.D. Also, I would like to acknowledge Drs. Miguel Garcia-Diaz and Stella Tsirka for their support as well as the Department of Pharmacological Sciences, including Odalis Hernandez, Janice Kito, Cynthia Wisekal, Lynda Perdomo-Ayala, Paul Stern, and Raymond Taffner. Dr. Michael Frohman, Dr. Markus Seeliger, Carron Allen, and the entire MSTP program have provided an enormous amount of support that have helped take care of any issue and always been willing to provide advice. Beyond Stony Brook, Dr. Kendal Broadie at Vanderbilt provided me my first research laboratory experience and was a valued mentor to me in my earliest years as a scientist. I always will value his trust in me and mentorship. Also, Drs. Cheryl Gatto and Lane Coffee were two early mentors, who were instrumental in my early scientific training at Vanderbilt. I also would like to thank Dr. Katherine Friedman at Vanderbilt, who I always counted on for mentorship and guidance throughout my time at Vanderbilt.

To my friends (including my MSTP cohort, graduate school friends, medical school friends, and college friends) and family (Aunts, Uncles, Cousins, and Aunt Diane), you have been the bedrock of my support throughout this program, and I could not have done this without you. Lastly, and most importantly, thank you to my Mom and Dad. There is not a day goes by that I am not thankful for the lessons you have taught me and the sacrifies you have made. I only strive to make you proud and achieve half of what you have dreamt for me. I love you more than words can express.

Chapter 1: General Introduction

1.1 Cilia

1.1a Discovery of cilia

The invent of the microscope heralded a new era of cell and microbiology. As Anton van Leeuwenhoek peered into his microscope in 1676, he noted protozoa that had "diverse incredibly thin little feet, or little legs, which were moved very nimbly" and, in so doing, created the first description of cilia (Haimo and Rosenbaum 1981). While several theories persisted as to the nature of these "little feet" for the next almost three centuries, the use of an electron microscope elucidated the canonical 9+2 configuration of cilia that we now know today (Fawcett and Porter 1954). However, even with these early beginnings, it is only in the last twenty years that the field of ciliary biology has flourished.

1.1b Types of cilia

While the two main classifications of cilia are immotile primary cilia and motile cilia (for further discussion, see sections *1.1d Primary cilia* and *1.1e Motile and multicilia*), their diversity reflects a wide range of biological functions (Choksi et al. 2014). Most, though, are variants of a single primary cilium and associated with specific functions. For example, two types of cilia involved in mechanosensation are the cilia of kidney epithelial cells as well as of the peripheral region of the ventral embryonic node. The former project into the tubule lumen to sense and regulate urine flow rate (Praetorius and Leipziger 2013). The latter are thought to detect the leftward fluid flow in the embryonic node and translate this signal into the formation of the left-right axis (Hirokawa et al. 2009). Cilia are also involved in the sensory processes of vision, olfaction, and hearing (Choksi et al. 2014). Sensory neurons of the retina epithelium have a specialized cilium with distinct

morphology that functions to cluster opsin photoreceptors. Olfactory neurons project 10-30 cilia into the mucosal epithelium of the nasal cavity and contain odorant receptors that permit the transduction of an odorant signal. Finally, inner and outer hair cells of the organ of Corti in the inner ear possess kinocilia, which arrange with stereocilia to sense vibration and fluid movement. Of the aforementioned cilia that are not associated with a specific receptor type, i.e. kidney cilia, nodal cilia on the peripheral cells, and kinocilia, the prevailing thought was that Ca^{2+} influx translated the mechanical stimulation into a cellular signal. However, recently, this has been called into question (Delling et al. 2016); hence, the exact mechanism for how mechanosensory cilia transduce the stimulus is currently controversial (Norris and Jackson 2016).

Beyond mammals, cilia are evolutionarily conserved structures that are found on most eukaryotes (Fisch and Dupuis-Williams 2011; Choksi et al. 2014). The embryonic epithelium of *Xenopus laevis*, for example, is multiciliated (Walentek and Quigley 2017). The spermatids and sensory neurons of the chordotonal organ are the only ciliated cell types in *Drosophila melanogaster* while the nematode *Caenorhabditis elegans* has an even more restricted profile of ciliated cell types with solely sensory neurons maintaining cilia. Furthermore, the flagella of the single-celled algae *Chlamydomonas reinhardtii* has been extensively studied and employed as a model system. Cilia are even found across pathogens ranging from *Tetrahymena thermophile* to *Trypanosoma cruzi* and *T. brucei*, the latter being causative for African trypanosomiasis (more commonly referred to as African sleeping sickness) (Langousis and Hill 2014). Of note, most of the cilia mentioned above have an evolutionarily conserved basal body and axonemal structure, highlighting

the importance of cilia to eukaryotic life (Carvalho-Santos et al. 2011; Fisch and Dupuis-Williams 2011).

1.1c Ciliary structure

The ciliary axoneme is nucleated from either a mother, or mature, centriole or basal body (Figure 1.1). A basal body is roughly 500 nanometers (nm) in length and 200 nm in width and composed of nine triplet microtubule bundles named as the A-, B-, and C-tubule from interior to exterior (Bettencourt-Dias and Glover 2007; Bettencourt-Dias et al. 2011). However, the C-tubule will terminate near the distal end prior to the beginning of the distal appendage (Gonczy 2012). Two centrioles, the mother and the daughter, along with the pericentriolar matrix (PCM) form the centrosome in every cell, which serves as the microtubule organizing center (MTOC) necessary for cell division (Nigg and Stearns 2011; Firat-Karalar and Stearns 2014). Centrioles therefore are replicated once per cell cycle and are thought to be templated by a cartwheel structure (Gonczy 2012). As a centriole matures, it acquires several accessory structures, including the subdistal and distal appendages, the basal feet, and the rootlet (Bettencourt-Dias and Glover 2007; Gonczy 2012). Importantly, while the basal foot and the subdistal appendage function in similar ways, only one or two basal feet are present on the centriole as opposed to nine subdistal appendages. A further discussion of the subdistal and distal appendages can be found in section *1.4 Centriolar maturation*.

Distal to the basal body in the proximal portion of the ciliary axoneme lies the transition zone, a structure comprised of nine microtubule doublets with no central pair, regardless of whether the cilium is motile, and Y-linkers that extend from the microtubule doublet to the ciliary membrane (Figure 1.1) (Czarnecki and Shah 2012). Additionally,

the Y-linkers establish membranous extensions that are referred to as the ciliary necklace (Gilula and Satir 1972). The transition zone is thought to function in maintaining a distinct ciliary compartment by limiting access of proteins and membrane to the ciliary axoneme (Czarnecki and Shah 2012; Reiter et al. 2012). While the exact composition of the fibrous Y-linkers is unknown, various protein complexes are known to localize to and be the functional units of the transition zone, including the NPHP (nephronophthisis)-associated, MKS (Meckel-Gruber syndrome)-associated, CEP290, and Inversin protein modules (Sang et al. 2011; Williams et al. 2011; Czarnecki and Shah 2012; Li et al. 2016a). Several studies have defined hierarchical relationships between these modules and the proteins within them; however, MKS-5/Retinitis pigmentosa GTPase regulator interacting protein-1-like (RPGrip1L) appears to be the master regulator of the transition zone as it is necessary for the proper recruitment of the NPHP, MKS, CEP290, and Inversin components (Sang et al. 2011; Williams et al. 2011; Czarnecki and Shah 2012; Jensen et al. 2015; Li et al. 2016a).

After the termination of the transition zone, the ciliary axoneme is then composed of either nine microtubule doublets with, if motile, or without, if immotile, a central pair of single microtubules, 9+2 or 9+0, respectively (Figure 1.1) (Bisgrove and Yost 2006). In most cilia, the B-tubule will terminate at some point prior to the ciliary tip (Satir 1968; Sale and Satir 1976; Fisch and Dupuis-Williams 2011). The exact place along the axoneme that each B-tubule stops varies amongst ciliary types and can do so even within an axoneme. The region prior to the end of the B-tubule is known as the doublet zone while the portion afterwards is referred to as the singlet zone. The ciliary tip complex is located at the most distal portion of the ciliary axoneme (Dentler and Rosenbaum 1977; Sale and

Satir 1977; Dentler 1980; Dentler and LeCluyse 1982; Dentler 1984). While this complex is an elusive structure, intraflagellar transport (IFT) and BBSome components, amongst others, are known to reside there to facilitate the rearrangement of transport trains bringing cargos to and from the ciliary tip (Wei et al. 2012).

1.1d Primary cilia

The primary immotile cilium is structurally relatively simple in comparison with most motile cilia as it has a 9+0 microtubule arrangement, lacking a central pair of microtubules and the decorations necessary for motility (Mahjoub 2013). Despite its simplicity, the primary cilim has an absolutely necessary function in vertebrate development as a hub for hedgehog (Hh) signaling (Goetz and Anderson 2010). In vertebrates, Hh signaling through the primary cilium regulates both early embryonic development and organogenesis and has been linked with tumorigenesis. Hence, understanding how primary cilia are formed and function is of great importance.

Through a compendium of studies, it is known that, in the absence of Hh, the receptor Patched1 localizes to cilia where it is thought to prevent ciliary entry of the Smoothened receptor and ciliary accumulation of Gli2 (Rohatgi et al. 2007; Goetz and Anderson 2010). Of note, while three forms of Gli proteins exist in vertebrates, the major Gli involved in activated Hh signaling is Gli2 (Ingham et al. 2011). Upon Hh binding, Patched1 translocates out of the cilia, allowing entry of Smoothened (Corbit et al. 2005; Rohatgi et al. 2007). Increased levels of ciliary Smoothened promote ciliary accumulation of Gli2 in complex with the negative regulator Suppresor of Fused (SUFU) (Tukachinsky et al. 2010; Zeng et al. 2010). Gli2 then dissociates with SUFU to activate transcription of downstream effectors (Humke et al. 2010).

Beyond Hh signaling, several Wnt signaling proteins are also involved in primary cilia formation and function as well as multicilia formation and function (Wallingford and Mitchell 2011). Dishevelled proteins, which transduce the Wnt signal in both canonical and non-canonical pathways, localize to the base of cilia (Park et al. 2008). Furthermore, Prickle1, a non-canonical Wnt signaling component, has been shown to be important for primary cilia formation and mediating cilia-related congenital abnormalities (Gibbs et al. 2016). For multicilia formation, the non-canonical, or planar cell polarity (PCP), pathway promotes proper docking and polarization of basal bodies at the apical cell surface through regulation of the actin cytoskeleton (Park et al. 2006; Park et al. 2008; Mitchell et al. 2009; Vladar et al. 2009; Hildebrandt et al. 2011). Finally, Chibby1 was initially identified as a Wnt signaling inhibitor and is necessary for cilia formation (Takemaru et al. 2003; Voronina et al. 2009; Steere et al. 2012; Lee et al. 2014). Hence, intriguing connections exist between cilia and Wnt signaling; however, the meaning of this interconnectedness is still to be elucidated.

1.1e Motile and multicilia

Motile cilia are distinct from primary immotile cilia based on the presence of a central pair of microtubules (the 9+2 microtubule arrangement) and axonemal components necessary for motility (Bisgrove and Yost 2006). Surrounding the central pair is a membranous inner sheath from which the nine radial spokes extend (Warner and Satir 1974; Pigino and Ishikawa 2012). The radial spokes, which are T-shaped structures that attach to the A-tubule with the longer process and to the inner sheath with the wider process, are thought to be a means of signal transduction between these elements to coordinate movement during ciliary beating. As the radial spokes connect the outer

microtubule doublets to the central pair, the inner and outer dynein arms extend from the A-tubule of an outer doublet to connect with the B-tubule of the adjacent doublets and coordinate a relative sliding motion of the microtubule doublets to ensure proper ciliary beating (Warner and Satir 1974; King 2016). While distinct sets of heavy, intermediate, and light chain dyneins compose the inner and outer dynein arms, it is the heavy chains that have ATPase activity and power this process (Porter et al. 1999; Porter and Sale 2000; Ibanez-Tallon et al. 2003). Finally, nexin-dynein regulatory complexes associate with the inner dynein arms and radial spokes to regulate dynein activity and thus ciliary movement (Warner and Satir 1974; Lin et al. 2011; Pigino and Ishikawa 2012; King 2016). The consequence of this machinery is a ciliary beat motion that has two phases: the effective and the recovery stroke (Brooks and Wallingford 2014). During the effective stroke, the cilium arcs to become perpendicular to the cell body as opposed to the recovery stroke, where the cilium is parallel to the cell body as it returns to its initial position.

Motility is exceptionally important to human health and biology, and, accordingly, several different types of motile cilia exist to serve a host of functions. The largest type of motile cilia is multicilia, which line the airway epithelium, the walls of the lateral ventricles of the brain, and the fallopian tube epithelium (Ibanez-Tallon et al. 2003; Brooks and Wallingford 2014; Spassky and Meunier 2017). At these distinct locations, multicilia propel the mucus and debris from out of our airways, circulate the cerebrospinal fluid in our brains, and facilitate the movement of the ovum along the oviduct. Besides multicilia, the sperm flagellum and the nodal cilia are other examples of motile cilia (Choksi et al. 2014; Linck et al. 2016). Nodal cilia, which lack a central pair, are unique amongst motile

cilia in that they move rotationally, rather than beat, to generate the leftward fluid flow across the embryonic node to establish the left-right axis (Lee and Anderson 2008). Interestingly, cells with the aforementioned disparate motile cilia types are regulated by the same transcriptional cascade (covered further in section *1.1g Transcriptional regulation of multiciliogenesis*).

1.1f Ciliogenesis of primary and multicilia

Primary or multicilia formation is a complex cellular process that follows a largely analogous pathway (Figure 1.2) (Pedersen et al. 2008; Nigg and Raff 2009). Primary cilia arise in a quiescent (G_0) cell from the mother centriole, distinguished from the daughter by the presence of appendage structures (Bettencourt-Dias and Glover 2007; Gonczy 2012). On the other hand, multiciliated cells must produce hundreds of centrioles *en masse* from the two centrioles, the mother and the daughter, that every cell contains (Brooks and Wallingford 2014). To solve this physiological problem, multiciliated cells replicate their centrioles via two pathways: 1) the centriolar and 2) the acentriolar pathways (Meunier and Spassky 2016). The centriolar pathway involves direct centriolar replication from the pre-existing centrioles (Bettencourt-Dias and Glover 2007; Bettencourt-Dias et al. 2011; Gonczy 2012; Meunier and Spassky 2016). It is thought that this pathway utilizes the mother, as opposed to the daughter, centriole as the template. The vast majority of the centrioles produced by a multiciliated cell will arise from the acentriolar pathway where fibrogranular structures termed deuterosomes act as sites of *de novo* centriolar generation (Klos Dehring et al. 2013; Zhao et al. 2013). While deuterosomes are understudied structures, recent studies have shed light on two proteins, CCDC78 and Deup1, which localize to and are critical for their function (Klos

Dehring et al. 2013; Zhao et al. 2013). Additionally, live imaging studies of cultured multiciliated ependymal cells from the subventricular zone (SVZ) of the lateral wall of the lateral ventricle of GFP-CETN2 mice suggest that deuterosomes originate from the daughter centriole (Jord et al. 2014). Furthermore, it was proposed from these live imaging studies that centriolar duplication on deuterosomes passes through three stages: 1) the halo stage (where nascent procentrioles are initially nucleated on the deuterosome), 2) the flower stage (where centriolar elongation occurs on the deuterosome), and 3) the basal body stage (where centrioles are released from the deuterosome).

After mass replication, centrioles mature by acquiring subdistal and distal appendages (Bettencourt-Dias and Glover 2007). At this point, formation of both primary and multicilia proceeds in a similar manner. Small vesicles are recruited to the distal appendage and then coalesce to form the larger ciliary vesicle, which is thought to promote docking of the centriole, or basal body, as it is now referred, with the apical cell surface via membrane fusion events (Sorokin 1962; Sorokin 1968; Li et al. 2015a). At this point, the axoneme is nucleated from the basal body via an intraciliary trafficking mechanism known as IFT (Rosenbaum and Witman 2002; Scholey 2003; Scholey 2008). Further discussion of both ciliary membrane biogenesis and IFT can be found in section *1.3 Ciliary trafficking*.

1.1g Transcriptional regulation of multiciliogenesis

Regulation of ciliogenesis in the multiciliated cells of the airway, brain ventricle, and fallopian tube epithelium requires a particularly complex transcriptional network (Figure 1.3), which is well-conserved amongst the different tissue types (Brooks and

Wallingford 2014). However, the specification of multiciliated cells in each context is distinct. For example, the Hippo-Yap pathway as well as the transcription factor Grainyhead-like 2 appear to be critical for establishing the airway mucociliary epithelium (Mahoney et al. 2014; Gao et al. 2015) while Hh signaling and Gli3 along with interactions between the extracellular matrix (ECM) and ECM receptor dystroglycan are suggested to promote commitment of radial glial cells to ependymal cells (McClenahan et al. 2016; Kyrousi et al. 2017). More work is clearly needed to understand these early cell fate decisions. However, the first step to commit to becoming a multiciliated cell in each of these contexts is regulated by Notch signaling as Notch inhibits Multicilin (MCIDAS) and Gemc1 (Stubbs et al. 2012; Brooks and Wallingford 2014; Ma et al. 2014; Kyrousi et al. 2015; Zhou et al. 2015; Arbi et al. 2016; Kyrousi et al. 2017). After being released from Notch repression, Multicilin in complex with E2F transcription factors, in particular E2F4 and E2F5, is sufficient to drive the entire downstream transcriptional cascade that leads to multicilia formation (Ma et al. 2014). Targets of Multicilin/E2F include the transcription factors p73, Myb, Rfx2, Rfx3, and FOXJ1, the rest of the transcriptional network regulating multiciliogenesis (Stubbs et al. 2012; Didon et al. 2013; Tan et al. 2013; Brooks and Wallingford 2014; Chung et al. 2014; Ma et al. 2014; Kistler et al. 2015; Kyrousi et al. 2015; Gonzalez-Cano et al. 2016; Jackson and Attardi 2016; Marshall et al. 2016; Nemajerova et al. 2016; Kyrousi et al. 2017; Quigley and Kintner 2017). Intriguingly, Gemc1 has also been shown to be one of the most upstream transcription factors along with Multicilin and can promote transcription of similar targets as the Multicilin/E2F complex (Kyrousi et al. 2015; Zhou et al. 2015; Arbi et al. 2016). However, there is conflicting evidence whether Gemc1 is sufficient to initiate the entire transcriptional

cascade (Kyrousi et al. 2015; Zhou et al. 2015; Arbi et al. 2016; Kyrousi et al. 2017). It is also noteworthy that TAp73, while downstream of Multicilin/E2F and Gemc1, is suggested to control the rest of the multiciliogenic transcriptional cascade, including Myb, Rfx2, Rfx3, and FOXJ1 (Gonzalez-Cano et al. 2016; Jackson and Attardi 2016; Marshall et al. 2016; Nemajerova et al. 2016). At the onset of multiciliogenesis, Multicilin/E2F and Myb direct expression of genes involved in deuterosome-mediated centriole biogenesis, such as Deup1 and CCDC78 (Stubbs et al. 2012; Tan et al. 2013; Ma et al. 2014). Also, cyclin O appears to be involved in the regulation of this process (Funk et al. 2015). Myb, Rfx2, and Rfx3 then fine-tune expression of FOXJ1 (Didon et al. 2013; Tan et al. 2013; Chung et al. 2014; Quigley and Kintner 2017), which is the first identified and most specific multiciliated cell transcription factor (Lim et al. 1997; Blatt et al. 1999). Although TAp73, Myb, Rfx2, and Rfx3 control expression of several proteins involved in various aspects of multiciliogenesis, such as basal body docking and axonemal formation, FOXJ1 is the main gene expression driver for proteins involved in multiciliogenesis (Lim et al. 1997; Blatt et al. 1999; Brooks and Wallingford 2014).

Importantly, this transcriptional network is similar amongst multiciliated epithelia. In addition, formation of nodal cilia and sperm flagella requires FOXJ1, suggesting that this transcription factor provides for expression of motility factors, such as dynein heavy, intermediate, and light chains (Blatt et al. 1999). Intriguingly, Rfx2 also appears to have a particularly important role in regulating spermiogenesis (Kistler et al. 2015; Shawlot et al. 2015; Wu et al. 2016). Moreover, Rfx factors not only promote multiciliogenesis but also support primary ciliogenesis, indicating conservation amongst the transcription units that control cilia formation. Support for this notion comes from the presence of DAF-19,

an ortholog of the Rfx proteins, in *C. elegans* (Swoboda et al. 2000). In summary, cilia are diverse organelles that have complex structure, function, and regulatory modules.

1.2 Cilia in disease

1.2a Ciliopathies

Only until recently, the underlying molecular and cellular basis of a wide spectrum of genetic disorders with extremely pleiotropic phenotypes puzzled clinicians and scientists (Hildebrandt et al. 2011). With the understanding that ciliary dysfunction was at the core of their pathology, a new disease class was coined as the ciliopathies. As mentioned above, ciliopathies exhibit a broad scope of symptoms, such as infertility, intellectual deficits, airway abnormalities, skeletal abnormalities, and cystic liver, kidneys, and pancreas, reflecting the diverse types and functions of cilia in human biology. In this continually expanding disease class, a few examples include: nephronophthisis (NPHP), polycystic kidney disease (PKD), Bardet-Biedl syndrome (BBS), Joubert syndrome, and Meckel-Gruber syndrome (MKS) (Waters and Beales 2011). Specifically, autosomal dominant PKD is a potentially lethal disease that causes end-stage renal disease later in adulthood (normally between the ages of 55 and 70) and is due to a mutation in either the *PKD1* or *PKD2* genes that encode for polcystin-1 or polycystin-2, respectively (Kim and Walz 2007; Torres and Harris 2007; Torres et al. 2007). Autosomal recessive PKD results in bilateral cystic kidneys early in life that may progress to end-stage renal disease at any point in life from the neonatal period to adulthood depending on the causative genetic mutation in the *PKHD1* gene that encodes for fibrocystin (Adeva et al. 2006). Interestingly, all three proteins associated with these two disorders are not essential for

cilia formation; however, since they are found to localize to primary cilia, these disorders are designated as ciliopathies (Igarashi and Somlo 2002; Pazour et al. 2002b; Yoder et al. 2002; Watnick and Germino 2003). NPHP, from which the transition zone proteins derive their names, also leads to end-stage renal disease, of which it is the most frequent genetic cause in individuals under 30 (Hildebrandt et al. 2009). Frequently associated with NPHP, Joubert syndrome causes intellectual deficits and ataxia and is strongly associated with the “molar-tooth” radiologic finding (Gleeson et al. 2004; Valente et al. 2005). Additionally, BBS and MKS are both multi-organ disorders. BBS, which arises from mutations in BBS genes, is a genetic obesity disorder characterized by diabetes mellitus, infertility, urinary tract malformation, cystic kidneys, a degenerative retina, cognitive deficits, and postaxial polydactyly (Ansley et al. 2003). MKS is one of the most devastating ciliopathies, which results in perinatal death (Salonen 1984; Paavola et al. 1997; Salonen and Paavola 1998). Its symptoms include *situs inversus*, bile-duct dilatation, lung hypoplasia, microphthalmia, occipital meningoencephalocele, cystic or malformed kidneys, and postaxial polydactyly. Clearly, ciliary dysfunction has wide-reaching effects on human health and disease that include and extend beyond the above diseases. Of note, many ciliopathies are caused by mutations in genes encoding transition zone proteins, suggesting that the transition zone is particularly important to ciliary function (van Reeuwijk et al. 2011). Furthermore, intense efforts are underway to identify novel mutations in ciliary genes associated with developmental defects and ciliopathies to further appreciate the role cilia play in human health.

1.2b Primary ciliary dyskinesia

Primary ciliary dyskinesia, also known as Kartagener's syndrome, was initially described in 1933 by Kartagener in a case report describing a patient with the classic triad of chronic sinusitis, bronchiectasis, and *situs inversus* (Knowles et al. 2013). In 1976 and then again in 1977, Afzelius and colleagues demonstrated that the symptoms associated with Kartagener's were due to ultrastructural defects of motile cilia, leading to the designation the "immotile cilia syndrome" (Afzelius 1976; Eliasson et al. 1977). However, upon recognition that these ultrastructural defects created ineffective beat patterns that did not prevent motility, the syndrome was again renamed to primary ciliary dyskinesia (PCD) to reflect this.

PCD is a genetic disorder of motile cilia characterized by chronic sinusitis that often develops to bronchiectasis, chronic otitis and rhinitis, recurrent lower respiratory tract infection, transient hearing loss and speech delays, *situs inversus* (in ~50% of cases due random organ placement from loss of rotational motility of nodal cilia), and male infertility (Escudier et al. 2009; Boon et al. 2013; Hosie et al. 2014). Hydrocephalus, or enlargement of the fluid-filled brain ventricles, often also associates with PCD. These manifestations are often a result of structural defects in the motility apparatus, including the inner and outer (more common) dynein arms, radial spokes, and the central pair apparatus (Leigh et al. 2009a; Mitchison et al. 2012; Onoufriadis et al. 2013; Zhang et al. 2014; Olcese et al. 2017). Accordingly, the genetic mutations linked to PCD have mainly been found in genes encoding for outer dynein arm heavy chain (e.g. DNAH5, DNAH9, DNAH11), intermediate chain (e.g. DNAI1, DNAI2), light chain (e.g. DNAL1), dynein assembly (e.g. DNAAF1, DNAAF3, CCDC39, CCDC40, DRC1, HEATR2), radial spoke

(e.g. RSPH1, RSPH4A, RSPH9), or central pair proteins (e.g. HYDIN, SPAG1, SPAG17) (Tilley et al. 2014). As such, genetic testing is now a more common mechanism for confirming a PCD diagnosis. However, the gold standard is examination by electron microscopy (EM) of airway cilia for defects in axonemal structure (Leigh et al. 2009b; Rugina et al. 2014). Besides genetic testing and EM, immunofluorescence (IF) analysis for DNAH5 is another diagnostic test used as PCD patients with outer dynein arm defects have been found to have altered localization patterns of DNAH5 in the ciliary axoneme (Fliegauf et al. 2005). Finally, nasal nitric oxide testing has also become a useful screening test for PCD as patients demonstrate a substantially reduced level of nitric oxide production (Chodhari et al. 2004). Therapy is unfortunately mainly focused on symptom management with many treatment mechanisms being extrapolated from studies on cystic fibrosis patients (Knowles et al. 2013). A final note about PCD is that, while it is a genetic disorder of motile cilia and the genetics reflect this, it is also recognized that mutations in genes for ciliary proteins that are not involved in motility may affect primary cilia as well as motile cilia and cause combinatorial disorders, such as polycystic kidney disease with PCD (Fliegauf et al. 2007; Waters and Beales 2011). Hence, it is necessary to understand both primary and motile cilia as well as their differences to enable enhanced treatment of PCD as well as other ciliary disorders.

1.2c Motile and multicilia in human disease and disorder

While PCD is the prototypical disorder of motile cilia, defective motile and multicilia are an integral component of the pathogenesis of several genetic and non-genetic respiratory disorders (Tilley et al. 2014). For example, cystic fibrosis (CF) is a genetic disorder that results in abnormally thick mucus and mucus plugging due to mutations in

the *CFTR* gene, which lead to recurrent infections, bronchiectasis, and chronic lung disease (Riordan et al. 1989; Boucher 2004). The defective CFTR chloride ion channel causes dehydration of the airway epithelium and altered mucus composition, which hinders mucociliary transport (Boucher 2007; Rubin 2007). While ciliary dysfunction is not the primary cause of the pathology, loss of cilia or cilia with altered axonemal structure or ciliary membrane are seen in progressing and advanced CF (Boucher 2004; Ehre et al. 2014). In addition to CF, smoking has been shown to cause a shortening and loss of cilia, which reduce mucociliary clearance (Leopold et al. 2009; Hessel et al. 2014). As smoking has also been linked to reduced expression of ciliary proteins, it is postulated that this delays the regeneration of cilia after they are lost, further enhancing this phenotype (Tilley et al. 2014). With compromised cilia in healthy smokers (Leopold et al. 2009), it is not surprising that ciliary defects exacerbate the disease course of individuals with chronic obstructive pulmonary disorder (COPD) as cilia in COPD patients are even shorter than healthy smokers (Camner et al. 1973; Hessel et al. 2014). Interestingly, one suggested mechanism for the shorter cilia in COPD patients is smoke-induced ciliophagy, an autophagic process by which cilia are rescinded and that might prove therapeutically useful (Lam et al. 2013; Cloonan et al. 2014). Furthermore, smokers with chronic bronchitis also exhibit axonemal structural abnormalities similar to those observed in CF patients, which contributes to this pathology (Katz and Holsclaw 1980). Beyond smoking, environmental pollutants lead to ciliary defects and lower ciliary beat frequencies (Pedersen 1990; Carson et al. 1994; Riechelmann et al. 1994; Calderon-Garciduenas et al. 1998), and biopsies from asthmatics demonstrate that ciliary loss via epithelial shedding as well as ciliary structural abnormalities further aggravate problems with

mucociliary clearance in these patients (Dunnill 1960; Erle and Sheppard 2014; Tilley et al. 2014). Thus, airway cilia are an important component of human health and contribute to a wide array of human diseases.

The effects of diseased multicilia and motile cilia can also be seen in conditions outside of the airway. In the brain, the status of ependymal cilia influences the progression of and can be a direct cause of hydrocephalus, both congenital and acquired (Banizs et al. 2005; Tissir et al. 2010; Ohata et al. 2014; Wang et al. 2016). Laterality defects, including *situs inversus* and heterotaxy, can result from perturbations in fluid-flow across the embryonic node, for which the nodal cilia are responsible (Fliegauf et al. 2007; Lee and Anderson 2008). Finally, male and female infertility may both be affected by defects in multicilia and motile cilia as decreased ciliary beating in the fallopian tube can play a role in female infertility and defective flagellar beating of the sperm has a marked impact on male fertility (Linck et al. 2016). In conclusion, a surprising multitude of disorders have been linked with ciliary dysfunction, highlighting the necessity for future studies into how defective cilia contribute to pathology.

1.3 Ciliary trafficking

1.3a Ciliary membrane biogenesis

The recruitment and formation of the ciliary membrane is a complex process that was first elucidated by Sergei Sorokin in the 1960's (Sorokin 1962; Sorokin 1968). In an elegant series of EM studies of neonatal chick and mammalian tissues, Sorokin first hinted at the possible importance of ciliary vesicle formation in ciliogenesis. To establish a ciliary vesicle, small vesicles are recruited to the distal appendage (Figure 1.4). After a

series of small vesicles have attached to the distal appendage, they coalesce via membrane fusion events to form a larger vesicle known as the ciliary vesicle, which then invaginates (Yee and Reiter 2015). Afterwards, the basal body with the ciliary vesicle either begins to extend an axoneme with small vesicles contributing to ciliary membrane growth or is transported to the apical surface where the ciliary vesicle will fuse with the apical cell membrane (Li et al. 2015a). Once a basal body has docked with the apical cell surface, it is thought that vesicles are then targeted to the periciliary membrane region of the apical cell surface to promote ciliary membrane growth via lateral diffusion of membrane, a process potentially mediated and regulated by the transition fibers, as the distal appendages are referred to after basal body docking (Rohatgi and Snell 2010; Reiter et al. 2012; Wei et al. 2015).

1.3b Molecular mechanisms of ciliary membrane recruitment and formation

The molecular events controlling membrane recruitment to the centriole and basal body are an area of intense study in the field. Rab proteins are a superfamily of Ras-like GTPases that regulate membrane trafficking between cellular compartments (Zerial and McBride 2001). With greater than 60 Rab proteins in mammals, they are well-poised to orchestrate membrane trafficking events as their ability to be activated and deactivated by guanine nucleotide exchange factors (GEFs) and GTPase-activating proteins (GAPs), respectively, provides tight spatiotemporal control over their activity (Grosshans et al. 2006; Stenmark 2009).

To initiate ciliary membrane formation and small vesicle recruitment to the distal appendage, Rab11 is known to be trafficked from the trans-Golgi network to the centriole via its association with the appendage proteins Odf2 and centriolin to promote Rabin8

centriolar recruitment (Wu et al. 2005; Knodler et al. 2010; Westlake et al. 2011; Hehnly et al. 2012; Vetter et al. 2015). Rabin8 is the Rab8 GEF, which recruits and activates Rab8 to the centriole (Nachury et al. 2007; Yoshimura et al. 2007; Westlake et al. 2011; Feng et al. 2012). Rab8 then promotes recruitment of small vesicles, presumably post-Golgi in origin, as Rab8 localizes to the trans-Golgi network, to the distal appendage and, after basal body docking, will continue to facilitate membrane recruitment to the basal body (Huber et al. 1993; Nachury et al. 2007; Yoshimura et al. 2007; Feng et al. 2012). As Rab8 is an important identifier of ciliary membrane, it is not surprising that its proper centriolar and ciliary localization, while dependent mainly on Rabin8, is also controlled by the transition zone proteins Ahi1, Cc2d2a, and CEP290 (Kim et al. 2008; Hsiao et al. 2009; Bachmann-Gagescu et al. 2015). In addition to Rab11 and Rab8, other Rab proteins, such as Rab28 and Rab5, are implicated in ciliogenesis (Yoshimura et al. 2007; Stenmark 2009; Boehlke et al. 2010; Jensen et al. 2016). Rab5 is particularly interesting due to its association with endocytic membranes, which provides an enticing link between ciliary membranes and endocytosis (Zerial and McBride 2001; Grosshans et al. 2006; Stenmark 2009). Recently, the Eps15 homology domain (EHD) family members EHD1 and EHD3, which are also involved in endosomal membrane trafficking, were implicated in the fusion of small vesicles to form the ciliary vesicle and proposed to act in parallel with the Rab11-Rabin8-Rab8 protein cascade (Lu et al. 2015b). Hence, several lines of evidence are starting to pinpoint a role of endocytosis and the endosome recycling compartment in ciliogenesis. Other than endocytosis, both the Rab11-Rabin8-Rab8 network and Arl13b, another important regulator of ciliary membrane biogenesis, have been associated with multiple components of the exocyst complex, which is known to be

important for membrane trafficking, tethering, and remodeling events that are prevalent throughout ciliogenesis (Wu et al. 2005; Yoshimura et al. 2007; Das and Guo 2011; Feng et al. 2012; Hehnly et al. 2012; Seixas et al. 2016).

ADP-ribosylation factor (Arf) and Arf-like (Arl) small GTPases also function in ciliary membrane targeting and formation (Li et al. 2012; Deretic 2013). Particularly, Arl3, Arl6, Arl13b, and Arf4 have been shown to be involved in trafficking of membrane or membrane receptors to cilia (Li et al. 2012). For example, Arl6/BBS3 has a role in the trafficking of ciliary membrane receptors as it co-migrates with and appears to regulate IFT in the cilium (Jin et al. 2010; Liew et al. 2014). Of particular note, Arf4 regulates ciliary membrane trafficking in complex with Rab11 and a Rab11 effector FIP3, suggesting a synergy between Arf/Arl proteins and Rab proteins in ciliary membrane trafficking (Mazelova et al. 2009; Wang et al. 2012; Deretic 2013; Sung and Leroux 2013; Vetter et al. 2015). Finally, Arl13b is a well-known ciliary membrane protein that is mutated in Joubert syndrome (Cantagrel et al. 2008; Li et al. 2012). Consistent with this, Arl13b knockout (KO) mice display phenotypes similar to those seen in patients with Joubert syndrome (Caspary et al. 2007). Arl13b has been demonstrated to be involved in multiple steps of ciliogenesis from regulating ciliary membrane length to the correct transport of ciliary membrane receptors (Cevik et al. 2010; Humbert et al. 2012; Cevik et al. 2013; Lu et al. 2015a; Seixas et al. 2016). Clearly, this complex network of membrane trafficking that promotes cilia formation is an exciting and understudied area that is critically important to understanding ciliogenesis and the progession of ciliopathies.

1.3c Intraflagellar transport

IFT is the bidirectional transport system that moves cargo proteins along the cilium (Rosenbaum and Witman 2002; Scholey 2003; Scholey 2008). First discovered in *C. reinhardtii*, IFT is essential for ciliary growth, structure, and maintenance through the delivery of tubulins and other axonemal components to their sites of incorporation within the ciliary compartment (Kozminski et al. 1993; Deane et al. 2001; Rosenbaum and Witman 2002). With more than 20 core protein subunits, two major IFT sub-complexes have been identified: the (1) IFT-B and (2) IFT-A sub-complexes (Taschner et al. 2012; Bhogaraju et al. 2013). IFT-B is thought to mediate anterograde transport in association with kinesin motors while IFT-A is implicated in retrograde transport via dynein motors. To prevent collisions between these anterograde and retrograde IFT trains, anterograde IFT particles move on the B-tubule while retrograde IFT particles employ the A-tubule for transport (Stepanek and Pigino 2016). Besides the requisite association of IFT proteins with kinesin and dynein motors, IFT particles associate and co-migrate with the BBSome along cilia (Wei et al. 2012; Zhang et al. 2012; Sung and Leroux 2013; Williams et al. 2014). Originally identified as mutated in BBS and through tandem-affinity purification experiments with BBS4, the BBSome is an octameric complex that consists of eight conserved BBS proteins and has been proposed to regulate the assembly, rearrangement, and turnaround of IFT particles at both the ciliary base and tip (Ansley et al. 2003; Nachury et al. 2007; Nachury 2008; Jin and Nachury 2009; Zaghloul and Katsanis 2009; Wei et al. 2012; Williams et al. 2014). Interestingly, the BBSome also has been shown to interact with Rabin8, which suggests a mechanistic link between ciliary membrane biogenesis and IFT (Nachury et al. 2007; Jin et al. 2010). Taken together, the

building of a ciliary axoneme is a complicated cellular trafficking process in which a multitude of protein networks must precisely coordinate to ensure faithful ciliogenesis at each point.

1.4 Centriolar maturation

1.4a Subdistal appendage

The appendage structures of centrioles are an important marker of centriolar maturation (Figure 1.5) (Bettencourt-Dias and Glover 2007; Gonczy 2012). The more proximal of the two appendages is the subdistal appendage, whose main function, despite being dispensable for ciliogenesis, is to connect the basal body with the microtubule network (Quintyne et al. 1999; Mogensen et al. 2000; Dammermann and Merdes 2002; Delgehyr et al. 2005; Guarguaglini et al. 2005; Kunimoto et al. 2012). While the exact composition of the subdistal appendage is a mystery, recent work by Mazo and colleagues elucidated two protein groups that make up the subdistal appendage: the 1) Odf2 and 2) ninein groups (Mazo et al. 2016). The Odf2 group consists of Odf2, CEP128, and centriolin while the ninein group consists of ninein, CEP170, Kif2a, and the p150glued/dynactin complex. Through CRISPR/Cas9 gene editing techniques in human retinal pigment epithelial 1 (RPE1) cells and RNAi-mediated knockdown (KD) in HeLa cells, the same group proposed that Odf2, CEP128, centriolin, and ninein are recruited in this sequential order and then ninein recruits the rest of its protein group constituents to form the subdistal appendage. Interestingly, several similarities in functionality and composition exist between the subdistal appendages and the basal feet; however, nine subdistal appendages extend radially from the basal body whereas only one or two basal

feet extend from the basal body (Bettencourt-Dias and Glover 2007; Bettencourt-Dias et al. 2011; Gonczy 2012). Moreover, Odf2, a protein common to both subdistal appendages and basal feet, appears to function slightly differently in each context as it is important for appendage assembly at the subdistal appendage and for proper basal body polarization at the basal foot (Ishikawa et al. 2005; Kunimoto et al. 2012). Thus, although recent studies have shed light on the composition and function of the subdistal appendage, further work is needed to understand its role in ciliogenesis.

1.4b Distal appendage

In comparison to the subdistal appendage, which is the more proximal appendage structure, the distal appendage has been more extensively studied, particularly in primary ciliogenesis (Figure 1.5) (Graser et al. 2007; Schmidt et al. 2012; Joo et al. 2013; Sillibourne et al. 2013; Tanos et al. 2013; Ye et al. 2014). Emanating from the B-tubules of mature centrioles or basal bodies, the distal appendages, or transition fibers as they are known at the ciliary base, are nine fibrous radial extensions that anchor the basal body to the apical cell membrane and are indispensable for ciliogenesis (Reiter et al. 2012; Wei et al. 2015). As a central structure to ciliogenesis, stable isotope labeling by amino acids in cell culture (SILAC) mass spectrometry was employed to identify the core distal appendage protein module, which includes: 1) CEP83/CCDC41, 2) CEP89/CEP123, 3) SCLT1, 4) FBF1, and 5) CEP164 (Tanos et al. 2013). These proteins are sequentially recruited to the distal appendage as CEP83 recruits both SCLT1 and CEP89 and SCLT1 then recruits FBF1 and CEP164. Odf2 and C2cd3 are two upstream proteins of this core distal appendage protein unit and therefore are required for distal appendage assembly (Ishikawa et al. 2005; Ye et al. 2014). It is particularly

interesting that Odf2 is required for both subdistal and distal appendage formation, suggesting that it may coordinate the behaviors of the two appendage structures. However, more work is needed to discern the exact role of Odf2 in both contexts.

The distal appendage plays a crucial role in vesicle docking during ciliogenesis. Many constituents of the core protein unit, including CEP83, CEP89, and CEP164, are necessary for small vesicle recruitment, ciliary vesicle formation, and basal body docking in primary cilia formation (Schmidt et al. 2012; Joo et al. 2013; Sillibourne et al. 2013). However, to achieve these and other functions, these distal appendage proteins have several downstream effectors, including Tau-tubulin kinase 2 (TTBK2) and Chibby1 (Cby1) (Wei et al. 2015). Additionally, distal appendage proteins coordinate with the Rab11-Rabin8-Rab8 protein cascade to promote ciliary vesicle formation and basal body docking (Reiter et al. 2012).

The cilium is a privileged domain from the rest of the cellular space; nonetheless, trafficking from the cytoplasm to the cilium and *vice versa* readily occurs. To both maintain the ciliary compartment as distinct from the cytoplasm but ensure ease of transport for ciliary proteins, which can be >100 kDa, the existence of a ciliary pore complex, very much akin to the nuclear pore complex, has been speculated (Nachury et al. 2010; Wei et al. 2015). As the transition fibers are structures that help to demarcate the basal body and axonemal components of cilia, they are proposed to be the ciliary pore complex (Reiter et al. 2012; Wei et al. 2015). Furthermore, the transition fibers in conjunction with the transition zone have been suggested to make up a ciliary gate complex that helps to select for entry and exit of ciliary proteins. While certain lines of evidence support these notions, such as the discovery of ciliary localization signals

(Mazelova et al. 2009), it is still unclear if these functionalities can be ascribed to the transition fibers and will be the subject of future investigations.

1.4c Chibby1, a distal appendage effector protein

Chibby1 (Cby1) is a small 15-kDa coiled-coil protein that was originally identified in a screen utilizing the yeast Ras recruitment system for cofactors of the C-terminus of β-catenin (Takemaru et al. 2003). This initial report of Cby1 showed that the functional consequences of the interaction between Cby1 and β-catenin were to compete with and thus block Lef1 binding of β-catenin, preventing β-catenin-mediated transcriptional activation. Additional work has demonstrated that Cby1 regulates β-catenin activity by facilitating the nuclear export of β-catenin via interactions with 14-3-3 proteins (Li et al. 2008; Takemaru et al. 2009; Li et al. 2010; Killoran et al. 2015). This dual inhibition of β-catenin by Cby1 results in the promotion of adipocyte differentiation and amelioration of the tumorigenic effect of β-catenin (Li et al. 2007; Li et al. 2008; Takemaru et al. 2009; Li et al. 2010).

While initially discovered as a Wnt/β-catenin antagonist, Cby1 was surprisingly found to play a major role in ciliogenesis upon creation of the Cby1 KO mouse (Takemaru et al. 2003; Voronina et al. 2009). Excitingly, Cby1 KO mice displayed chronic sinusitis and rhinitis, polycystic kidneys, pancreatic degeneration, sub-fertility, and hydrocephalus and polydactyly at low frequency (Voronina et al. 2009; Lee et al. 2014). It should be noted that a portion of Cby1 KO mice die prior to weaning; however, with the use of a special diet, Cby1 KO mice can survive to adulthood without gross abnormalities, except for polydactyly and hydrocephalus at low frequency. These phenotypes were found to be caused by loss of both primary and motile cilia (Voronina et al. 2009; Steere et al. 2012;

Burke et al. 2014; Lee et al. 2014). Further investigation revealed that Cby1 localized solely to the mother centriole, which suggested that it might be an appendage protein (Steere et al. 2012).

Analysis by transmission EM (TEM) of Cby1 KO trachea uncovered roles for Cby1 in basal body docking and ciliary vesicle formation (Voronina et al. 2009; Burke et al. 2014). Consistent with these roles and the specific localization to the mother centriole, super-resolution structured illumination microscopy (SIM) revealed that Cby1 makes a ring pattern, characteristic of transition fiber proteins, that is more apical and narrower than CEP164 rings (Burke et al. 2014). Immuno-EM for Cby1 confirmed that it indeed does reside at the distal appendages/transition fibers (Burke et al. 2014). Bolstering the notion that Cby1 is a *bona fide* distal appendage/transition fiber effector protein, Cby1 binds and is recruited by the distal appendage protein CEP164 (Burke et al. 2014).

In an effort to further elucidate Cby1 function in ciliogenesis, tandem-affinity purification of Cby1 binding partners followed by mass spectrometry was performed and identified the membrane-binding BAR-domain containing proteins family with sequence similarity 92, members A and B (FAM92A and 92B) as Cby1 interactors (Li et al. 2016b). FAM92A and 92B also co-localize with Cby1 in ring structures at the ciliary base upon SIM imaging (Li et al. 2016b). Intriguingly, co-expression of FAM92 proteins and Cby1 induces Rab8-positive tubules, implying that FAM92A and 92B cooperate with Cby1 to remodel Rab8-positive membranes (Li et al. 2016b). Taken together, this data suggests that FAM92A and 92B may also be distal appendage/transition fiber effector proteins that could potentially facilitate ciliary vesicle formation through their membrane remodeling activities.

1.4d CEP164, the first identified genuine distal appendage protein

Centrosomal protein of 164 kDa (CEP164) was originally identified as a centriolar protein in a proteomic analysis of the human centrosome using mass spectrometry (Andersen et al. 2003). Subsequently, CEP164 was uncovered as a novel regulator of primary cilia formation in an small-interfering RNA (siRNA) KD screen of centrosomal proteins (Graser et al. 2007). In the same study, the production of a validated antibody against CEP164 as well as immuno-EM analysis indicated that CEP164 is a distal appendage protein, making it the first identified distal appendage protein. Since this initial report, SILAC mass spectrometry experiments have confirmed and extended these data to indicate that CEP164 is a core distal appendage protein (see section *1.4b Distal appendage*) (Tanos et al. 2013).

As the first protein recognized as a distal appendage component, CEP164 was also the first appendage protein implicated in small vesicle docking to the basal body in serum-starved CEP164 KD RPE1 cells (Schmidt et al. 2012). To mediate the attachment of these small vesicles, the C-terminus of CEP164 is the centriolar localization domain and recruits Rabin8 via direct protein-protein interactions (Schmidt et al. 2012). In line with its function in ciliary vesicle formation, Cby1 is then recruited to the basal body by CEP164 and stabilizes this CEP164-Rabin8 interaction to promote Rab8 and small vesicle recruitment (Burke et al. 2014). In this manner, CEP164 harnesses the Rab11-Rabin8-Rab8 pathway to facilitate primary ciliogenesis.

Highlighting these and other potential roles in cilia formation, mutations in the *CEP164* gene are linked with two ciliopathies, NPHP and BBS (Chaki et al. 2012; Maria et al. 2016). The initial mutation was discovered through whole-exome resequencing

followed by homozygosity mapping of a Saudi family with a child with Leber congenital amaurosis, which is linked to genes mutated in NPHP (Chaki et al. 2012). This patient was found to have a homozygous point mutation that removed a termination codon, extending the open reading frame by 57 amino acid residues. Additional sequencing of families affected by NPHP identified three recessive point mutations in the *CEP164* gene, implicating it as a NPHP-associated disease gene and giving it the additional designation of *NPHP15*. A recent report that performed whole-exome sequencing followed by homozygosity mapping of a Pakistani family with a BBS-like disorder described a missense mutation in the *CEP164* gene, extending the genes associated with BBS to further include *CEP164* (Maria et al. 2016). A key point of both studies is the broad clinical phenotypes displayed by the patients with *CEP164* mutations, indicating its importance to human biology and that further mutations in the *CEP164* gene are still yet to be found.

Beyond its role in cilia, CEP164 has also been shown to be important for the DNA damage response and G_2/M checkpoint (Sivasubramaniam et al. 2008; Schmidt et al. 2012; Slaats et al. 2014). Consistent with this, CEP164 KD was associated with cell cycle defects, accumulations of DNA lesions, proliferation defects, and increases in apoptosis, all of which were proposed to partly underlie NPHP pathogenesis in those patients with *CEP164* mutations (Sivasubramaniam et al. 2008; Chaki et al. 2012; Slaats et al. 2014). However, a recent report of a CEP164 KO cell line has both confirmed a role for CEP164 in primary ciliogenesis but called into question its role in regulating the DNA damage response and the cell cycle (Daly et al. 2016). Thus, further elucidation is still needed to investigate the role of CEP164 in physiology and development to appreciate its cellular function and contribution to human pathology.

1.4e New roles for the distal appendage proteins CEP164 and Chibby1

In the present study, I have discerned novel functions for the distal appendage protein CEP164 and its effector and interactor Cby1 in multiciliated cells through the use of mouse models. First, I elucidate a role for Cby1 in the maintenance of ciliary morphology and in the regulation of IFT processes through examination of Cby1 KO ciliated cells. Then, I establish a novel conditional mouse model for CEP164, which displays phenotypes similar to those observed in PCD, and extend findings from primary cilia to multicilia while also detecting unique differences between the two systems. Of importance, CEP164 is known to regulate vesicle docking in primary cilia and maintains that role in multicilia, yet it differentially regulates access of ciliary membrane proteins to the ciliary membrane compartment. In summary, the distal appendages, or transition fibers, are a critical nexus in both primary and multicilia and only through studies, such as the present, can we appreciate their importance to ciliary biology as well as human health and disease.

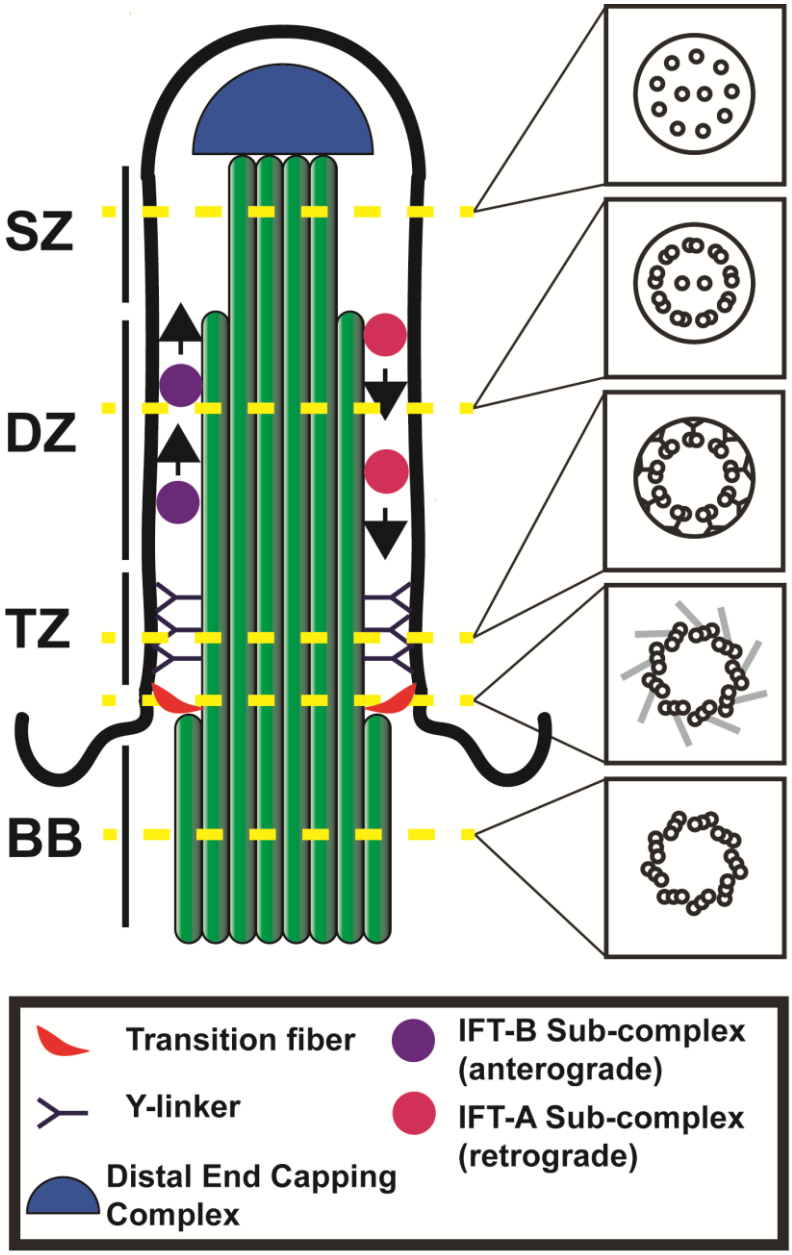

Figure 1.1: Ciliary ultrastructure.
A ciliary axoneme is nucleated from a basal body (BB), which is made of nine microtubule triplets. The transition fibers that emanate radially from the B-tubule attach the basal body to the apical cell surface. Distal to the transition fibers, the transition zone (TZ) contains Y-linkers that connect the microtubule doublets of the axoneme to the ciliary membrane. The rest of the axoneme is composed of a doublet zone (DZ) and a singlet zone (SZ). The doublet zone contains either a 9+0 or 9+2 microtubule doublet arrangement while the singlet zone contains either a 9+0 or 9+2 microtubule singlet arrangement. Shown here is a motile cilium as it has a 9+2 microtubule arrangement. At the distal tip of the ciliary axoneme, a capping complex mediates the rearrangement of the intraflagellar transport (IFT) trains from the anterograde to retrograde particles.

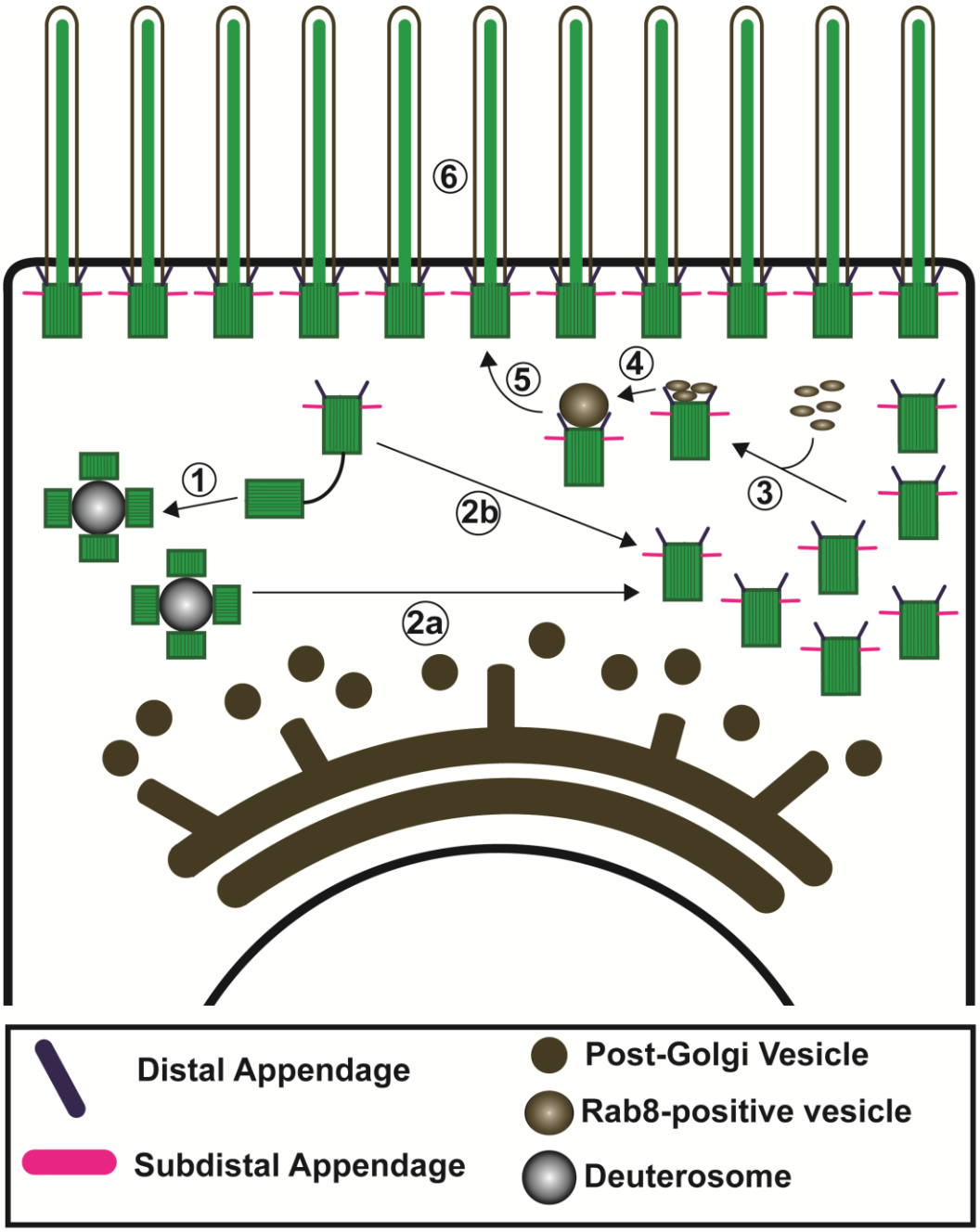

Figure 1.2: Multiciliogenesis.
Multiciliated cells initially form fibrogranular structures called deuterosomes (step 1) to allow for a majority of centriole duplication (step 2a). A small fraction of centriole amplification comes from direct replication of the existing centrioles (step 2b). After centriole duplication occurs, small vesicles, thought to be post-Golgi in origin, will dock to the distal appendage (step 3) and then eventually coalesce to form the ciliary vesicle (step 4). After ciliary vesicle formation, the basal body, as a centriole is referred to now, then migrates to and docks with the apical cell surface (step 5). Finally, intraflagellar transport processes allow axonemal extension to occur (step 6).

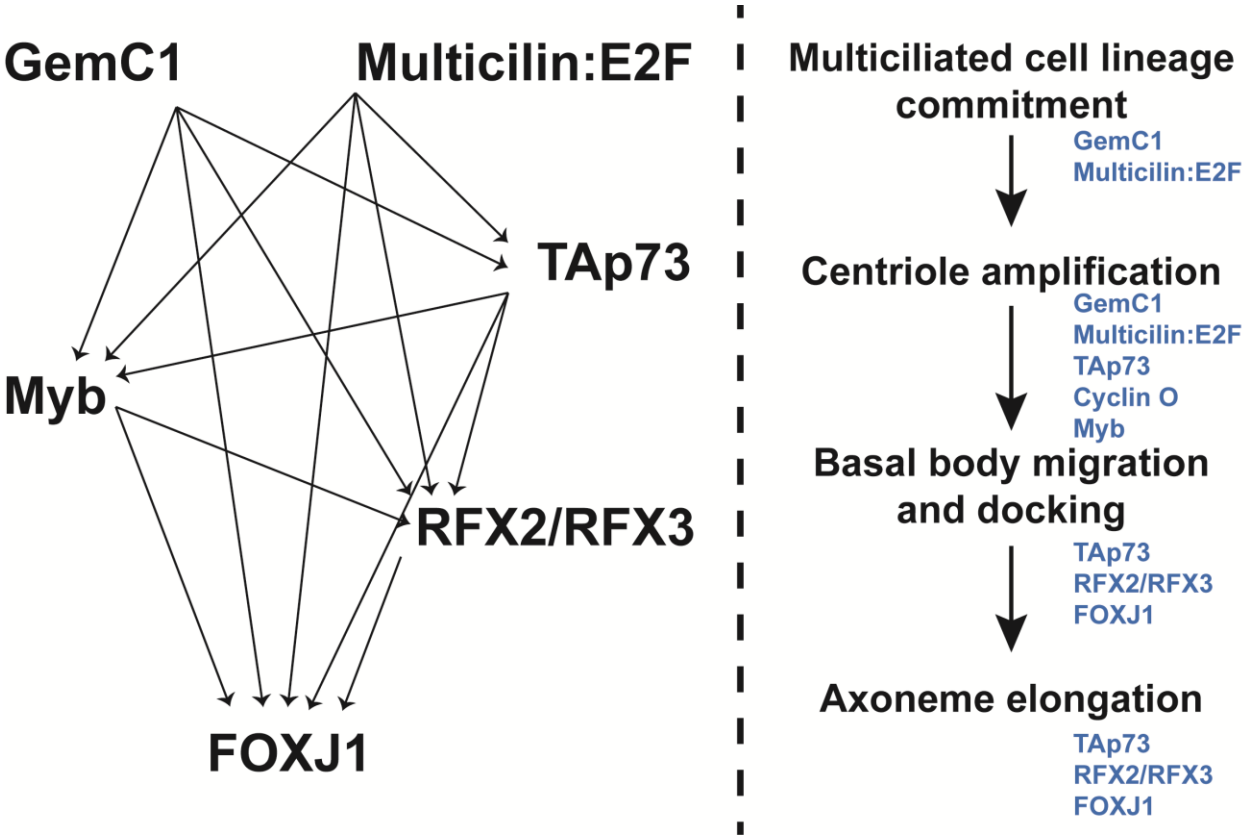

Figure 1.3: Transcriptional network regulating multiciliogenesis.
The hierarchy of transcription factors that govern multiciliogenesis is shown to the left of the dashed line. The steps that these transcription factors regulate are shown to the right of the dashed line with the individual transcription factors that control each step listed below in blue. GemC1 and Multicilin in complex with E2F transcription factors (Multicilin:E2F) control commitment to a multiciliated cell fate and expression of all downstream transcription factors. TAp73 also controls all downstream effectors along with the centriole amplification, basal body migration and docking, and axoneme elongation steps. Myb promotes expression of RFX factors and FOXJ1 and primarily regulates centriole ampliciation along with cyclin O. The core unit of TAp73, RFX2/RFX3, and FOXJ1 then regulates both basal body migration and docking as well as axoneme elongation. As made clear in this diagram, FOXJ1 is the main driver of all steps of multiciliogenesis after centriole duplication events.

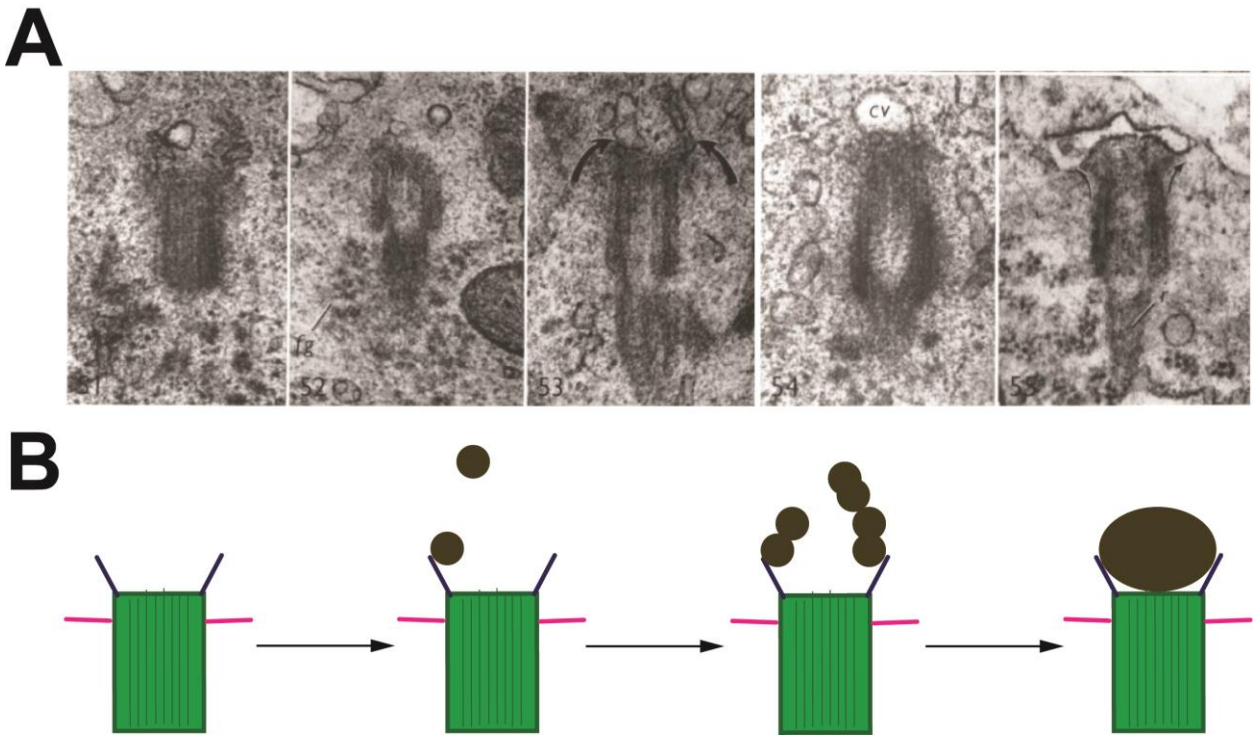

Figure 1.4: Ciliary vesicle formation.
(A) A series of electron micrographs of rat lungs that show the recruitment of small vesicles to the distal appendage followed by formation of the ciliary vesicle and flattening of the ciliary vesicle in primary ciliogenesis. These images are adapted from (Sorokin 1968). (B) Ciliary vesicle formation starts with the recruitment of EHD proteins and the small GTPase Rab11 on presumably post-Golgi vesicles, which associate with the distal appendage. Rab11 then recruits and activates the Rab8 GEF Rabin8. Rabin8 then recruits and activates Rab8, which facilitates further small vesicle transport to the distal appendage and subsequent ciliary vesicle formation.

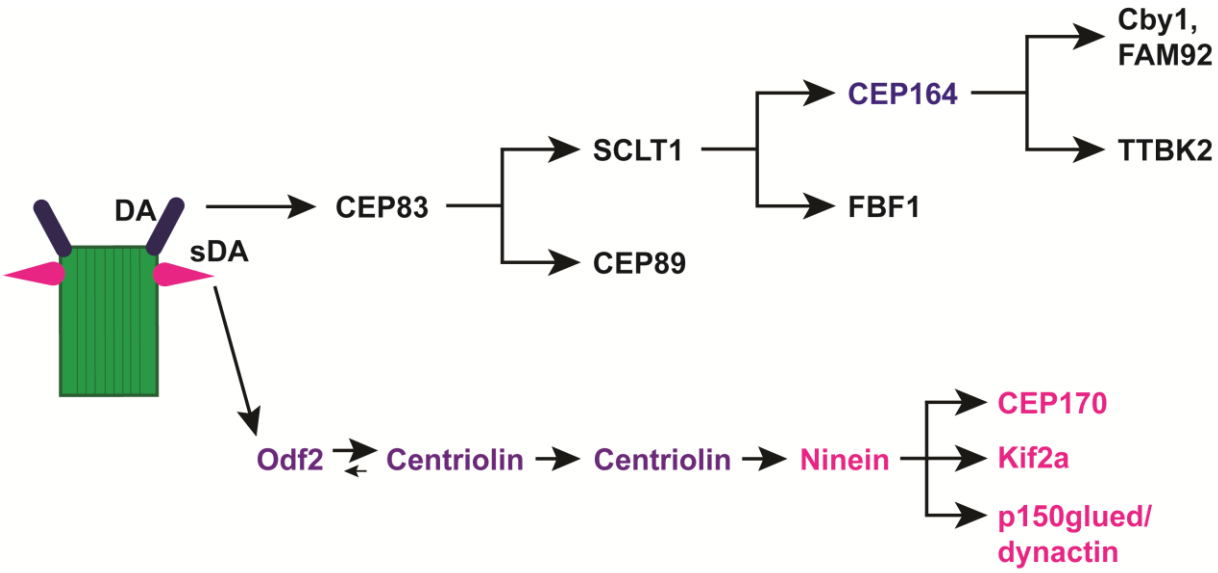

Figure 1.5: Subdistal and distal appendage formation.
The subdistal (sDA) and distal (DA) appendages decorate the distal end of a mature centriole. To form the subdistal appendage, Odf2 is recruited first, which, in turn, leads to the sequential recruitment of CEP128, centriolin, and ninein. Odf2, CEP128, and centriolin are thought to compose an Odf2 protein module (purple). After ninein is recruited to the subdistal appendage, it will then facilitate transport of CEP170, Kif2a, and the p150glued/dynactin complex, which together with ninein compose the ninein protein module (magenta). Distal appendage assembly, on the other hand, starts with CEP83, which recruits CEP89 and SCLT1. The latter then is responsible for FBF1 and CEP164 recruitment. CEP83, CEP89, SCLT1, FBF1, and CEP164 make up a core distal appendage protein unit. Downstream effectors that bind and are recruited by CEP164 include Cby1, FAM92A, FAM92B, and TTBK2.

Chapter 2: Chibby1 maintains ciliary morphology through regulation of intraflagellar transport particles in airway ciliated cells

Parts and data of the following chapter have been reproduced from (Siller SS, et al. 2015).

2.1 Introduction

Despite a wide range of phenotypes observed in the Cby1 KO mouse, the major effects of Cby1 loss are found in the upper airways and lungs (Voronina et al. 2009; Love et al. 2010; Burke et al. 2014). Histological examination of Cby1 KO tissues shows signs of sinusitis and otitis media (Voronina et al. 2009). In agreement with this finding, when challenged with *Pseudomonas aeruginosa*, an infectious pathogen found in CF and PCD patients, bacterial debris and mucus are evident in Cby1 KO sinus (Voronina et al. 2009). Surprisingly, though, both Cby1 wild type (WT) and KO mice effectively clear the bacteria from their lungs. However, Cby1 KO mice do have perturbed mucociliary transport. Furthermore, despite appearing normal at birth, Cby1 KO lungs progressively demonstrate enlarged alveolar sacs, as represented by an increased distance between alveolar walls, and increased airway luminal area, which are suggestive of certain aspects of the morphological changes observed in bronchiectasis (Love et al. 2010). Collectively, these phenotypes reflect many of the pathologies seen in PCD and CF patients, including the chronic sinusitis and otitis media, the impaired mucociliary transport, and bronchiectasis.

Analysis via histology, IF, and electron microscopy (EM) of airway tissue and primary cultures of mouse tracheal epithelial cells (MTECs) revealed that Cby1 KO mice have a dramatic reduction in airway cilia, providing insight into how the absence of Cby1 leads to PCD phenotypes (Voronina et al. 2009; Love et al. 2010; Steere et al. 2012;

Burke et al. 2014). Importantly, Cby1 function in ciliogenesis is evolutionarily conserved as reports in both *D. melanogaster* and *X. laevis* find ciliary defects upon Cby1 loss (Enjolras et al. 2012; Shi et al. 2014). To further understand the role of Cby1 in airway ciliated cell differentiation, localization studies determined that Cby1 is expressed in cytoplasmic foci, similar to that seen for other centriolar proteins, in early differentiation stages and in close association with basal bodies during their migration and docking to the cell surface in later stages (Love et al. 2010; Burke et al. 2014). As the axoneme extends and is maintained via IFT processes (discussed in section *1.3c Intraflagellar transport*), Cby1 is then found at the distal transition fibers/proximal transition zone and persists at this location after ciliogenesis is complete in fully differentiated ciliated cells (Love et al. 2010; Enjolras et al. 2012; Steere et al. 2012; Burke et al. 2014; Lee et al. 2014; Shi et al. 2014). The expression of Cby1 during airway ciliated cell differentiation is known to facilitate ciliary vesicle formation by stabilizing a CEP164-Rabin8 interaction (Burke et al. 2014). On the other hand, a role for Cby1 during later stages of differentiation or in maintenance of airway ciliated cells, when it continues to reside at the ciliary base, remains to be elucidated.

Here, I report that Cby1 functions to maintain proper ciliary structure and morphology through the regulation of IFT particle localization along cilia. Cby1 KO airway ciliated cells develop a fraction of cilia with a paddle-like morphology and a dilated ciliary tip *in vitro*. I show that the IFT-B protein IFT88 accumulates within these tip distortions in both primary and multicilia. Additionally, I demonstrate that the other IFT-B proteins IFT20 and IFT57 accumulate with IFT88 at the ciliary tip while the IFT-A protein IFT140 and the BBSome component BBS5 do not. These findings indicate that Cby1 plays an

integral role in the modulation of IFT protein localization and ciliary structure. Taken together with the predominant localization of Cby1 at the ciliary base, I propose that Cby1 is involved in proper IFT particle assembly at the ciliary base. Hence, loss of Cby1 would affect IFT particle composition, which leads to defects in IFT particle rearrangement at the ciliary tip and the abnormal ciliary morphology observed in Cby1 KO airway ciliated cells. These ciliary tip dilations then contribute to the PCD phenotypes observed in Cby1 KO mice via the hindrance of mucociliary transport.

2.2 Materials and methods

2.2a Mouse strains

The generation of Cby1 KO mice has been previously described (Voronina et al. 2009). Cby1 WT or KO mice were obtained by intercrossing Cby1 heterozygous mice on a mixed C57BL/6J and 129/SvJ background. Genotyping was conducted with PCR analysis using published primer sequences. For PCR analysis, tails were digested with Proteinase K (10 mg/mL) and 10X ThermoPol buffer (New England Biolabs, B9004S) in distilled water at 55^{o}C overnight and then heat-inactivated at 95^{o}C. After digestion, genomic tail DNA is then mixed with primer mix (10 pmol/µL for each primer), 2X Taq master mix (Promega, M7123), and distilled water. This mixture is then subjected to 35 cycles of 1 min at 95^{o}C, 1.5 min at 55^{o}C, and 2 min at 72^{o}C in a thermocycler and held at 4^{o}C until electrophoresed.

2.2b Ethics statement

All mice were handled in accordance with NIH guidelines, and all protocols were approved by the Institutional Animal Care and Use Committee (IACUC) of Stony Brook University (#2010-1393).

2.2c Plasmids and reagents

The lentiviral expression construct for FLAG-hCby1 has been previously described (Burke et al. 2014). Briefly, a cDNA encoding for FLAG-hCby1 was subcloned into a 2nd generation lentiviral transfer vector pEF1α-IRES-EGFP (gift from Dr. I. Lemischka, Mount Sinai Medical Center). All chemicals were purchased from Sigma-Aldrich unless otherwise noted.

2.2d Lenviral production

Sub-confluent HEK293T cells were transiently transfected with the FLAG-hCby1 construct, VSV-G envelope plasmid (Addgene), and the pMDLg/pRRE packaging plasmid (Addgene) in a 1:1:1 ratio utilizing polyethylenimine (PEI) standard transfection protocols. Viral media was then collected 48, 72, and 96 hours post-transfection and sterile filtered.

2.2e Preparation of primary culture of mouse tracheal epithelial cells

Primary cultures of mouse tracheal epithelial cells (MTECs) were prepared as previously described (Figure 2.1) (You et al. 2002; Vladar and Stearns 2007; Vladar and Brody 2013). 6-week- to 6-month-old Cby1 WT or KO mice were euthanized by CO_2 asphyxiation. Tracheas from these mice were then freshly dissected from the thyroid cartilage to the bifurcation of the bronchi, using sterile technique, and placed in ice-cold Ham's F-12 media (Cellgro, 10-080-CV). These tracheas were cleaned of muscle, fascia,

and debris in Ham's F-12 media in a tissue culture hood, bisected longitudinally, and incubated overnight at 4^{o}C with 2 mL/5 tracheas of sterile filtered 1.5 mg/mL pronase (Roche, 10165921001) in Ham's F-12 media plus 100 U/mL penicillin/streptomycin (P/S; Corning, 30-002-CI).

Tracheal epithelial cells were then isolated by adding 10% fetal bovine serum (FBS) (Sigma, F2442) to the tracheas and gently inverting the tube with the tracheas 15-20 times. Tracheas were transferred to another tube with 4 mL of cold Ham's F-12 media with 10% FBS and 100 U/mL P/S, which was again gently inverted 15-20 times. This process was repeated twice more. Tracheas were then discarded, and the media was pooled and spun at 1,200 rpm for 10 min at 4^{o}C. Afterwards, the supernantant was aspirated, and the pelleted cells were resuspended in 200 µL DNase solution (0.5 mg/mL crude pancreatic DNase I [Sigma, DN-25] in Ham's F-12 plus 100 U/mL P/S and 10 mg/mL bovine serum albumin [BSA] stock, consisting of BSA [Fisher, BP-1605-100] and Hank's Balanced Salt Solution [HBSS] without Ca^{2+} and Mg^{2+} [Sigma, H9394]) to remove genomic DNA contamination. After a 5 min incubation with the DNase solution on ice, the cells were spun again at 1,200 rpm for 10 min at 4^{o}C. The pelleted cells were then resuspended with MTEC Basic solution plus 10% FBS and placed at 37^{o}C with 5% CO_2 for 3 to 4 hrs to allow fibroblasts to settle and attach to the Primaria culture dish (Falcon). MTEC Basic solution consisted of Dulbecco's Modified Eagle's Medium (DMEM)/Ham's F-12 media (Cellgro, 15-090-CM) with 15 mM HEPES (Gibco, 15630-080), 4 mM glutamine (Gibco, 25-030-149), 0.03% sodium bicarbonate (Sigma, S8761), 2.5 µg/mL fungizone (Gibco, 15290-018), and 100 U/mL P/S.

After 3 to 4 hrs, the media were collected, and the culture dish washed twice with MTEC Basic media plus 10% FBS. The pooled media were spun down at 1,200 rpm for 10 min at 4^{o}C. The isolated tracheal epithelial cells from 4 tracheas were then seeded onto 12 collagen-coated Transwell permeable membranes made of either polycarbonate or polyester (6.5 mm insert, 0.4-µm pore size; Corning-Costar, 3413). The membranes were incubated with filtered collagen coating solution (rat tail collagen, type I [Corning, 354236] diluted to 50 µg/mL in 0.02 N acetic acid) overnight under ultraviolet light, allowed to air-dry for 5 min, and then washed 3X with phosphate-buffered saline (PBS), pH 7.4. The number of membranes seeded was changed based on the above ratios depending on the initial number of pooled tracheas. Finally, the seeded cultures were allowed to proliferate in MTEC Plus media with 10^{-8} M retinoic acid (RA) in both the apical and basal chambers of the Transwell. MTEC Plus media consisted of MTEC Basic media with 10 µg/mL insulin (Sigma, I-6634), 5 µg/mL human transferrin (Sigma, T-1147), 25 ng/mL epidermal growth factor (EGF) (BD Biosciences, 354001), 0.1 µg/mL cholera toxin (Sigma, C-8052), 30 µg/mL bovine pituitary extract (BPE) (Sigma, P1167), and 5% FBS. For lentiviral infection, collected viral media were added with MTEC Plus media supplemented with RA at a 1:1 ratio in the apical chamber for the first 48 hrs after seeding. Fresh media and virus were provided after the first 24 hrs of infection. Upon achieving confluency, an air-liquid interface (ALI) was established and maintained with 2% NuSerum media (MTEC Basic media and NuSerum [BD Biosciences, 355100, or Corning, 355500] with RA provided only in the basal chamber of the Transwell. The day that an ALI was created was considered ALI day 0 (ALId0). In this chapter, MTECs were maintained until ALId21 unless otherwise noted with a PBS wash and media change

every other day (in *Chapter 4*, MTECs were maintained until ALId14 unless otherwise noted).

2.2f Preparation of primary cultures of mouse embryonic fibroblasts

Primary cultures of Cby1 WT and KO mouse embryonic fibroblasts (MEFs) were prepared from mouse embryos between embryonic days 12.5 and 14.5, as described previously (Li et al. 2007). Briefly, the uteri of pregnant Cby1 heterozygous females were dissected with sterile technique in sterile PBS. Under a tissue culture hood, embryos were isolated in PBS, and the head, heart, and liver removed. The head was used for genotyping analysis. The remaining embryos were minced and incubated with 0.05% trypsin-EDTA (Invitrogen) for 20 min at 37^{o}C in 5% CO_2. The mixture was then passed through a syringe and needle to create a single-cell suspension. MEFs were then propagated in DMEM supplemented with 10% FBS (Denville Scientific) and 100 U/mL P/S. To induce ciliogenesis, MEFs seeded on coverslips in a 24-well tissue culture plate were serum-starved for 48 hrs after reaching confluency.

2.2g Western blotting

Western blotting was performed on Cby1 WT and KO AId21 MTEC lysates as previously described (Burke et al. 2014). Lysates were generated by washing MTEC cultures with PBS and lysing with SDS buffer, which consisted of 100 mM Tris-HCl, pH 6.8, 4% sodium dodecyl sulfate (SDS), 0.2% bromophenol blue, 20% glycerol, and 200 mM β-mercaptoethanol. These samples were then boiled at 95°C for 5 min, and SDS polyacrylamide gel electrophoresis was performed. The electrophoresed proteins were then transferred to nitrocellulose membranes (Bio-Rad). These membranes were then washed with Tris-buffered saline with 0.1% Tween-20 (TBS-T) 3X for 5 min each and

incubated with 5% milk for 1 hr, primary antibodies in milk for 1 hr, and horseradish peroxidase (HRP)-conjugated secondary antibodies in milk for 1 hr. Three 5 min PBS washes were performed before and after the secondary antibody incubation. All incubations and washes were at room temperature with agitation. Protein bands were visualized with chemiluminescent substrates and HyBlot CL films (Denville) that were developed by a Konica Medical Film Processor SRX-101A. The primary antibodies used were the following: rabbit anti-IFT88 (Proteintech) and mouse anti-GAPDH (Biodesign International).

2.2h Immunofluorescence staining

ALId21, unless otherwise noted, MTEC membranes or MEFs were washed with PBS and fixed with ice-cold methanol-acetone (used 1:1) at 4^{o}C for 20 min. Membranes were then washed 3X for 5 min in PBS, cut into quarters, and stored in PBS with 0.01% sodium azide. Samples were blocked and permeabilized with 5% goat serum in antibody solution (PBS with 0.2% Triton X-100 and 5% BSA) for 1 hr at room temperature. Primary antibodies were incubated in antibody solution overnight at 4^{o}C at dilutions specified in section *2.2i Antibodies for immunofluorescence staining*. After 3X PBS washes for 5 min each at room temperature, samples were blocked and permeabilized again in antibody solution for 1 hr at room temperature, followed by secondary antibody incubation for 1 hr at room temperature. All secondary antibodies were diluted with antibody solution and used at a dilution of 1:250. MTEC membranes were then washed with PBS 3X for 5 min each at room temperature and counterstained for 2 min with DAPI, followed by two 5 min PBS washes and a PBS rinse at room temperature. Samples were then mounted with Fluoromount-G (SouthernBiotech).

2.2i Antibodies for immunofluorescence staining

The primary antibodies used were: rabbit anti-IFT88 (1:250; Proteintech), mouse anti-IFT88 (1:250; Proteintech), rabbit anti-IFT20 (1:250; gift from G. Pazour, University of Massachusetts Medical School, Worcester, MA), rabbit anti-IFT57 (1:500; Proteintech), rabbit anti-IFT140 (1:500; Proteintech), rabbit anti-BBS4 (1:500; gift from M. Nachury, Stanford University, Palo Alto, CA), rabbit anti-BBS5 (1:200; Proteintech), mouse anti-Cby1 27-11 (1:300; in-house) (Cyge et al. 2011), mouse anti-acetylated α-tubulin (A-tub) (1:1000; Sigma-Aldrich). The secondary antibodies used were: DyLight 488-conjugated goat anti-rabbit IgG (Vector Laboratories), DyLight 549-conjugated goat anti-mouse IgG (Jackson ImmunoResearch), DyLight 549-conjugated goat anti-rabbit IgG (Vector Laboratories), Alexa Fluor 647-conjugated goat anti-mouse IgG2b (Invitrogen), Alexa Fluor 488-conjugated goat anti-mouse IgG (Invitrogen).

2.2j Fluorescence microscopy

Epifluorescence images of MEFs were taken on a Leica DMI6000B epifluorescence microscope with an HCX PL Fluotar 100X/1.3 NA oil objective equipped with a DFC300FX camera. Confocal images were obtained on a Zeiss LSM Meta 510 laser scanning confocal microscope with a 63X/1.4 NA objective or a Leica SP5 or SP8X with a tunable white light laser (WLL) confocal microscope on a HC PL APO 100X/1.4 NA oil objective. For SIM imaging, MTECs were imaged using a Nikon N-SIM with a 100x/1.49 NA objective equipped with an Andor iXon3 897 EMCCD camera. All confocal and SIM images were analyzed with LSM Image Browser (Carl Zeiss), Leica Application Suite X, or Nikon Elements (Nikon) and further processed using Adobe Photoshop and Illustrator.

2.2k Scanning electron microscopy

Scanning EM (SEM) was performed as previously described (Voronina et al. 2009; Love et al. 2010; Burke et al. 2014). Briefly, ALId21 MTEC membranes were fixed with filtered 2% EM grade paraformaldehyde (PFA) (Sigma) and 2% glutaraldehyde in PBS and then dehydrated in a graded ethanol series to 100%. After dehydration, samples were processed through a graded series of ethanol-hexamethyldisilazane (HMDS; Electron Microscopy Sciences) to 100% HMDS. Preparations were then air-dried, mounted on scanning EM stubs, and sputter coated with gold prior to imaging with a scanning electron microscope (LEO1550; Carl Zeiss). Images were analyzed and processed with Adobe Photoshop and Illustrator as described above.

2.2l Statistical analysis

Two-tailed Student's t-tests were used for quantification analysis as indicated, and $p<0.05$ was considered significant.

2.3 Results

2.3a Loss of Cby1 leads to dilated distal tips of cilia in airway ciliated cells

To investigate the effect of loss of Cby1 on mature airway cilia, I exploited the well-established MTEC primary culture system (You et al. 2002; Vladar and Stearns 2007; Hoh et al. 2012; Vladar and Brody 2013). To generate primary cultures of MTECs, isolated tracheal cells were seeded at low density onto a semipermeable, collagen-coated membrane and subsequently allowed to proliferate for ≤7 days (Figure 2.1). Once confluent, an ALI was created to induce multiciliated cell differentiation. As we reported previously (Burke et al. 2014), at 9-14 days post-ALI induction (ALId9-14), a majority of

Cby1 WT cells were fully differentiated while Cby1 KO MTECs showed a reduction in the number of fully differentiated cells and of cilia per ciliated cell (data not shown).

We then performed SEM on Cby1 WT and KO- MTECs at ALId21 to assess the effects of Cby1 loss on ciliary maintenance and morphology. Consistent with previous findings (Voronina et al. 2009; Love et al. 2010; Burke et al. 2014), the number of cilia in Cby1 KO MTECs was reduced when compared to Cby1 WT MTECs. Surprisingly, in a fraction of cilia present on Cby1 KO MTECs, I found abnormalities in ciliary structure at the distal end. These ciliary malformations displayed a characteristic paddle-like morphology with a large, distended distal tip structure (Figure 2.2, arrowheads). The dramatic ballooning of the ciliary tip was an infrequent event in MTECs from Cby1 KO mice; however, such ciliary structural defects were not observed in MTECs from Cby1 WT mice. Thus, despite their low frequency, these dilations of the ciliary tip were specific for the loss of Cby1. These findings suggest that Cby1 is critical for proper ciliary architecture in mature airway ciliated cells.

2.3b The IFT-B subunit IFT88 aggregates in Cby1 KO airway ciliated cells

The IFT system plays an essential role in the biogenesis and maintenance of cilia via trafficking of cargo proteins along axonemal microtubules (Rosenbaum and Witman 2002; Scholey 2008; Sung and Leroux 2013). Prior studies have demonstrated that mutations in the genes that encode for IFT-A components lead to a ciliary bulge morphology, which often contains vesicular accumulation in the dilated distal tips (Pazour et al. 1998; Piperno et al. 1998; Huangfu and Anderson 2005; Eggenschwiler and Anderson 2007; Tsao and Gorovsky 2008; Iomini et al. 2009; Qin et al. 2011; Liem et al. 2012; Sung and Leroux 2013). Specific examples include IFT122 mutants in *T.*

thermophila and mice and IFT144 mutants in *C. reinhardtii* and mice (Tsao and Gorovsky 2008; Iomini et al. 2009; Qin et al. 2011; Liem et al. 2012). Beyond IFT, mutants for the motor constituents dynein heavy and light chains and multiple BBSome components in *C. reinhardtii* and mice have also exhibited bulge phenotypes (Pazour et al. 1998; Porter et al. 1999; Cole 2003; Shah et al. 2008). I therefore hypothesized that IFT-associated proteins are misregulated in fully differentiated Cby1 KO ciliated cells with paddle-like cilia. To examine this possibility, I performed IF staining of IFT88, an IFT-B subunit (Rosenbaum and Witman 2002; Bhogaraju et al. 2013; Sung and Leroux 2013), in ALId21 Cby1 WT and KO MTECs (Figure 2.3A). In Cby1 WT MTECs, intense IFT88 signals were detectable at the basal body with weak punctate signals also present along the ciliary axoneme (Yang et al. 2013). In contrast, I detected aberrant accumulations of IFT88 in Cby1 KO ciliated cells (Figure 2.3A, arrowheads). IFT88 aggregations were significantly more frequently observed in Cby1 KO ciliated cells (18.2±3.5% of ciliated cells) compared to Cby1 WT ciliated cells (1.7±0.3% of ciliated cells) ($p=0.018$; $n=4$) (Figure 2.3B). Interestingly, the numbers of large IFT88 accumulations per ciliated cell were highly variable with a range of 1 to 10 bulges. Next, I assessed IFT88 protein levels in ALId21 Cby1 WT and KO MTEC lysates by immunoblotting to determine if IFT88 aggregates were caused by alterations in protein expression (Figure 2.3C). No apparent differences in IFT88 protein levels were detectable between Cby1 WT and KO MTECs, suggesting that the accumulation of IFT88 in Cby1 KO ciliated cells is primarily a localization defect.

I then attempted to rescue the IFT88 accumulation phenotype with lentivirus-mediated expression of Flag-tagged full-length human Cby1 (hCby1) (Figure 2.3D). In ALId21 Cby1 KO MTECs, many infected ciliated cells demonstrated normal IFT88

localization patterns (when compared to Cby1 WT ciliated cells in Figure 2.3A). However, neighboring uninfected Cby1 KO ciliated cells displayed IFT88 accumulations (Figure 2.3D, arrowheads). Overall, the frequency of ciliated cells with IFT88 aggregates was reduced by ~50% in infected Cby1 KO ciliated cells (data not shown). These data confirm that the IFT88 accumulations are attributable to the loss of Cby1 and suggest that Cby1 is required for normal distribution of IFT88 along cilia.

2.3c Loss of Cby1 causes IFT88 mislocalization at the distal tip of primary cilia

IFT is a critical process for the generation and maintenance of both primary and multicilia (Bisgrove and Yost 2006; Scholey 2008; Goetz and Anderson 2010; Brooks and Wallingford 2014). I therefore examined IFT88 localization in a well-established model for primary ciliogenesis: serum-starved MEFs that were derived from Cby1 WT and KO embryos between embryonic days 12.5 and 14.5 (Archer and Wheatley 1971; Ocbina and Anderson 2008). Consistent with my findings in multiciliated cells, IFT88 accumulations were observed at the distal end of primary cilia with a significantly increased frequency in Cby1 KO MEFs (42.3±7.9% of ciliated cells) compared to Cby1 WT MEFs (20.2±3.6% of ciliated cells) ($p=0.038$; $n=3$) (Figure 2.4A, arrowheads, and B). These data indicate that Cby1 performs a similar function to regulate distribution of IFT-associated proteins in both primary and multicilia.

2.3d IFT88 accumulates in the bulge structure at the ciliary tips in Cby1 KO airway ciliated cells

I suspected that the IFT88 accumulations in Cby1 WT MTECs (Figure 2.3A) might reflect IFT particle accumulation within the bulged, dilated ciliary tip structures as observed by SEM (Figure 2.2). To resolve the exact location of these IFT88 aggregates,

I utilized three-dimensional SIM (3D-SIM) to image ALId21 Cby1 WT and KO MTECs co-stained with antibodies for IFT88 and A-tub (Fig. 4). 3D-SIM provides two-fold increased resolution compared to conventional confocal microscopy in each of the x-, y-, and z-dimensions, which permits visualization beyond the diffraction limit. 3D-SIM imaging easily revealed that the large IFT88 accumulations present in Cby1 KO MTECs were enclosed within large, distended circular loops of A-tub-positive ciliary axonemes at the distal ends of cilia (Figure 2.5). Thus, it is likely that defects in IFT or inherent to IFT particles result in the accumulation of IFT particles at the ciliary tip and subsequent formation of paddle-like cilia.

In Cby1 KO ciliated cells without large IFT88 masses, I observed a relatively normal IFT88 distribution pattern. However, moderate enrichment in IFT88 signal at the ciliary tip in Cby1 KO MTECs was readily apparent upon 3D-SIM imaging (Figure 2.6). These moderate IFT88 accumulations were more frequent than the larger aggregates, suggesting that they may represent a precursor step to the formation of more pronounced paddle-shaped cilia.

2.3e Cby1 regulates ciliary localization of IFT-B sub-complex members in ciliated cells

The IFT complex consists of >20 subunits that are grouped into two distinct sub-complexes: the IFT-B and IFT-A sub-complexes (Bhogaraju et al. 2013; Sung and Leroux 2013). As IFT88 is one of the IFT-B complex members, we speculated that other IFT-B and IFT-A sub-complex components might also be misregulated and accumulate within the bulges in Cby1 KO ciliated cells. We therefore evaluated the ciliary localization of the IFT-B proteins IFT20 and IFT57 and the IFT-A protein IFT140 by IF staining (Figure 2.7,

top three rows of panels). IFT20, IFT57, and IFT140 all demonstrated normal localization patterns in ALId21 Cby1 WT MTECs as reported previously (data not shown) (Pazour et al. 2002a; Follit et al. 2006; Sedmak and Wolfrum 2010). In contrast, in ALId21 Cby1 KO MTECs, the IFT-B proteins IFT20 and IFT57 showed robust accumulations (Figure 2.7, top two rows of panels) that colocalized with the IFT88 aggregates that were found to correspond to the bulge structures by 3D-SIM imaging (Figure 2.5). Interestingly, the IFT-A subunit IFT140 was not detectable as aggregates with IFT88 (Figure 2.7, dotted line enclosures in third row of panels). Hence, solely the IFT-B, not IFT-A, proteins, and presumptively the sub-complex, accumulate at the dilated ciliary tips of Cby1 KO ciliated cells. These observations suggest that IFT-B proteins are, most likely, not trafficked out of the ciliary compartment efficiently in Cby1 KO ciliated cells despite apparently normal trafficking of IFT-A complex members. Thus, this raises the interesting possibility that Cby1 influences the proper rearrangement of IFT particles at the ciliary tip from anterograde to retrograde transport.

Similar to the bulge phenotype observed in ALId21 Cby1 KO MTECs, mouse mutants for the BBSome component BBS1, BBS2, BBS4, or BBS6 develop bulges filled with vesicular structures near the distal tips of cilia in airway epithelia (Shah et al. 2008). Hence, I hypothesized that Cby1 might be required for the proper localization and function of the BBSome. To address this possibility, I performed IF staining for BBS5 in Cby1 KO MTECs at ALId21 (Figure 2.7, bottom row of panels). Surprisingly, BBS5 did not demonstrate aberrant accumulation with IFT88 (Figure 2.7, dotted line enclosures in bottom row of panels). Thus, Cby1 does not appear to regulate BBSome localization

although I cannot rule out the possibility that other BBSome components might be mislocalized or that the BBSome might be dysfunctional in the absence of Cby1.

2.4 Discussion

In this chapter, I present evidence that Cby1 is required for normal ciliary architecture and IFT localization in ciliated cells of MTEC cultures. IFT is a bidirectional process that requires both IFT-B and IFT-A complexes and anterograde kinesin and retrograde dynein motor proteins (Rosenbaum and Witman 2002; Scholey 2008; Sung and Leroux 2013). Based on studies of mutant phenotypes and IFT particle dynamics, it has been proposed that a unique complement of both IFT-B and IFT-A transport and motor proteins mediates anterograde and retrograde IFT, respectively. This proposed model would necessitate that the anterograde IFT-B complex and kinesins carry retrograde IFT-A proteins and dyneins to the ciliary tip as cargo and that the retrograde IFT-A complex and dyneins transport the anterograde components back to the cytoplasm. Hence, massive rearrangement of the IFT particle and its associated proteins, including kinesins and dyneins, must take place at the ciliary tip for proper ciliary extension and maintenance (Qin et al. 2004; Wei et al. 2015). Thus, a failure to rearrange the IFT particle at the ciliary tip, as documented in IFT-A or BBSome mutants, leads to the formation of bulge structures (Piperno et al. 1998; Huangfu and Anderson 2005; Shah et al. 2008; Tsao and Gorovsky 2008; Iomini et al. 2009; Qin et al. 2011; Liem et al. 2012). In the absence of Cby1, the IFT-B component IFT88 accumulates within the bulged, dilated ciliary tips of both Cby1 KO primary cilia and multicilia (Figures 2.2-5). In agreement with this observation, the *D. melanogaste*r IFT88 homolog is found to

accumulate in the embryonic chordotonal cilia of the Cby1 mutant fly (Enjolras et al. 2012), indicating that the function of Cby1 as an IFT regulator is evolutionarily conserved. Interestingly, solely other IFT-B sub-complex members amass with IFT88 in Cby1 KO ciliated cells (Figure 2.7), suggesting that anterograde IFT occurs normally in Cby1 KO ciliated cells while IFT-B components are either not properly loaded as cargos onto the retrograde IFT complex or unable to effectively exit the ciliary compartment. Coupled with the normal localization pattern of IFT-A proteins and BBSome members, we speculate that Cby1 is important for a switch from anterograde to retrograde IFT at the ciliary tip.

The BBSome has been shown to be a critical effector of IFT and proposed to be involved in IFT particle turnaround at the ciliary tip (Wei et al. 2012; Zhang et al. 2012; Williams et al. 2014). Furthermore, several BBS mouse mutants display bulge phenotypes in airway ciliated cells strikingly similar to those in Cby1 KO MTECs (Shah et al. 2008). Hence, it is particularly surprising that BBS5 demonstrated relatively normal distribution patterns in Cby1 KO MTECs (Figure 2.7). However, the possibility remains that other BBSome components may show altered distribution or that the BBSome may be dysfunctional in Cby1 KO ciliated cells. Thus, a potential connection between the BBSome complex and Cby1 is clearly an intriguing area of potential future exploration.

How might Cby1 regulate IFT rearrangement at the ciliary tip? An attractive model is that Cby1 localizes to the ciliary compartment along cilia, travels with the IFT particle, and directly impacts IFT particle rearrangement at the ciliary tip. I attempted with the use of several methodologies to detect Cby1 in the ciliary compartment in MTECs by IF staining. Intense Cby1 signal was observed at the base of cilia, consistent with previous

reports (Love et al. 2010; Enjolras et al. 2012; Steere et al. 2012; Burke et al. 2014; Lee et al. 2014; Shi et al. 2014); however, Cby1 was not clearly detectable in the ciliary compartment (data not shown). While it remains possible that the levels of Cby1 in the ciliary compartment are beyond the detection limit of our current methods, a more likely scenario is that Cby1 influences IFT particle assembly from its position at the ciliary base. Several lines of evidence support this proposal. Cby1 predominantly clusters around the transition fibers in mature ciliated cells (Love et al. 2010; Enjolras et al. 2012; Steere et al. 2012; Burke et al. 2014; Lee et al. 2014; Shi et al. 2014), which are known to be the sites critical for IFT particle assembly, docking, and entry into the ciliary compartment (Deane et al. 2001; Reiter et al. 2012; Daly et al. 2016). Interestingly, other transition fiber proteins, such as CEP164 and FBF1 (Schmidt et al. 2012; Wei et al. 2013; Cajanek and Nigg 2014; Oda et al. 2014), have also been shown to regulate IFT particle formation and ciliary entry, implying that particularly complex regulation of IFT processes may occur at the transition fibers. Thus, Cby1 may modulate recruitment of IFT components, assembly of IFT-motor complexes, and their efficient entry into the ciliary compartment at the ciliary base.

The trapping of IFT-B components at the ciliary tip is most likely a rate-limiting process, which accounts for the ~18% frequency with which we observe the more dramatic IFT88 accumulations (Figure 2.3B). Furthermore, the accumulation of IFT88 in only a subset of cilia implies a considerable heterogeneity in IFT among individual cilia and, hence, an explanation why not all cilia display overt morphological deficits at any given time. However, the more abundant presence of smaller IFT88 accumulations detectable with 3D-SIM imaging suggests an interesting model for bulge formation at the

ciliary tip (Figure 2.6). I propose that, subsequent to axonemal extension in Cby1 KO ciliated cells, IFT-B components accumulate at the ciliary tip due to defective retrograde trafficking of these IFT-B proteins. Thus, small accumulations of IFT-B proteins begin to form as a precursor state to the formation of larger accumulations of these IFT-B proteins, which cause bulge formation and paddle-like cilia. In support of this model, the frequency of large IFT88-positive bulges at the ciliary tips increased as Cby1 KO MTEC cultures were maintained for longer periods of time (data not shown). However, it is also conceivable that these bulges form during the early phases of ciliogenesis before cilia fully elongate. On the other hand, small versus large IFT88 accumulations may reflect the severity of the deregulation of IFT particle assembly and rearrangement. Recently, a novel mechanism for the release of ciliary G-protein coupled receptors (GPCRs) as well as IFT-B particles was uncovered in primary cilia as two reports demonstrated the capacity of primary cilia to produce extracellular vesicles from their tip. In both studies, the accumulation of GPCRs or IFT-B proteins preceded ciliary vesicle release, similar to what was observed for a portion of primary cilia in Cby1 WT MEFs (Figure 2.4B). Thus, it is reasonable to speculate that Cby1 might effect these membrane remodeling processes at the ciliary tip and influence the capacity and frequency of this event. Indeed, many predictions exist as the molecular underpinnings of how paddle-like cilia phenotypes develop are unclear.

Despite over twenty years elapsing since the discovery of IFT (Kozminski et al. 1993; Rosenbaum and Witman 2002), its complex regulation is still an area of much active research. Here, I propose that Cby1 is a regulator of IFT processes, including IFT particle assembly and rearrangement as its loss causes both mislocalization of IFT components

and alterations in ciliary structure. However, the exact molecular basis by which Cby1 regulates IFT processes warrants further investigation to provide novel insight into where Cby1 fits into a larger IFT regulatory network. Additionally, further examination of the underlying mechanism by which loss of Cby1 results in the formation of paddle-like cilia may help us to understand both how cilia are formed and maintained, how IFT misregulation leads to defects in ciliary structure, and how those morphological defects contribute to PCD phenotypes, particularly in the Cby1 KO mice.

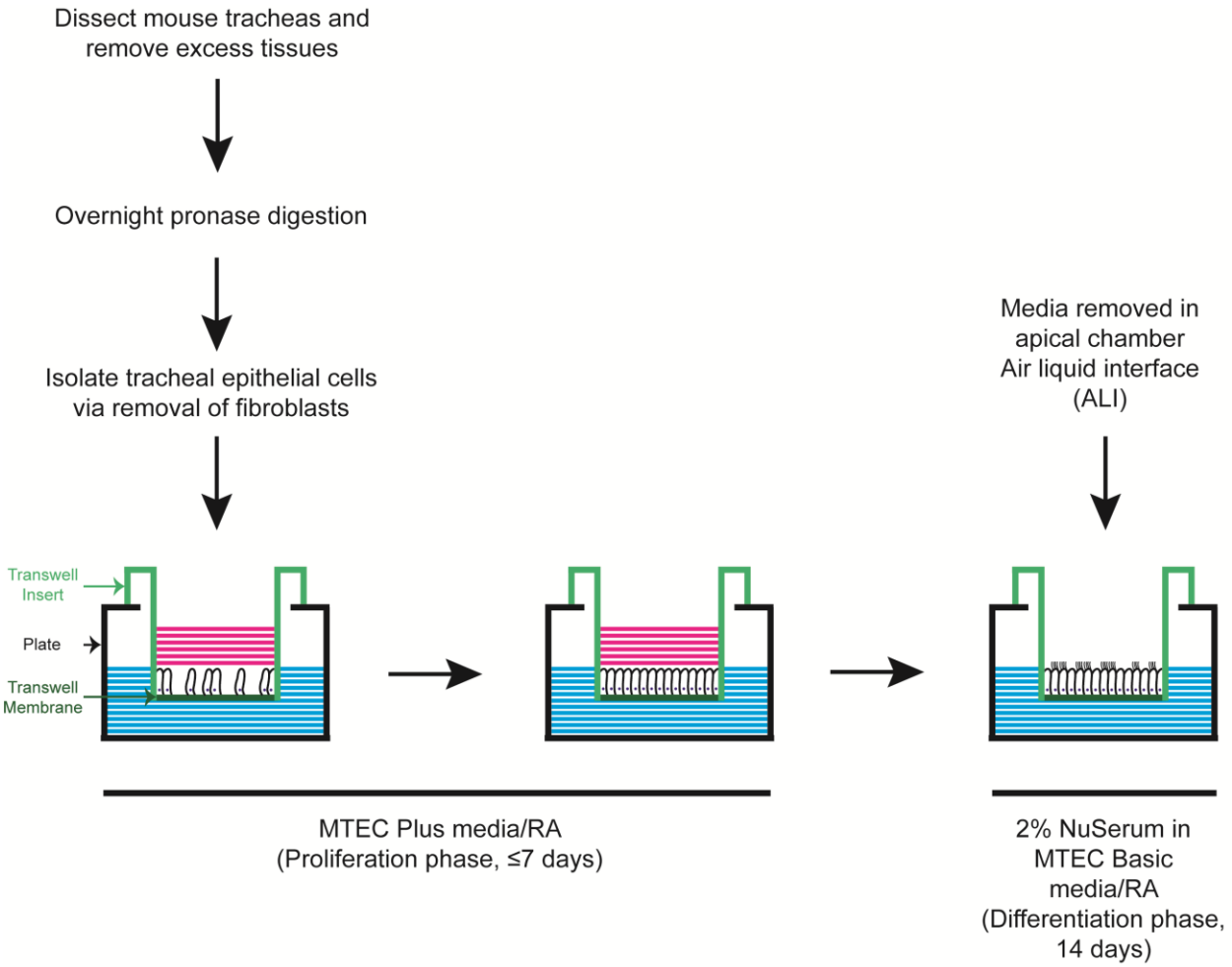

Figure 2.1: Generation of primary cultures of mouse tracheal epithelial cells (MTECs).
To establish primary cultures of mouse tracheal epithelial cells, tracheas from adult mice are dissected, cleaned of excess tissue and fascia, and allowed to incubate in pronase overnight to promote the dissociation of tracheal epithelial cells from the tissue. The following day the tracheal epithelial cells are isolated from fibroblasts and seeded onto collagen-coated Transwell membranes. These cultures are provided MTEC Plus media with RA that contains serum and essential growth factors in both the apical and basal chambers of the Transwell until confluent, which usually occurs within 7 days of seeding. After confluency is reached, the tracheal epithelial cells are provided 2% NuSerum in MTEC Basic media with RA in solely the basal chamber, establishing an air-liquid interface (ALI), to promote differentiation of the cultures. This differentiation phase normally requires 14 days until the cultures resemble the native tracheal epithelium. This figure was adapted from You et al. 2002.

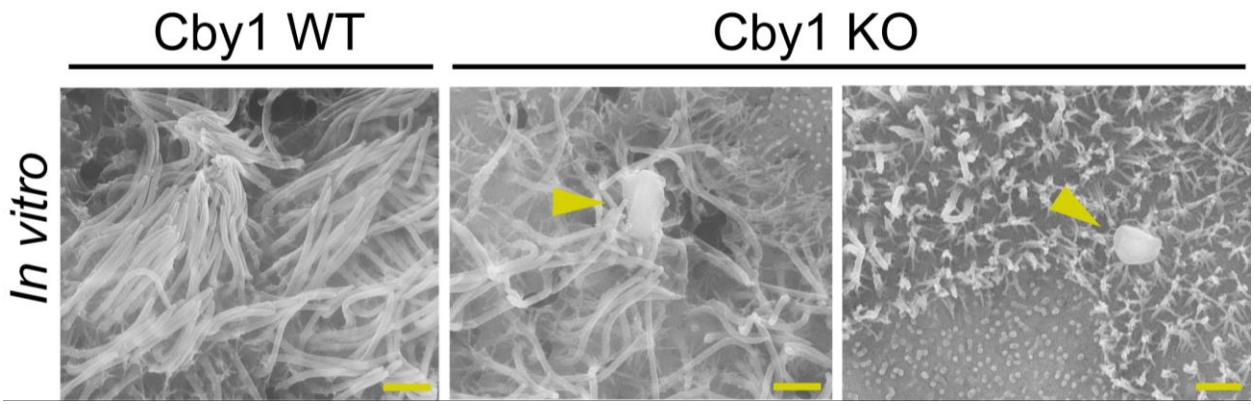

Figure 2.2: Ciliated cells of Cby1 KO airways display a bulge morphology at the ciliary tip.
Shown are scanning electron micrographs of ALId21 MTECs (*In vitro*) from adult Cby1 WT (left column) and KO (middle and right columns) tracheas. Cby1 KO MTECs demonstrated a paddle-like ciliary morphology with dilated distal tips (arrowheads). In addition to cilia, the apical surface of ciliated cells contains numerous microvilli. Scale bars, 1 µm.

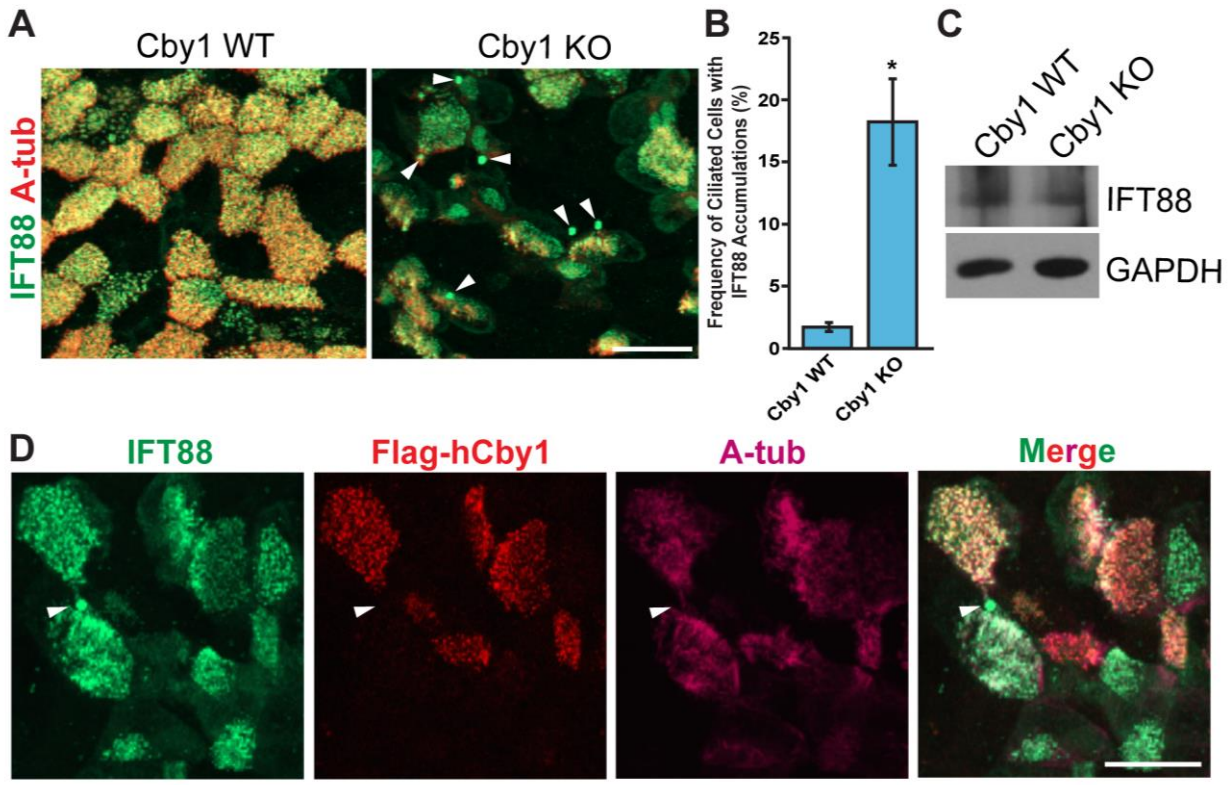

Figure 2.3: IFT88, a subunit of the IFT-B sub-complex, accumulates in Cby1 KO tracheal ciliated cells.

(A) Confocal images of Cby1 WT and KO MTECs at ALId21 colabeled for IFT88 (green) and the basal body/axonemal marker acetylated α-tubulin (A-tub) (red). Arrowheads indicate IFT88 accumulations in Cby1 KO ciliated cells. Scale bar, 20 µm. (B) Quantification of frequency of ciliated cells with IFT88 accumulations in ALId21 Cby1 WT and KO MTECs. Greater than 250 ciliated cells were counted from each of four individual MTEC preparations. Data presented as means ± SEM. *, $p<0.05$. (C) Western blot analysis of IFT88 and GAPDH (loading control) from ALId21 Cby1 WT and KO MTEC lysates. No differences in IFT88 protein expression were observed. (D) Confocal images show ALId21 Cby1 KO MTECs that were infected with lentiviruses that express Flag-tagged full-length human Cby1 (hCby1) and were immunostained for IFT88 (green), Flag-hCby1 (red), and A-tub (magenta). Uninfected Cby1 KO ciliated cells displayed IFT88 accumulations (arrowheads) while lentivirus-mediated expression of Flag-hCby rescued such accumulations. Scale bar, 20 µm.

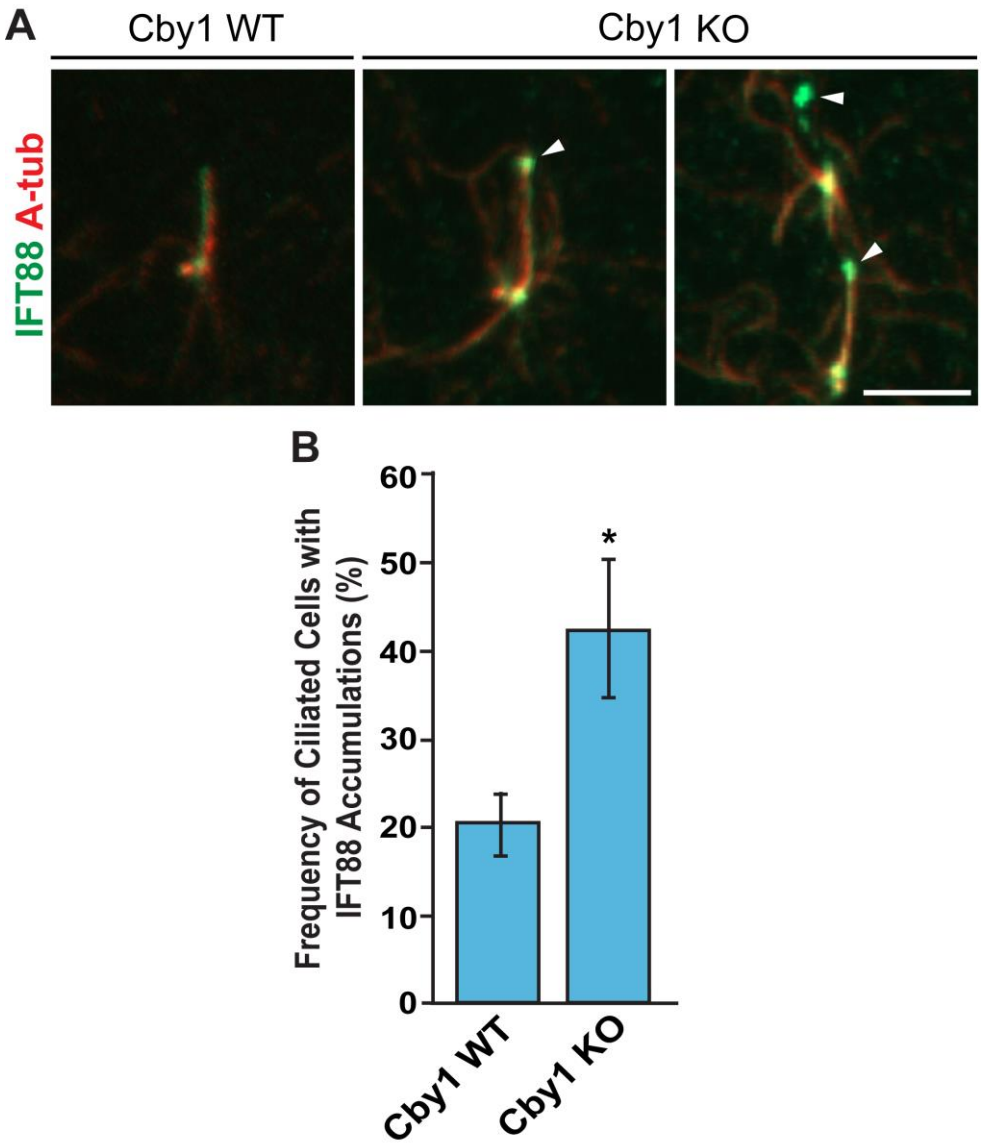

Figure 2.4: IFT88 aggregates at the distal tip of primary cilia are present in Cby1 KO MEFs.

(A) Confocal images of Cby1 WT and KO MEFs that were serum-starved for 48 hrs and stained for IFT88 (green) and A-tub (red). Accumulations of IFT88 (arrowheads) were found at the distal end of primary cilia in Cby1 KO MEFs. Scale bar, 5 µm. (B) Quantification of frequency of ciliated cells with IFT88 accumulations in serum-starved Cby1 WT and KO MEFs. Greater than 198 cells with primary cilia were counted from each of three individual MEF preparations. Data presented as means ± SEM. *, $p<0.05$.

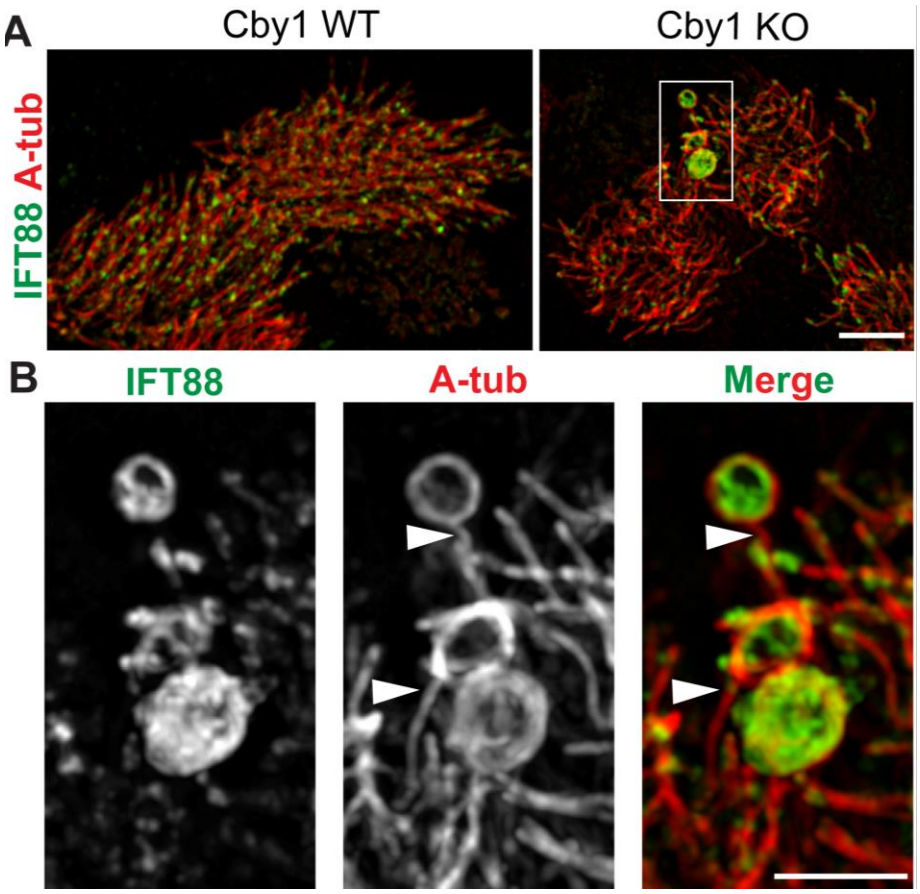

Figure 2.5: IFT88 accumulations are contained within the bulge structures at the dilated ciliary tips of Cby1 KO tracheal ciliated cells.
(A) Super-resolution 3D-SIM images of ALId21 Cby1 WT and KO MTECs colabeled for IFT88 (green) and A-tub (red). Scale bar: 5 µm. (B) Magnified images of the boxed area in (A) clearly demonstrate that IFT88 accumulations occurred within dilated A-tub-positive enclosures at the ciliary tip. Single channel images for IFT88 and A-tub staining are shown in grayscale. Ciliary axonemes, which harbor IFT88 accumulations, are indicated by arrowheads. Scale bar, 1 µm.

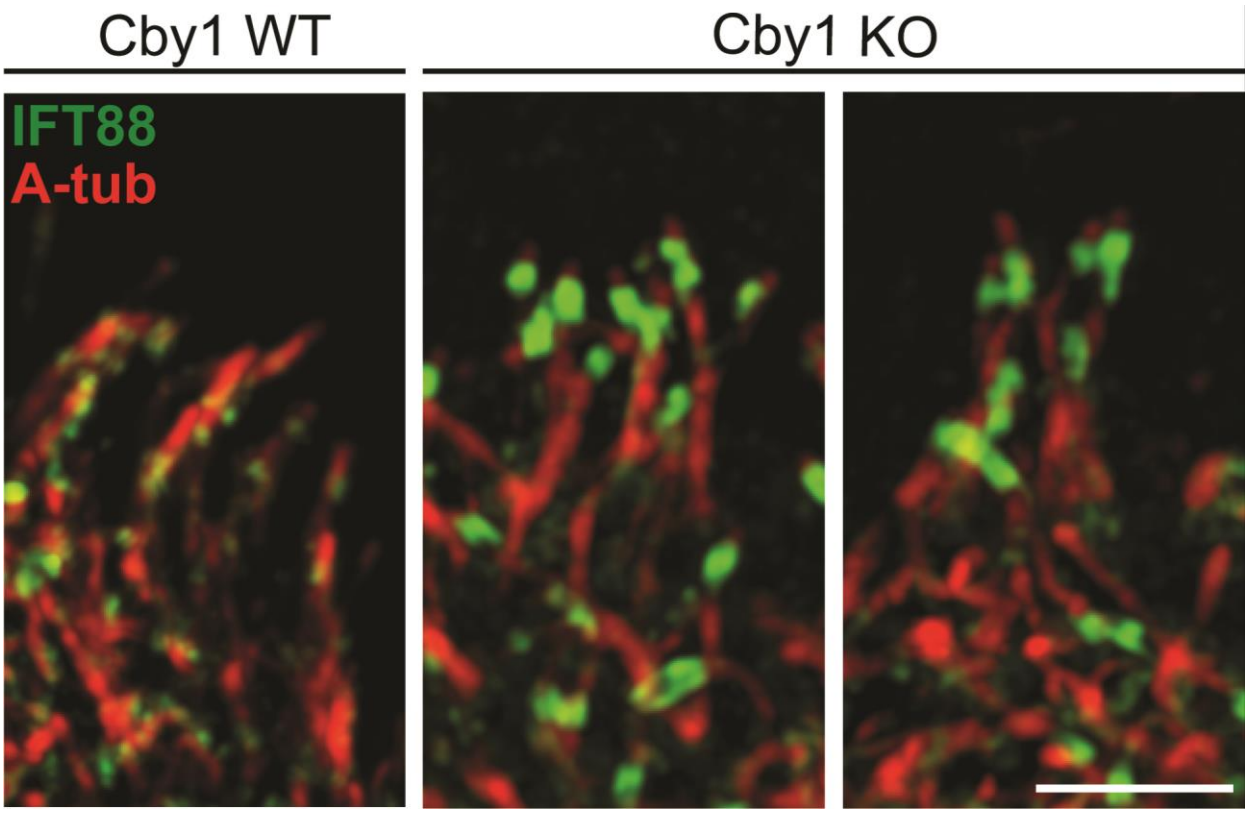

Figure 2.6: Small IFT88 accumulations were observed in at the ciliary distal ends in Cby1 KO tracheal ciliated cells.
3D-SIM images of cilia in Cby1 WT and KO MTECs at ALId21 colabeled for IFT88 (green) and A-tub (red). Moderate IFT88 accumulations at the ciliary tip were frequently found in Cby1 KO ciliated cells. Note that IFT88 accumulations, large or small, were not seen in Cby1 WT cilia. Scale bar, 1 µm.

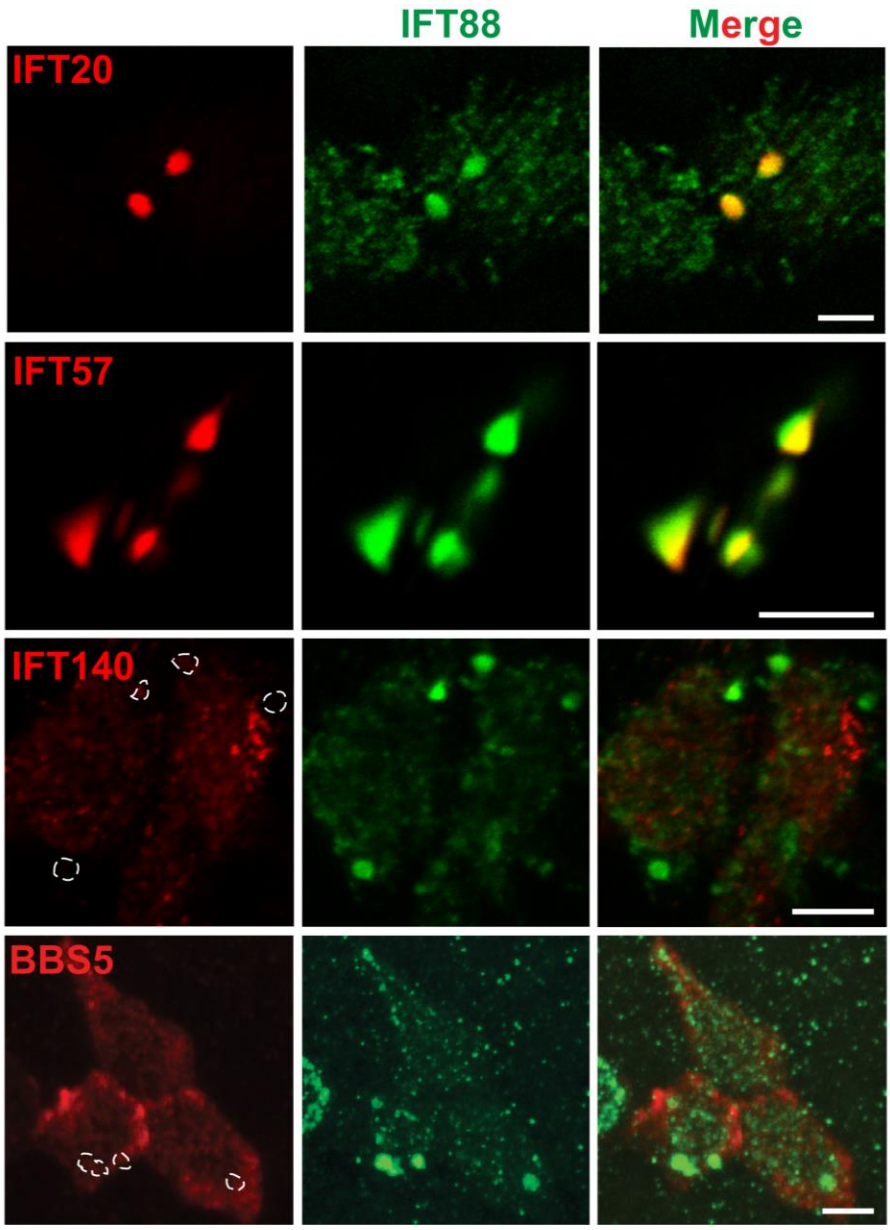

Figure 2.7: IFT-B, but not IFT-A or BBSome, consistuents exhibit localization patterns similar to IFT88 in Cby1 KO tracheal ciliated cells.
Shown are immunofluorescence confocal images of ALId21 Cby1 KO MTECs immunostained for IFT88 (green) and either IFT-B sub-complex members IFT20 or IFT57, IFT-A sub-complex member IFT140, or BBSome member BBS5 (red), as indicated. IFT20 and IFT57 localized in patterns similar to IFT88 while IFT140 and BBS5 did not accumulate with IFT88. Dashed enclosures correspond to the areas positive for IFT88 accumulations. Scale bars, 5 µm.

Chapter 3: CEP164 is essential for mammalian development and multiciliated tissues

In combination with Chapter 4, the data and text of this chapter are part of a current manuscript being prepared for submission (Siller SS, et al).

3.1 Introduction

The distal appendage and its core protein constituents are necessary for ciliogenesis based upon several studies conducted in mammalian cell culture systems (Graser et al. 2007; Joo et al. 2013; Sillibourne et al. 2013; Tanos et al. 2013). Though, the physiological function of the distal appendage and its components remain undefined as few animal models for the distal appendage proteins exist. Furthermore, due to the lack of animal models, the roles of the distal appendage and its associated proteins have not been interrogated in motile cilia and multicilia.

The first identified core distal appendage protein was CEP164, which has since been shown to be critical for primary cilia formation in KD and KO experiments using mammalian cell culture systems (Graser et al. 2007; Chaki et al. 2012; Schmidt et al. 2012; Cajanek and Nigg 2014; Daly et al. 2016). Furthermore, mutations in the *CEP164* gene have been associated with NPHP and BBS disorders (Chaki et al. 2012; Maria et al. 2016). Based on its essential role in primary ciliogenesis and disease associations, it is surprising that, thus far, the only animal data on CEP164 function comes from morpholino KD experiments in zebrafish. Two separate reports demonstrate that CEP164 KD in zebrafish causes cell death, a shortened and curved body axis, abnormal heart looping, pronephric tubule cysts, brain developmental abnormalities, and retinal dysplasia, many of which are reminiscent of ciliopathy phenotypes (Chaki et al. 2012;

Slaats et al. 2014). Hence, with such dramatic phenotypes in KD experiments, it is necessary to generate new animal KO models to further determine CEP164 function.

In this chapter, I report the first mouse model for CEP164. As all prior work had studied CEP164 in primary ciliogenesis and as protein function in motile cilia and multicilia can only be analyzed using animal model systems, I specifically aimed to generate a novel conditional KO mouse model in which CEP164 is deleted from multiciliated cells. To create these mice, a CEP164 KO-first mouse from the European Conditional Mouse Mutagenesis (EUCOMM) Program was utilized. Interestingly, mice homozygous for the CEP164 KO-first allele were embryonically lethal prior to embryonic day (E) 12.5 and demonstrated holoprosencephaly, cardiac defects, and a shortened posterior trunk. Further analysis of MEFs from these homozygous mice revealed that CEP164 was lost at the mother centriole, suggesting that these mice had no CEP164 expression. On the other hand, the conditional KO mouse model was viable to adulthood with only ~20% lethality around weaning age due to profound hydrocephalus. These mice showed a severe reduction in the number of airway, ependymal, and oviduct cilia with concomitant defective spermiogenesis. Consistent with these abnormalities, all adult conditional mice had hydrocephalus, and the males were found to be infertile. Therefore, this mouse model with CEP164 removed from multiciliated cells proves to be a powerful tool for further interrogation of CEP164 function in mammals and in multiciliogenesis.

3.2 Materials and methods

3.2a Generation of FOXJ1-Cre;CEP164$^{fl/fl}$ mice

CEP164 KO-first mice, which contain the promoter-driven Tm1a allele, were purchased from the EUCOMM program (Skarnes et al. 2011; Bradley et al. 2012). CEP164 KO-first mice were crossed with the flippase (Flp) deleter mouse line B6(C3)-Tg(Pgk1-FLPo)10Sykr/J (The Jackson Laboratory, #011065) to generate CEP164$^{fl/fl}$ mice (Rodriguez et al. 2000). Removal of the neomycin-resistance and *lacZ* cassettes was confirmed by polymerase chain reaction (PCR) genotyping analysis and subsequent electrophoresis as described in section *2.2a Statistical analysis*. Subsequently, CEP164$^{fl/fl}$ mice were crossed with FOXJ1-Cre mice to generate FOXJ1-Cre;CEP164$^{fl/fl}$ mice lacking CEP164 in multiciliated cells and the testis (Zhang et al. 2007). A colony of CEP164 KO-first mice was maintained by intercrossing heterozygous mice while FOXJ1-Cre;CEP164$^{fl/fl}$ mice were generated by breeding FOXJ1-Cre;CEP164$^{fl/+}$ with CEP164$^{fl/fl}$ mice. Primers for genotyping were: WT allele for CEP164 KO-first, 5'-CCATCTGTCCAGTACCATTAAAAA-3' and 5'-CCCAGAATACAACATGGGAGA-3' (215 bp); KO allele for CEP164 KO-first, 5'-CCATCTGTCCAGTACCATTAAAAA-3' and 5'-GAACTTCGGAATAGGAACTTCG-3' (148 bp); CEP164 floxed allele, 5'-CCATCTGTCCAGTACCATTAAAAA-3' and 5'-CCCAGAATACAACATGGGAGA-3' (WT allele, 215 bp; floxed allele, 415 bp); FOXJ1-Cre, 5'-CGTATAGCCGAAATTGCCAGG-3' and 5'-CTGACCAGAGTCATCCTTAGC-3' (327 bp). For statement of protocols and guidelines regarding animal husbandry, see section *2.2b Ethics statement*.

3.2b Histology and X-gal staining

Trachea, testis, and oviduct were dissected from adult mice euthanized via CO_2 asphyxiation. Samples were then fixed with 4% PFA in PBS overnight at 4°C, paraffin-embedded, sectioned at 5 µm, stained with hematoxylin and eosin using standard protocols, and mounted with Permount (Fischer Scientific). For X-gal staining, testes from control WT or CEP164 KO-first heterozygous mice were fixed with 2% PFA and 0.25% glutaraldehyde in PBS overnight at 4°C, embedded in the Optimal Cutting Temperature (OCT) compound (Fisher Scientific), and snap-frozen in liquid nitrogen-cooled 2-methylbutane. The tissues were then sectioned at 5 µm, washed twice for 5 min each in wash buffer (0.01% sodium deoxycholate, 2 mM $MgCl_2$, and 0.02% NP-40 in PBS), incubated with X-gal (1 mg/ml) in wash buffer and cyanide solution (100 mM potassium ferricyanide and 100 mM potassium ferrocyanide in water) for 48 hours at room temperature, washed twice for 5 minutes in wash buffer, and mounted with Permount.

3.2c Immunofluorescence staining and imaging

MEFs were prepared from E8.5 embryos as described in section *2.2f Preparation of primary cultures of mouse embryonic fibroblasts*, and IF was performed as outlined above in section *2.2h Immunofluorescence staining*. For IF analysis of oviducts, paraffin sections were subjected to antigen retrieval with citrate buffer (pH 6.0), blocked with normal horse serum, and incubated with primary and secondary antibodies, followed by mounting with Prolong Gold with DAPI (Invitrogen). Epifluorescence images, as well as images of tissue histology, were taken on a Leica DMI6000B epifluorescence microscope with an HCX PL Fluotar 100X/1.3 NA oil objective equipped with a DFC300FX camera

and handled on Leica Application Suite X software. All images were further processed with Adobe Photoshop and Illustrator.

3.2d Subventricular zone whole mount dissection and analysis

SVZ whole mounts were dissected as described previously (McClenahan et al. 2016). Briefly, adult mice were anesthetized and decapitated. After brain removal, the lateral wall of the lateral ventricle was dissected and fixed in 4% PFA in PBS for 30 min on ice. Whole mounts were washed with PBS, blocked in blocking solution (10% donkey serum with 0.1% Triton X-100 in PBS), and incubated with primary antibody for 24 hours at 4°C and secondary antibody for 2 hours at room temperature in blocking solution. Whole mount fields were randomly selected for imaging with a Leica SP8X with a tunable WLL confocal microscope on a HC PL APO 100X/1.4 NA oil objective from the anterior-dorsal region of the SVZ.

Images were processed and quantified using the FIJI/ImageJ software as previously described (McClenahan et al. 2016). Outlines of the apical borders of cells and the borders of basal body patches were traced manually in ImageJ. Absolute areas were directly calculated and reported whereas fractional areas were calculated by dividing the basal body patch area by the apical cell surface area. The centroid of each area was calculated in FIJI/ImageJ, and the vector from the center of the cell and center of the basal body patch was then calculated based on those values. Basal body patch displacement was calculated by taking the magnitude of this vector. Fractional displacement was calculated by dividing the magnitude of the vector running from the center of the cell to the center of the basal body patch by the magnitude of a manually

drawn vector running from the center of the cell through the center of the basal body and terminating at the cell border.

3.2e Antibodies for immunofluorescence staining

The primary antibodies used were: rabbit anti-CEP164 (1:200; Sigma), rabbit anti-Cby1 1418P (1:250; in-house) (Voronina et al. 2009), rabbit anti-FAM92A (1:200; Proteintech), mouse β-catenin (1:500; BD Transduction), rabbit anti-γ-tubulin (G-tub; 1:1000; Sigma), mouse anti-A-tub (1:1000; Sigma), and mouse anti-γ-tubulin (1:200; Sigma). The secondary antibodies used were: DyLight 488-conjugated goat anti-rabbit IgG (Vector Laboratories), DyLight 549-conjugated horse anti-mouse IgG (Vector Laboratories), and DyLight 488-conjugated horse anti-mouse IgG (Vector Laboratories).

Descriptions of statistical analyses used in this chapter can be found in section *2.2l Statistical analysis*.

3.3 Results

3.3a CEP164 is indispensable for early mouse embryogenesis

CEP164 is composed of 1460 amino acids and contains a WW domain along with three coiled-coil domains (Figure 3.1A). To elucidate the physiological function of CEP164 in mammals, the CEP164 KO-first mouse line from the EUCOMM Program was obtained (Figure 3.1B) (Skarnes et al. 2011; Bradley et al. 2012; Cevik et al. 2013). This mouse line contains the promoter-driven Tm1a allele that carries the neomycin-resistance and *lacZ* gene cassettes. As I initially expanded our CEP164 KO-first mouse colony, I noted that mice heterozygous for the KO-first allele appeared healthy and fertile while no

homozygous mice were born, suggesting embryonic lethality. To address this possibility, I examined embryos from heterozygous intercrosses at various stages of gestation. At E7.5 (Figure 3.2), CEP164 KO-first homozygous embryos showed no obvious morphological abnormalities; however, at E9.5 (Figure 3.2) and E10.5 (data not shown), homozygous embryos exhibited holoprosencephaly, cardiac looping defects, an edematous pericardial sac, and a truncated posterior trunk. Resorptions were consistently observed at E12.5 and all later stages examined. These data demonstrate that CEP164 is necessary for mammalian embryogenesis.

CEP164 has been shown to be essential for primary ciliogenesis in mammalian cultured cells and zebrafish embryos (Graser et al. 2007; Schmidt et al. 2012; Cajanek and Nigg 2014; Slaats et al. 2014; Daly et al. 2016). To confirm the lack of CEP164 protein expression in homozygous CEP164 KO-first embryos and the critical role of CEP164 in primary ciliogenesis, I utilized primary cultures of MEFs, which are established model systems for the study of primary cilia (Archer and Wheatley 1971; Ocbina and Anderson 2008). MEFs were prepared from E8.5 embryos due to the lethality of homozygous CEP164 KO-first embryos, grown to confluence, and serum-starved for 48 hours to induce ciliogenesis (Figure 3.3). IF staining revealed that CEP164 localized at the base of cilia in control MEFs, whereas no CEP164 was found at the centrioles of homozygous MEFs. Consistent with prior reports and the dramatic embryonic phenotypes, MEFs homozygous for the CEP164 KO-first allele failed to ciliate upon serum starvation (Figure 3.3).

Using siRNA-mediated KD experiments in human RPE1 cells, it has been previously shown that CEP164 recruits both Cby1 and FAM92A to the ciliary base to

facilitate primary ciliogenesis (Burke et al. 2014; Li et al. 2016b). Indeed, in contrast to control MEFs, neither Cby1 nor FAM92A were detected at the centrioles of homozygous MEFs for the CEP164 KO-first allele (Figure 3.3). Thus, my results validate previous data suggesting a fundamental role for CEP164 in primary ciliogenesis and the recruitment of Cby1 and FAM92A to basal bodies. Additionally, the lack of primary cilia in these homozygous MEFs indicates that CEP164 regulates mammalian embryogenesis, at least in part, through its function in primary ciliogenesis.

3.3b Loss of CEP164 in FOXJ1-positive tissues in mice leads to defective multiciliogenesis

CEP164 plays an essential role in primary ciliogenesis (Schmidt et al. 2012; Cajanek and Nigg 2014; Daly et al. 2016); however, the role of CEP164 in multiciliogenesis had not been elucidated, and no CEP164-KO animal models were available to investigate its physiological functions *in vivo*. I therefore employed the CEP164 KO-first mouse line to generate a mouse model that lacks CEP164 in multiciliated cells (Figure 3.1B). To this end, a heterozygous CEP164 KO-first mouse was crossed with a Flp deleter mouse to remove both the *lacZ* and neomycin-resistance cassettes (Rodriguez et al. 2000). The resultant mouse ($CEP164^{fl/fl}$) has two loxP sites flanking exon 4 of the *CEP164* gene, which encodes a part of the WW domain (Figure 3.1A). FOXJ1 is a forkhead transcription factor expressed in multiciliated cells in the airways, brain ventricles, and oviducts as well as in the testis (Blatt et al. 1999; Brody et al. 2000). Thus, I bred the $CEP164^{fl/fl}$ mouse with a FOXJ1-Cre transgenic mouse that expresses Cre recombinase under the control of the FOXJ1 promoter to remove CEP164 expression from multiciliated cells and the testis (Zhang et al. 2007). Cre-mediated

recombination results in the excision of exon 4 and a frameshift, leading to a truncation at amino acid position 65 (Figure 3.1A). Correct recombination was verified by PCR genotyping (Figure 3.1C and D). A majority of FOXJ1-Cre;CEP164$^{fl/fl}$ mice lived to adulthood without gross abnormalities, except for 19.0% that succumbed to death due to severe hydrocephalus around weaning and another 24.1% that exhibited mild hydrocephalus, which resolved itself later.

Histological assessment of the trachea (Figure 3.4) and sinus (data not shown) from FOXJ1-Cre;CEP164$^{fl/fl}$ adult mice showed a marked decrease in the number of airway cilia in comparison to control specimens from CEP164$^{fl/fl}$ mice. Indicative of impaired mucociliary clearance from reduced airway cilia, these mice frequently produced coughing- or sneezing-like noises. As noted above, 19.0% of FOXJ1-Cre;CEP164$^{fl/fl}$ mice displayed severe hydrocephalus with a prominently domed head around weaning (Figure 3.5A, left panels); however, all FOXJ1-Cre;CEP164$^{fl/fl}$ adult mice examined showed substantial ventricular enlargement (middle panels). The high penetrance of hydrocephalus prompted me to examine the status of ependymal cilia by IF staining of whole mounts of the SVZ. As expected, IF staining for the ciliary marker acetylated α-tubulin (A-tub) demonstrated a clear reduction in the number of ependymal cilia in FOXJ1-Cre;CEP164$^{fl/fl}$ SVZ whole mounts compared to control CEP164$^{fl/fl}$ samples (Figure 3.5A, right panels). Consistent with this, quantification of basal body locations, based on γ-tubulin staining (G-tub; Figure 3.5B), on the apical surface of ependymal cells in FOXJ1-Cre;CEP164$^{fl/fl}$ mice revealed significant perturbations in the patch area and displacement (Figure 3.5C and D), indicating that basal bodies are fewer and mispositioned spatially at

the apical surface of ependymal cells. Thus, CEP164 is critical for multiciliogenesis in both mammalian airways and ependymal cells lining the brain ventricles.

3.3c CEP164 is important for normal differentiation of male and female reproductive tissues

As FOXJ1 is highly expressed in the ciliated cells of the oviduct epithelium as well as in the testis (Blatt et al. 1999; Brody et al. 2000), I next examined reproductive tissues in FOXJ1-Cre;CEP164$^{fl/fl}$ mice. In the oviduct of adult FOXJ1-Cre;CEP164$^{fl/fl}$ mice, cilia were reduced in number as evaluated by both histology (Figure 3.6A) and IF staining for A-tub (Figure 3.6B) compared to control CEP164$^{fl/fl}$ tissues. Surprisingly, however, FOXJ1-Cre;CEP164$^{fl/fl}$ females were fertile, suggesting that the remaining cilia are sufficient to sustain normal function. In stark contrast, FOXJ1-Cre;CEP164$^{fl/fl}$ males were completely infertile. Histological analysis revealed variable degrees of degenerative changes in the seminiferous tubules of FOXJ1-Cre;CEP164$^{fl/fl}$ adult testes. In general, I noticed a significant reduction in the number of late-stage germ cells (Figure 3.7A). In a subset of seminiferous tubules, germ cells were entirely depleted with solely Sertoli cells present (Figure 3.7A, asterisk). Additionally, no mature sperms were present in the epididymis of FOXJ1-Cre;CEP164$^{fl/fl}$ mice. In support of these extensive phenotypes, X-gal staining of testis sections from heterozygous CEP164 KO-first mice carrying a *lacZ* reporter showed broad CEP164 expression with particularly intense staining in differentiating spermatids (Figure 3.7B). Overall, these results demonstrate that FOXJ1-Cre;CEP164$^{fl/fl}$ mice exhibit phenotypes consistent with impaired multiciliogenesis and provide a useful model system to study the mechanisms of multiciliogenesis and its associated diseases.

3.4 Discussion

Despite the clear importance of the distal appendage for ciliogenesis, no mammalian model for investigating distal appendage protein function exists. In this chapter, I report the first mouse model of a distal appendage/transition fiber protein where CEP164 is removed in FOXJ1-positive cells of the airways, brain, oviduct, and testis (Figure 3.1). In the process of generating this conditional mouse model, I observed that the homozygous mouse from the initially-obtained CEP164 KO-first line exhibits early embryonic lethality prior to E12.5 as well as holoprosencephaly, an edematous cardiac sac, cardiac looping defects, and a truncated posterior trunk at E9.5 (Figure 3.2). Furthermore, I determined that MEFs homozygous for the CEP164 KO-first allele had no centriolar CEP164 and were unable to form cilia (Figure 3.3), indicating that the loss of primary cilia may be causative, in part, for the phenotypes observed.

The defects in the homozygous CEP164 KO-first embryos are similar to those in seen upon CEP164-KD in zebrafish (Chaki et al. 2012; Slaats et al. 2014), underscoring the importance of CEP164 in vertebrate and, now, mammalian development. Additionally, the homozygous CEP164 KO-first embryos bear a striking resemblance to the mouse mutants for the ciliary genes *Kif3a* (Marszalek et al. 1999; Takeda et al. 1999), *Kif3b* (Nonaka et al. 1998), and *polaris* (Murcia et al. 2000), emphasizing the critical role cilia play in mammalian development and the essential functions of certain ciliary genes and the proteins they encode. While much focus has been placed on transition zone proteins because of the numerous disease mutations found in the genes that encode them (van Reeuwijk et al. 2011), my data coupled with that from other ciliary mouse

mutants suggest that a subset of ciliary genes are an absolute requisite for mammalian development. It will be necessary to further interrogate ciliary gene function in mammalian development through the use of mouse models, and, to this end, the homozygous CEP164 KO-first mouse model should facilitate these studies. Of note, however, these results do not preclude the possibility that CEP164 may serve other cilia-independent functions during embryogenesis. Further work will be needed to fully appreciate CEP164 function during mammalian development. To this end, it will be interesting to cross the KO-first allele with a germline Cre mouse to create a true whole-body KO for CEP164 to tease out its functionality during mammalian development.

In spite of the large portion of the population affected by genetic and/or chronic disorders involving multicilia, few mouse models to interrogate the mechanisms of their formation and physiology exist. Thus, I generated a conditional mouse model that lacks CEP164 in FOXJ1-positive multiciliated tissues and the testis. Most of these mice live to adulthood, except for 19.0% who die due to substantial hydrocephalus. Furthermore, CEP164 removal in these tissues results in hydrocephalus as well as a profound loss of airway and ependymal cilia (Figure 3.4 and 3.5). In light of these phenotypes, the FOXJ1-Cre;CEP164$^{fl/fl}$ mouse should serve as a powerful tool to study diseases of multicilia, such as PCD, and further understand how defective multicilia contribute to the pathology of chronic respiratory diseases, such as cystic fibrosis, asthma, and COPD. Though, one caveat to this mouse model is the use of the FOXJ1 promoter to drive Cre expression. FOXJ1 is one of the most specific transcription factors for ciliated cells but turns on later in multiciliated cell differentiation (see section *1.1g Transcriptional regulation of multiciliogenesis*) (Lim et al. 1997; Blatt et al. 1999; Brody et al. 2000). Thus, in the future,

the use of upstream transcriptional regulators of multiciliogenesis to drive Cre expression in this mouse model may provide greater insights into the pathogenesis of PCD and multicilia-related disorders.

Besides airway and brain phenotypes, I also observed defects in both the female (Figure 3.6) and male (Figure 3.7) reproductive tracts when CEP164 expression is lost, suggesting that CEP164 regulates reproductive development. Interestingly, CEP164 loss has disparate effects on the male and female reproductive tracts, particularly, as FOXJ1-Cre;CEP164$^{fl/fl}$ male mice are infertile while FOXJ1-Cre;CEP164$^{fl/fl}$ female mice appear to be fertile. Furthermore, CEP164 is widely expressed during sperm differentiation, and its loss results in a substantially thinner seminiferous epithelium and, in some cases, complete loss of germ cells. As the first data to implicate CEP164 in sperm development, future investigation is warranted into the biological mechanisms for how CEP164 controls sperm differentiation. CEP164 though is now amongst a host of proteins, including RFX2 (Kistler et al. 2015; Shawlot et al. 2015; Wu et al. 2016), TAp73 (Holembowski et al. 2014; Marshall et al. 2016; Nemajerova et al. 2016), IFT20 (Follit et al. 2006; Zhang et al. 2016), and SPAG6 (Li et al. 2015b), with crucial roles in both ciliogenesis and sperm development.

The CEP164$^{fl/fl}$ mouse will prove to be an invaluable resource to investigate CEP164 function in other tissue- and organ-specific contexts. For example, the current conditional KO mouse model displays a robust hydrocephalus phenotype and corresponding defects in basal body patch size and displacement, which reflect changes in the number and spatial positioning of basal bodies at the apical surface of ependymal cells (Figure 3.5). These differences may be unique to CEP164 function in ependymal

cells, as opposed to airway ciliated cells, and should be the subject of future inquiries. In addition, very few mouse models exist to tease out the relationship between defective cilia and the pathogenesis of hydrocephalus, for which the FOXJ1-Cre;CEP164$^{fl/fl}$ mouse may serve useful. Finally, could CEP164 have cilia-dependent or -independent actions in other parts of the brain or in other tissues? By crossing the CEP164$^{fl/fl}$ mouse with various Cre lines, questions such as these can be addressed.

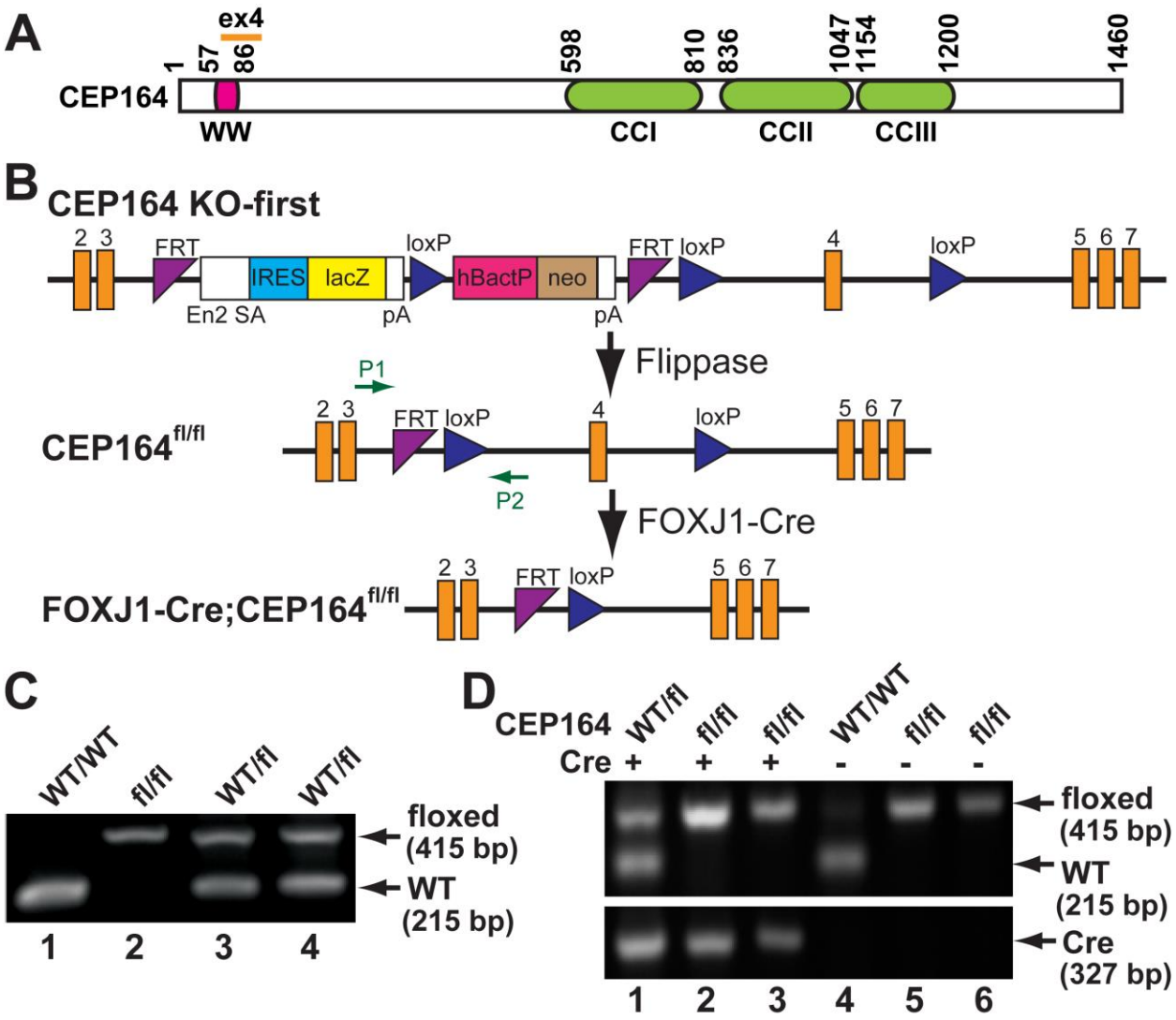

Figure 3.1: Generation of FOXJ1-Cre;CEP164$^{fl/fl}$ mice.
(A) Schematic diagram of CEP164 protein structure illustrating the WW domain and the three coiled-coiled (CC) domains. The N-terminal portion of the protein, encoded by exon 4 (ex4), which was removed upon Cre-mediated recombination, is depicted. The numbers indicate amino acid positions. (B) Shown are the original CEP164 KO-first allele, the floxed (fl) allele after removal of *lacZ* and neomycin cassettes upon crossing with flippase (Flp) deleter mice, and the final allele with exon 4 excised after Cre-mediated recombination driven by the FOXJ1 promoter. (C) PCR genotyping analysis confirming the generation of the CEP164$^{fl/fl}$ mouse. The locations for genotyping primers (P1 and P2) for detection of the floxed allele (415 bp) and wild-type (WT) allele (215 bp) are indicated by green arrows in (B). (D) PCR genotyping analysis using tail genomic DNA confirming the generation of the FOXJ1-Cre;CEP164$^{fl/fl}$ mouse.

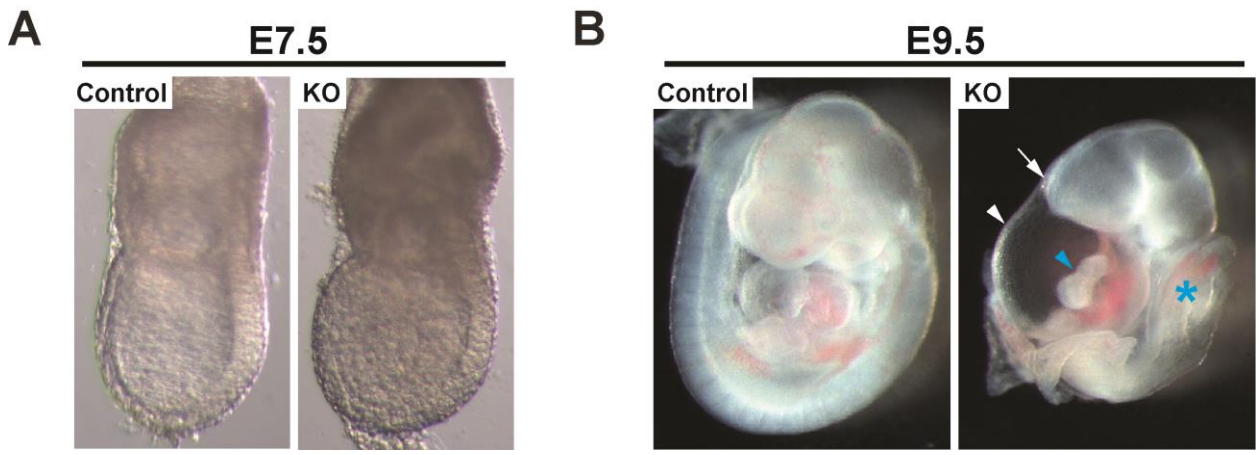

Figure 3.2: CEP164 is essential for early embryonic development.
Comparison of control (WT or heterozygous) embryos with CEP164-knockout (KO) littermates at E7.5 (A) and E9.5 (B). At E7.5, KO embryos were indistinguishable from control littermates. In contrast, E9.5 KO embryos displayed holoprosencephaly (arrow), an edematous pericardial sac (white arrowhead), cardiac looping defects (blue arrowhead), and a truncated posterior trunk (blue asterisk).

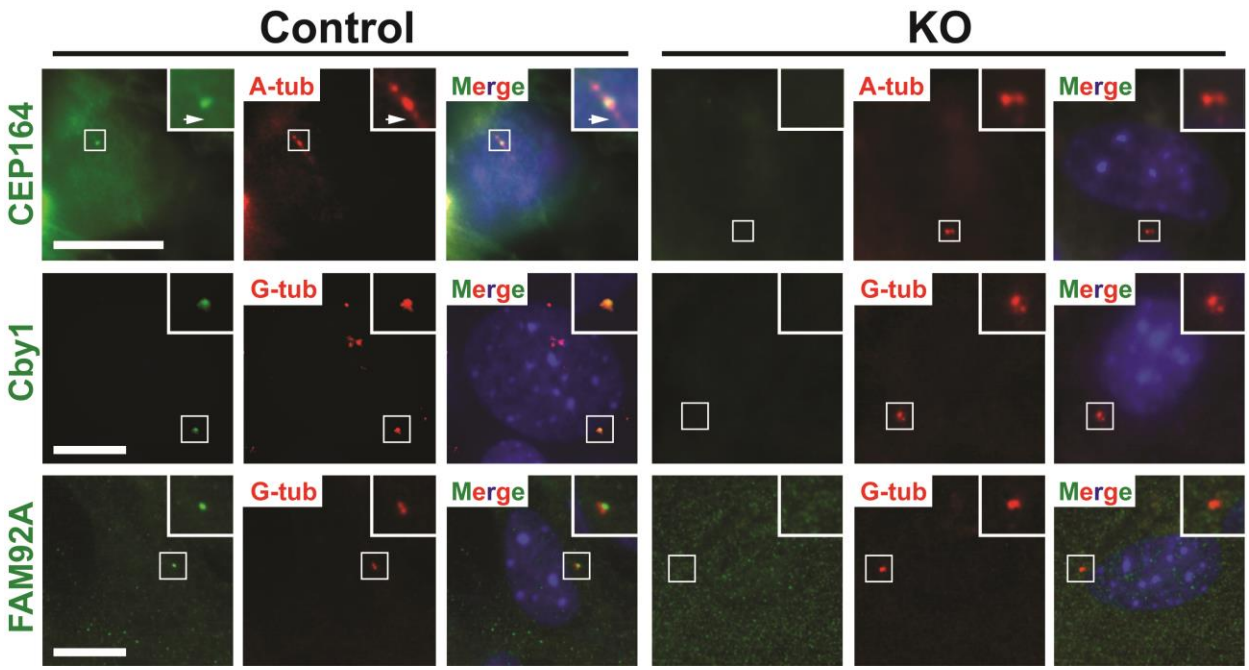

Figure 3.3: CEP164 is essential for primary ciliogenesis.
Epifluorescence images of serum-starved mouse embryonic fibroblasts (MEFs) derived from E8.5 control or KO embryos. Control MEFs were either WT or heterozygous. MEFs were double-labeled for CEP164, Cby1, or FAM92A (green) and A-tub or the basal body marker γ-tubulin (G-tub) (red) as indicated. Nuclei were visualized by DAPI (blue). The boxed regions are enlarged in the insets, highlighting the loss of CEP164, Cby1, and FAM92A centriolar localization in CEP164-KO MEFs. Arrows point to primary cilia. Scale bars, 20 µm.

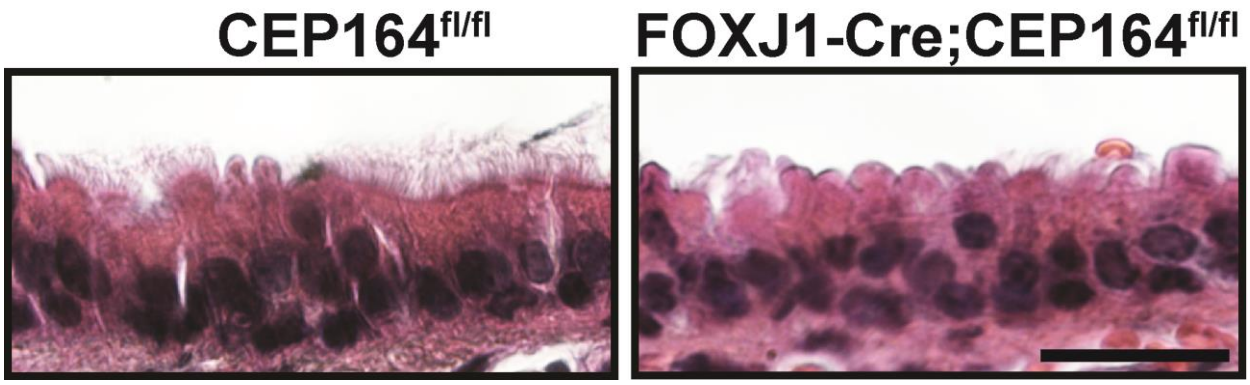

Figure 3.4: Loss of CEP164 results in reduced airway cilia.
Hematoxylin and eosin (H&E)-stained tracheal sections from control CEP164$^{fl/fl}$ and FOXJ1-Cre;CEP164$^{fl/fl}$ adult mice. Scale bar, 20 µm.

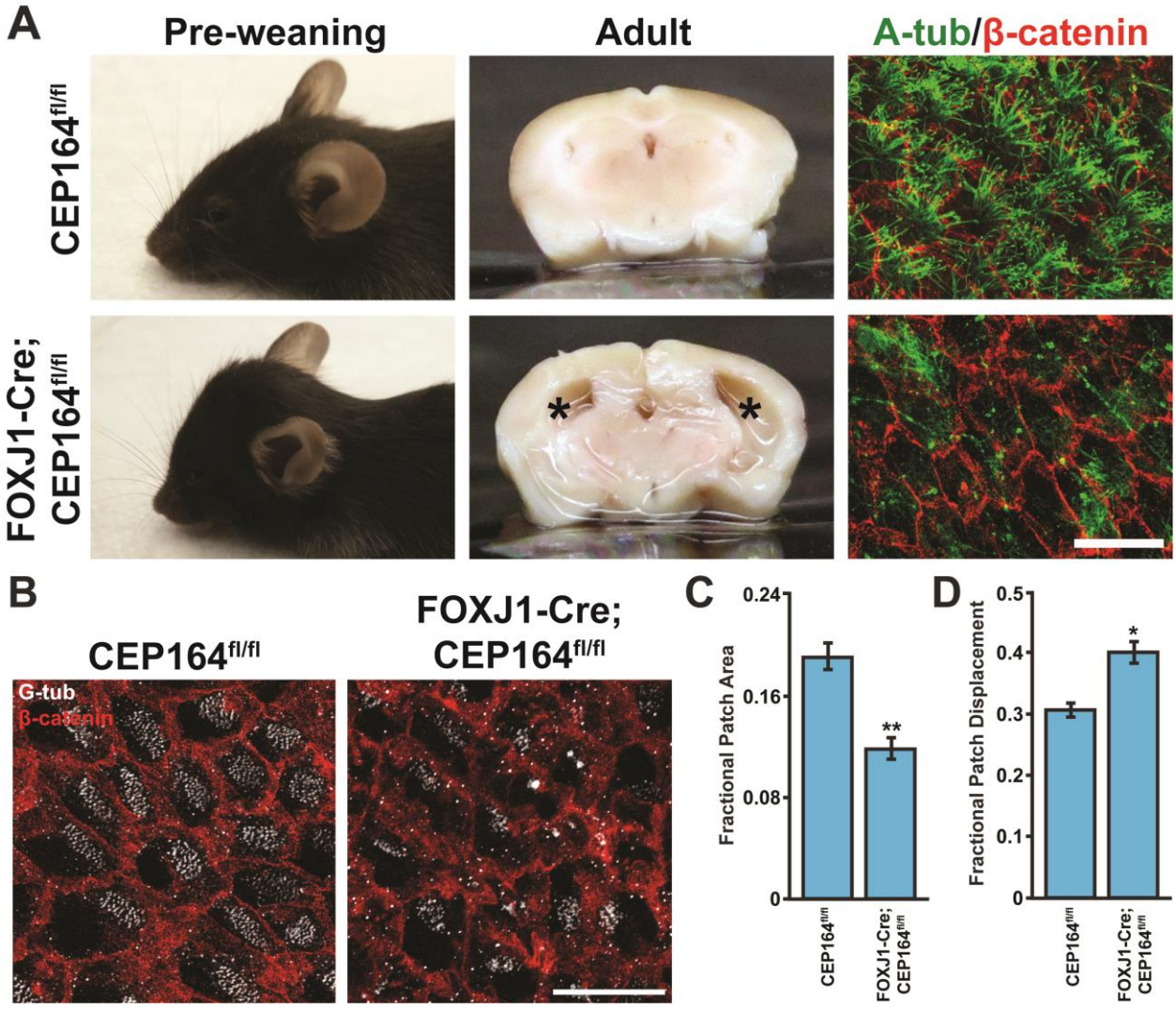

Figure 3.5: Ablation of CEP164 in the FOXJ1-positive tissues of the brain results in loss of ependymal cilia and hydrocephalus.

(A) Shown are lateral views of pre-weaning mice (left panels), coronal sections of adult brains (middle panels), and IF staining for A-tub (green) and β-catenin (red) in whole mounts of the adult subventricular zone (SVZ) (right panels). Asterisks denote enlarged lateral ventricular spaces indicative of hydrocephalus. Scale bar, 25 μm. (B) SVZ whole mount preparations from CEP164$^{fl/fl}$ or FOXJ1-Cre;CEP164$^{fl/fl}$ adult mice were immunostained for γ-tubulin (G-tub) (white) and β-catenin (red). β-catenin demarcates the cell boundaries, and γ-tubulin labels basal bodies that are found in patches in ependymal ciliated cells. Scale bar, 25 μm. (C) Quantification of basal body patch areas. Basal body patch areas relative to total apical cell surface are significantly reduced in CEP164-KO ependymal ciliated cells. (D) Quantification of the displacement of basal body patches. The displacement of the basal body patches from the cell center relative to the radius of the apical cell surface is significantly increased in the absence of CEP164. For quantification in (C) and (D), n=3. Error bars represent ±SEM. *, $p<0.05$. **, $p<0.005$.

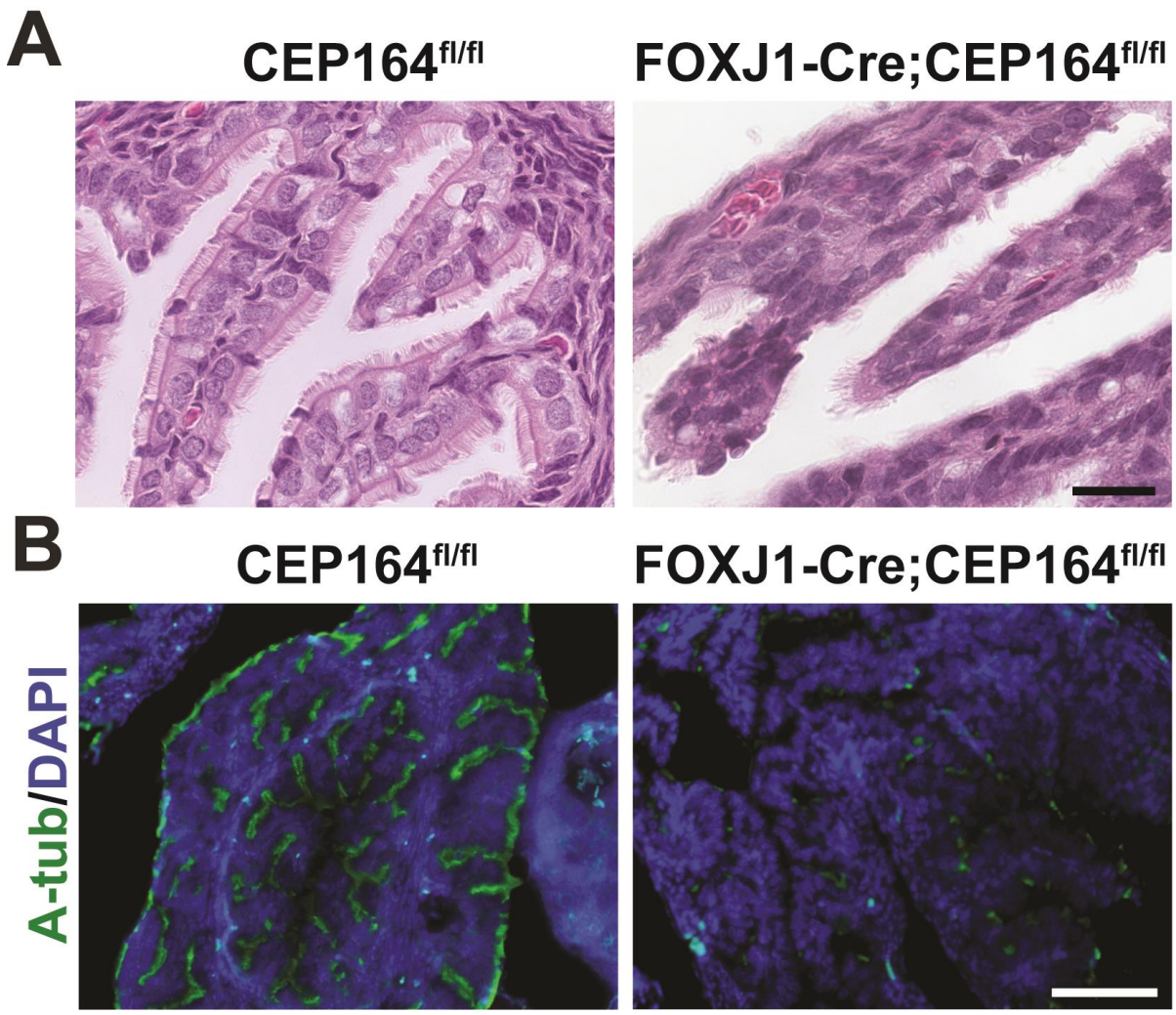

Figure 3.6: CEP164 removal leads to loss of oviduct cilia in the female reproductive tract.
(A) H&E staining of oviduct sections from CEP164$^{fl/fl}$ and FOXJ1-Cre;CEP164$^{fl/fl}$ adult mice. Scale bar, 10 µm. (B) IF staining of oviduct sections for A-tub (green) and DAPI (blue). Scale bar, 50 µm.

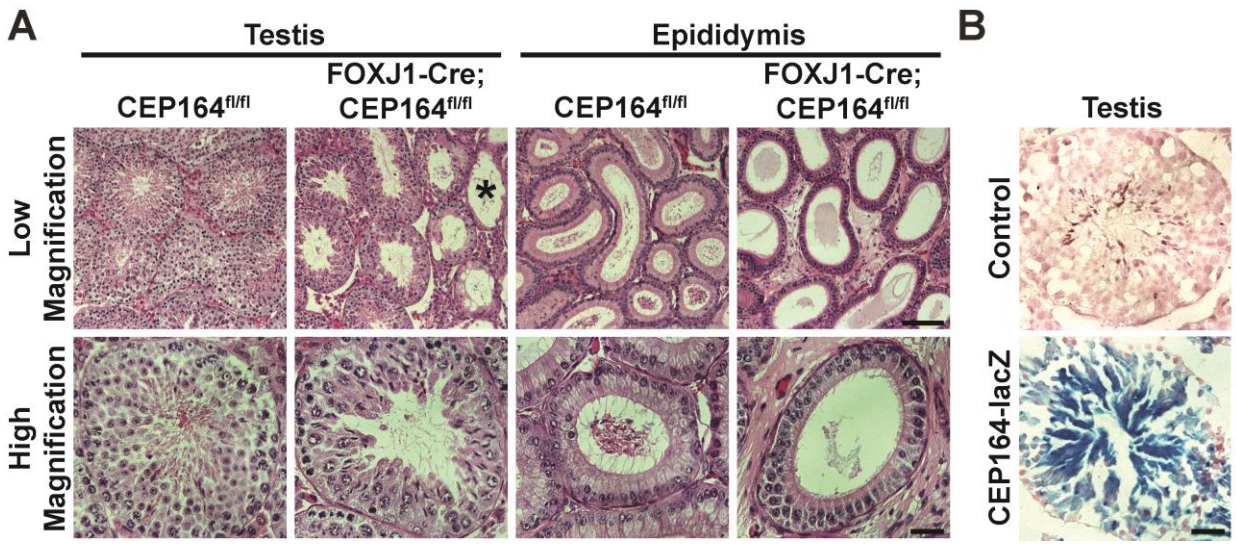

Figure 3.7: CEP164 plays an important role in proper development of female and male reproductive systems.
(A) H&E staining of both testis and epididymis from 3-month-old CEP164$^{fl/fl}$ and FOXJ1-Cre;CEP164$^{fl/fl}$ mice. Asterisk denotes seminiferous tubule lacking germ cells. Scale bars, 100 μm for low magnification and 40 μm for high magnification. (B) X-gal staining of testis sections from a control WT mouse and a mouse heterozygous for the CEP164 KO-first allele that contains a *lacZ* reporter. Scale bar, 40 μm.

Chapter 4: CEP164 plays multiple roles in airway ciliogenesis

In combination with Chapter 3, the data and text of this chapter are part of a current manuscript being prepared for submission (Siller SS, et al).

4.1 Introduction

CEP164 is an essential regulator of primary ciliogenesis in both mammalian cell culture and zebrafish models (Graser et al. 2007; Chaki et al. 2012; Schmidt et al. 2012; Cajanek and Nigg 2014; Oda et al. 2014; Slaats et al. 2014; Daly et al. 2016). As a distal appendage protein, a main action of CEP164 in primary ciliogenesis is the recruitment of small vesicles to the distal end of the mother centriole to permit ciliary vesicle formation and subsequent basal body docking events (Schmidt et al. 2012). On a molecular level, the C-terminus of CEP164, which is responsible for its centriolar localization, interacts with Rabin8 to promote Rab8 recruitment and activation to the mother centriole and ciliary membrane (Schmidt et al. 2012). Furthermore, Cby1, which is recruited by the C-terminus of CEP164, stabilizes this CEP164-Rabin8 interaction to facilitate ciliary membrane biogenesis (Burke et al. 2014).

While the C-terminus of CEP164 has important functionality in localizing CEP164 to the centriole and interacting with Rabin8, over-expressing solely the C-terminus leads to an inhibition of primary ciliogenesis (Schmidt et al. 2012). Explaining this peculiar finding, the N-terminus of CEP164 interacts with TTBK2, a kinase that is responsible for the phosphorylation of and subsequent removal of the centriolar capping protein CP110 (Goetz et al. 2012; Cajanek and Nigg 2014; Oda et al. 2014). By facilitating CP110 removal from the mother centriole, CEP164 allows primary ciliogenesis to proceed (Cajanek and Nigg 2014; Oda et al. 2014; Yadav et al. 2016). Intriguingly, CP110 has

been shown to prevent Rab8 centriolar and ciliary localization, a function attributed to an interaction between CP110 and CEP290 (Tsang et al. 2008). However, taken together, these data suggest that the mediator between CP110 and Rab8 is, in part, CEP164.

Besides vesicular docking and TTBK2 recruitment, CEP164 has also been shown to interact with and promote centriolar and ciliary localization of the lipid phosphatase inositol polyphosphate-5-phosphatase E (INPP5E) (Humbert et al. 2012), which converts PtdIns(3,4,5)P3 and PtdIns(4,5)P2 to PtdIns(3,4)P2 and PtdIns(4)P, respectively (Dyson et al. 2016). Recent studies have highlighted a delicate balance in phosphoinositol lipid composition of centriole-associated membrane and ciliary membrane (Chavez et al. 2015; Garcia-Gonzalo et al. 2015). At the ciliary base, PtdIns(4,5)P2 predominates whereas the ciliary membrane contains mainly PtdIns(4)P (Nakatsu 2015). When INPP5E function is perturbed, this balance is altered, which results in ciliogenesis defects (Bielas et al. 2009; Jacoby et al. 2009; Luo et al. 2012; Dyson et al. 2016; Xu et al. 2016). Thus, in this third mechanism, CEP164 regulates primary ciliogenesis. However, whether these actions of CEP164 are conserved or whether new roles for CEP164 exist in multiciliogenesis has never been assessed, in part, because no animal models existed.

In this chapter, I employ the conditional mouse model developed in *Chapter 3* to elucidate CEP164 function in multiciliogenesis. I find that CEP164 is important for proper multiciliogenesis by regulating small vesicle recruitment, ciliary vesicle formation, and basal body docking. Experiments using the MTEC system reveal that CEP164 is required for the normal basal body localization of Cby1 and its interactors FAM92A and 92B. Moreover, I provide evidence that CEP164 has unique functions in primary versus multicilia and plays a novel role in differentially controlling the trafficking of ciliary

membrane proteins in multiciliated cells. Altogether, this study harnesses a powerful new mouse model to shed light on multiple indispensable roles of CEP164 in airway ciliated cell differentiation.

4.2 Materials and methods

4.2a Transmission electron microscopy

Samples used for TEM were processed using standard techniques (Love et al. 2010; Burke et al. 2014). Briefly, MTEC membranes and adult tracheas were fixed by immersion in filtered 2.5% PFA, EM grade, (Sigma) and 2% glutaraldehyde in PBS overnight at 4^{o}C. After fixation, samples were washed in PBS, placed in 2% osmium tetroxide in PBS, dehydrated in a graded series of ethanol, and embedded in Embed812 resin (Electron Microscopy Sciences). Ultrathin sections of 80 nm were cut with a Leica EM UC7 ultramicrotome and placed on Formvar-coated slot copper grids. Sections were then counterstained with uranyl acetate and lead citrate and viewed with a FEI Tecnai12 BioTwinG^2 electron microscope. Digital images were acquired with an XR-60 CCD digital camera system (Advanced Microscopy Techniques) and further processed with Adobe Photoshop and Illustrator.

4.2b Tracheal culture and quantification of centrioles bound to vesicles

Centrioles in tracheal ciliated cells were analyzed for the presence or absence of docked vesicles as previously described (Burke et al. 2014). In brief, tracheas were dissected from P8 mice and cultured for 16 hours in a 5% CO_2 at 37^{o}C in DMEM supplemented with 10% FBS, 100 U/ml penicillin/streptomycin, 1 µg/ml insulin, and 300

ng/ml dexamethasone in the presence of 1 µM paclitaxel. Tracheas were then processed for TEM as described above in section *4.2a Transmission electron microscopy*.

4.2cPurification of NPHP1 antibody

The antibody was raised against the C-terminal coiled-coil domain and SH3 domain of human NPHP1 at Open Biosystems. To purify this antibody, the C-terminal domain of NPHP1 was expressed in BL21 *E. coli*. After lysing the cells with 0.5% NP-40 in PBS, sonicating, and spinning, the supernatant was applied to GST-Bind Resin (Novagen) in a Bio-Rad column. The C-terminal fragment was then covalently cross-linked to the beads with 40 mM dimethyl pimelimidate (DMP) for 1 hr at 4^{o}C. This reaction was then quenched with 40 mM ethanolamine for 45 min at 4^{o}C. After subsequent washes with 0.2 M glycine-HCl, pH 2.5, and 1 M dipotassium phosphate, the serum from the terminal bleed was then incubated with the beads overnight at 4^{o}C. The antibody was then eluted with 0.2 M glycine-HCl, pH 2.5, in seven fractions, which were neutralized with 1 M dipotassium phosphate. The first three and second three fractions were pooled and dialyzed with PBS overnight at 4^{o}C. Glycerol was then added to each antibody aliquot to 50%.

4.2d Antibodies for immunofluorescence staining

The primary antibodies used were: rabbit anti-CEP164 (1:200; Sigma), rabbit anti-Cby1 1418P (1:250; in-house) (Voronina et al. 2009), rabbit anti-FAM92A (1:200; Proteintech), rabbit anti-FAM92B (1:200; Proteintech), rabbit anti-IFT88 (1:250; Proteintech), rabbit anti-IFT20 (1:250; gift from G. Pazour, University of Massachusetts Medical School, Worcester, MA), rabbit anti-CP110 (1:200; Proteintech), rabbit anti-TTBK2 (1:100; Proteintech), rabbit anti-Rab8a (1:200; Proteintech), rabbit anti-Rab11a

(1:200; Proteintech), rabbit anti-Arl13b (1:200; Proteintech), rabbit anti-INPP5E (1:100; Proteintech), rabbit anti-NPHP1 (1:200; in-house), rabbit anti-CCDC92 (1:200; Proteintech), mouse anti-FOXJ1 (1:200; gift from S. Brody, Washington University, St. Louis, MO), and mouse anti-A-tub (1:1000; Sigma). The secondary antibodies used were: DyLight 488-conjugated goat anti-rabbit IgG (Vector Laboratories), DyLight 549-conjugated horse anti-mouse IgG (Vector Laboratories), DyLight 488-conjugated horse anti-mouse IgG (Vector Laboratories), and DyLight 549-conjugated goat anti-rabbit IgG (Vector Laboratories).

Descriptions of additional methods used in this chapter can be found in sections *3.2a Generation of FOXJ1-Cre;CEP164fl$^{/fl}$ mice*, *2.2e Preparation of primary culture of mouse tracheal epithelial cells*, *2.2h Immunofluorescence staining*, *2.2j Fluorescence microscopy*, and *2.2l Statistical analysis*.

4.3 Results

4.3a CEP164 is critical for multiciliogenesis during differentiation of airway ciliated cells

To gain insight into the molecular basis of the defective multiciliogenesis in the absence of CEP164 observed in *Chapter 3*, I again employed primary cultures of MTECs, a well-characterized *in vitro* model for airway differentiation and ciliogenesis (You et al. 2002; Vladar and Stearns 2007; Hoh et al. 2012; Vladar and Brody 2013). As described above, MTEC cultures are created by seeding isolated tracheal epithelial cells at low density onto a semipermeable, collagen-coated membrane and permitting them to

proliferate until confluent for ≤7 days (Figure 2.1). Differentiation then proceeds in a semi-synchronous manner after an ALI is established with low-serum media. At ALId14, the cultures contain both ciliated and non-ciliated cells and resemble the native tracheal epithelium.

Using the MTEC system and the conditional mouse model generated in *Chapter 3*, I first sought to determine the efficiency of FOXJ1-Cre-mediated CEP164 removal as well as whether it has any impact on the ciliated cell lineage. Hence, I performed IF staining of ALId14 MTECs for CEP164 and FOXJ1. While intense CEP164 signals were detectable at the ciliary base of FOXJ1-positive ciliated cells in CEP164$^{fl/fl}$ MTEC cultures at ALId14, CEP164 expression was lost or greatly reduced in ~90% of FOXJ1-positive ciliated cells in FOXJ1-Cre;CEP164$^{fl/fl}$ MTEC cultures, revealing highly efficient Cre-mediated recombination (Figure 4.1A). Interestingly, there was a modest decrease in the number of FOXJ1-positive cells present in FOXJ1-Cre;CEP164$^{fl/fl}$ (32.1%) vs. CEP164$^{fl/fl}$ (41.7%) MTEC cultures (Figure 4.1B). These data suggest that CEP164 may play some role in the maintenance and/or survival of ciliated cells. Clearly, this requires further detailed investigation in the future.

Next, I assessed the extent of ciliogenesis in ALId14 MTECs from CEP164$^{fl/fl}$ and FOXJ1-Cre;CEP164$^{fl/fl}$ mice by IF staining for CEP164 and A-tub (Figure 4.3A). As expected, CEP164-KO ciliated cells showed profound defects in ciliogenesis. To my surprise, however, CEP164-KO ciliated cells were able to extend cilia, albeit short and sparse (Figure 4.3A, zoomed image), in sharp contrast to its absolute requirement for primary ciliogenesis (Graser et al. 2007; Schmidt et al. 2012). To precisely quantify the percentages of ciliated cells at different stages of ciliogenesis as described (unciliated;

stage I: presence of an elongated primary cilium and foci of centrosomal/ciliary proteins; stage II: centriolar duplication stage with centrioles clustered to one side in the cytoplasm; stage III: basal body docking stage with apically located and evenly distributed basal bodies that an lack elongated axoneme; stage IV: axoneme elongation stage) (Figure 4.2) (Vladar and Stearns 2007), I fixed CEP164$^{fl/fl}$ and FOXJ1-Cre;CEP164$^{fl/fl}$ MTECs at ALId5, d7, and d14 and conducted IF staining for A-tub. As shown in Figure 4.3B, impaired ciliogenesis in FOXJ1-Cre;CEP164$^{fl/fl}$ MTEC cultures was evident at ALId5 and more pronounced at ALId14 with a large decrease in the number of stage IV ciliated cells and concomitant increases in the numbers of stage II and III cells. The increased number of non-ciliated cells at ALId14 was in line with the decrease in FOXJ1-positive cells seen in ALId14 FOXJ1-Cre;CEP164$^{fl/fl}$ MTECs (Figure 4.1B). Moreover, a vast majority of stage IV ciliated cells in FOXJ1-Cre;CEP164$^{fl/fl}$ MTEC cultures extended only short and scarce cilia (Figure 4.3C). Corroborating this observation, CEP164$^{fl/fl}$ MTEC cultures had 46.5±1.4% of total cells that were fully ciliated with abundant cilia, whereas only 4.9±1.1% of cells in FOXJ1-Cre;CEP164$^{fl/fl}$ MTEC cultures appeared fully ciliated, which most likely corresponds to CEP164-positive ciliated cells that escaped Cre-mediated recombination. Collectively, these data indicate that loss of CEP164 in airway ciliated cells results in defective ciliogenesis and ciliated cell differentiation.

4.3b CEP164 is required for ciliary vesicle formation and basal body docking during airway ciliated cell differentiation

The dramatic increase in the number of stage III ciliated cells in ALId14 FOXJ1-Cre;CEP164$^{fl/fl}$ MTEC cultures (Figure 4.3B) suggested that CEP164 regulates docking of basal bodies to the apical cell surface (Vladar and Stearns 2007). To investigate this

possibility, I performed TEM on both CEP164$^{fl/fl}$ and FOXJ1-Cre;CEP164$^{fl/fl}$ adult tracheas. In control CEP164$^{fl/fl}$ ciliated cells, basal bodies were properly docked to the apical cell surface with cilia extending into the lumen (Figure 4.4A). In contrast, many basal bodies were found undocked in the cytoplasm of FOXJ1-Cre;CEP164$^{fl/fl}$ ciliated cells with only a few cilia. In agreement with the IF staining of MTECs (Figure 4.3A), I frequently noted shortened cilia in FOXJ1-Cre;CEP164$^{fl/fl}$ adult tracheas (Figure 4.5A). I also confirmed the presence of many undocked, cytoplasmic basal bodies in ALId14 MTECs from FOXJ1-Cre;CEP164$^{fl/fl}$ mice using TEM (data not shown). Furthermore, I found that the transition fibers as well as the Y-linkers of the transition zone were present in the absence of CEP164 (Figure 4.5B and C), suggesting that CEP164 is not an essential structural component of the transition fibers.

Basal body docking defects often result from the inability of distal appendages to recruit small vesicles in order to assemble ciliary vesicles (Li et al. 2015a; Wei et al. 2015). CEP164 has been shown to be responsible for the recruitment of small vesicles to distal appendages during early stages of primary ciliogenesis in RPE1 cells (Schmidt et al. 2012). To test if this is the case in multiciliated cells, P8 tracheas were cultured *ex vivo* in the presence of the microtubule-stabilizing agent taxol and subjected to TEM analysis. Taxol has previously been shown to block apical migration of basal bodies and enrich for basal bodies bound to vesicles (Boisvieux-Ulrich et al. 1989). In control CEP164$^{fl/fl}$ tracheas, 67% of cytoplasmic basal bodies were associated with vesicles, whereas only 34% of basal bodies in FOXJ1-Cre;CEP164$^{fl/fl}$ tracheas were attached to vesicles (Figure 4.4B and C). Worthy of note, many of the vesicles bound to the cytoplasmic basal bodies in FOXJ1-Cre;CEP164$^{fl/fl}$ tracheas were smaller and had not coalesced to form ciliary

vesicles. Collectively, the TEM data support the notion that CEP164 plays key roles in small vesicle recruitment and ciliary vesicle formation during multiciliogenesis.

4.3c CEP164 recruits Chibby1, FAM92A, and FAM92B to basal bodies in multiciliated cells

It has been previously reported that Cby1 is important for ciliary vesicle formation and basal body docking in airway ciliated cells (Burke et al. 2014). During primary ciliogenesis, CEP164 is essential for Cby1 recruitment to the distal appendages of mother centrioles via protein-protein interactions. Cby1 then recruits the membrane-binding BAR domain-containing proteins FAM92A and 92B to basal bodies to facilitate primary ciliogenesis (Li et al. 2016b). IF staining of ALId14 MTECs revealed that Cby1 recruitment to basal bodies was substantially reduced in CEP164-KO ciliated cells (Figure 4.6A). Similarly, the basal body recruitment of both FAM92A and 92B was severely diminished in CEP164-KO compared to control ciliated cells (Figure 4.6B and C). These data clearly indicate that CEP164 lies upstream of Cby1, FAM92A, and FAM92B and recruits them to the distal appendages/transition fibers to regulate ciliary vesicle formation, basal body docking, and ciliated cell differentiation.

4.3d The loss of CEP164 in multiciliated cells does not influence the basal body localization of IFT components and CP110

It was demonstrated that CEP164-KD leads to a significant reduction in the levels of IFT components at the base of primary cilia in RPE1 cells (Schmidt et al. 2012; Cajanek and Nigg 2014). I therefore examined the effects of CEP164 loss on localization of the IFT components IFT88 and IFT20 in multiciliated cells (Figure 4.7). Surprisingly, in contrast to primary cilia, both IFT proteins were clearly detectable at basal bodies in

CEP164-KO ciliated cells at similar levels to control ciliated cells. Consistent with this as IFT carries tubulins and other cargos to build the axoneme, the axonemal 9+2 microtubule structure was found to be intact in CEP164-KO ciliated cells upon TEM analysis (Figure 4.5D). During primary ciliogenesis, CEP164 recruits TTBK2 to mother centrioles (Cajanek and Nigg 2014; Oda et al. 2014). TTBK2 in turn promotes removal of the distal end-capping protein CP110 and recruitment of IFT proteins to initiate ciliogenesis . Thus, CEP164-KD RPE1 cells fail to remove CP110 from the mother centriole, thereby preventing ciliogenesis from procedding upon serum starvation (Cajanek and Nigg 2014; Oda et al. 2014). In contrast, I found that, in multiciliated cells, CP110 was constitutively present at nascent centrioles (data not shown) as well as at the basal bodies of elongating and mature cilia (Figure 4.8A). The basal body localization of CP110 was not overtly affected in CEP164-KO ciliated cells. TTBK2 was mainly detectable at the tip of a subset of cilia at comparable levels in both control and CEP164-KO ciliated cells (Figure 4.8B). These findings suggest that CEP164 is dispensable for the proper localization of IFT particles and CP110 to centrioles/basal bodies in multiciliated cells and highlight potential differences between primary and multiciliogenesis.

4.3e Distribution of ciliary membrane proteins is perturbed in CEP164-KO ciliated cells

During primary ciliogenesis, Rab11 recruits Rabin8, which in turn recruits and activates Rab8 at centrosomes (Nachury et al. 2007; Knodler et al. 2010; Feng et al. 2012; Vetter et al. 2015). Rab8 then promotes membrane trafficking to the base of cilia to facilitate ciliary membrane assembly (Sorokin 1962; Sorokin 1968; Nachury et al. 2007). As mentioned above, CEP164 is known to bind Rabin8 and mediate Rab8

recruitment and activation (Schmidt et al. 2012). Furthermore, Cby1 binds CEP164 to facilitate the CEP164-Rabin8 interaction and Rab8 activation, thereby promoting ciliary vesicle formation and subsequent basal body docking in airway ciliated cell differentiation (Burke et al. 2014). I therefore hypothesized that CEP164 might affect the Rab11-Rabin8-Rab8 cascade in multiciliated cells and immunostained ALId14 MTECs from CEP164$^{fl/fl}$ and FOXJ1-Cre;CEP164$^{fl/fl}$ mice with antibodies for Rab8 and Rab11 (Figure 4.9). Utilizing super-resolution 3D-SIM, I found that the ciliary and basal body localization of both Rab8 and Rab11 was substantially reduced in CEP164-KO ciliated cells compared to control ciliated cells. Of particular note, Rab11 has been reported to predominantly localize to a pericentrosomal compartment in cycling cells or a peri-basal body compartment in quiescent cells with primary cilia (Knodler et al. 2010). In contrast, Rab11 localization extended to a proximal region of multicilia, again highlighting differences between primary and multicilia. These data point to potential alterations in the trafficking and formation of ciliary membranes in CEP164-KO ciliated cells.

Next, I sought to determine if other ciliary membrane proteins exhibited altered localization patterns upon loss of CEP164. The ciliary protein Arl13b specifically associates with the ciliary membrane via palmitoylation and functions in vesicle and ciliary trafficking as well as multiple other cellular processes (Cevik et al. 2010; Larkins et al. 2011; Cevik et al. 2013; Lu et al. 2015a; Seixas et al. 2016). Additionally, Arl13b forms a functional complex with CEP164 to target INPP5E to the primary cilium (Humbert et al. 2012), which is important for primary ciliogenesis and maintaining proper ciliary membrane lipid composition (Bielas et al. 2009; Jacoby et al. 2009; Luo et al. 2012; Chavez et al. 2015; Garcia-Gonzalo et al. 2015; Dyson et al. 2016; Xu et al. 2016).

Furthermore, genetic mutations in Arl13b and INPP5E are linked to the ciliopathy Joubert syndrome (Cantagrel et al. 2008; Bielas et al. 2009). Hence, I investigated whether the loss of CEP164 has any effect on the ciliary localization of Arl13b and INPP5E. Intriguingly, 3D-SIM imaging revealed that, in CEP164-KO ciliated cells, Arl13b robustly accumulated in short cilia and that the ciliary localization of INPP5E was modestly, yet consistently, increased along the entire length of the short cilia (Figure 4.10). These results, combined with the diminished ciliary recruitment of Rabs in CEP164-KO ciliated cells, implicate that CEP164 is involved in the trafficking and formation of ciliary membranes in multiciliated cells.

CEP164 has been shown to directly interact with the NPHP protein module of the transition zone (Chaki et al. 2012). As the transition zone with the transition fibers is thought to form the ciliary gate that controls protein localization in and outside the ciliary compartment, I determined if CEP164 loss effected NPHP protein localization in a similar manner as to Arl13b and INPP5E in ALId14 MTECs. Indeed, although intense signals tightly localized to the ciliary base in CEP164-WT ciliated cells, NPHP1 had reduced signal at the ciliary base, but more diffuse staining along cilia in CEP164-KO ciliated cells (Figure 4.11). In the same study that uncovered the interaction between CEP164 and the NPHP protein module, the mother centriole-specific protein CCDC92 was also identified as an interactor (Chaki et al. 2012). Thus, I stained ALId14 MTECs for CCDC92 and demonstrated that, CCDC92 signal was modestly decreased in CEP164-KO ciliated cells (Figure 4.12). Taken together, CEP164 differentially regulates ciliary protein localization and the recruitment of ciliary membranes during airway multiciliogenesis.

4.4 Discussion

CEP164-KD experiments in mammalian cell culture experiments provided the first insights that CEP164 is critical for proper basal body docking and ciliary vesicle formation (Schmidt et al. 2012). Here, I validate and extend these findings to multiciliogenesis (Figure 4.4). One caveat to this data is the use of the promoter region of the FOXJ1 transcription factor to drive Cre expression. FOXJ1 is one of the most specific, but also most downstream, transcription factors for multiciliated cell differentiation (Figure 1.3) (Blatt et al. 1999; Brody et al. 2000; Brooks and Wallingford 2014); hence, by employing an earlier transcription factor to drive Cre expression, different phenotypes might be found, including roles for CEP164 in centriole duplication. On the other hand, by utilizing a tamoxifen-inducible Cre expression system, roles of CEP164 in ciliary maintenance in multiciliated cells could be explored in the future.

By harnessing a conditional KO mouse model for CEP164 and the MTEC system, I provide evidence that CEP164 is dispensable for the proper structure of the distal appendage/transition fiber (Figure 4.5B). These data suggest that the distal appendage/transition fiber is not solely a structural docking site for small vesicles and subsequent ciliary vesicle formation; rather, certain proteins of the distal appendage/transition fiber are, in part, the key actors. As CEP164 appears dispensable for distal appendage/transition fiber structure, but not function, what could be the organizer of this distal appendage/transition fiber structure? Possible candidates are the other four core proteins, particularly CEP83 and CEP89, both of which play roles in basal body docking and ciliary vesicle formation and are proposed to lie upstream of CEP164 (Joo et al. 2013; Sillibourne et al. 2013; Tanos et al. 2013). Further upstream of CEP83

and CEP89 though are C2cd3 and Odf2/Cenexin (Ishikawa et al. 2005; Ye et al. 2014). Additional studies are needed to elucidate the exact structural composition of the distal appendage/transition fibers as well as the necessary proteins to organize these structural components.

Cby1, FAM92A, and FAM92B are all recruited to basal bodies in airway ciliated cells by CEP164 (Figure 4.6). Interestingly, I observed a small amount of Cby1 present at the basal bodies in CEP164-KO ciliated cells. CEP164 may therefore not be the sole protein responsible for Cby1 recruitment to the basal bodies. It has been previously reported that Odf2/Cenexin binds to Cby1 and localizes to the basal body in a Cby1-independent manner (Steere et al. 2012). It is then tempting to speculate that Odf2 may facilitate Cby1 recruitment to the basal bodies, especially as Odf2 is upstream of distal appendage formation (Ishikawa et al. 2005). My findings do align with previous data that CEP164 is necessary for FAM92A localization to the mother centriole in RPE1 cells (Li et al. 2016b). FAM92A and 92B are BAR-domain containing proteins, a class of proteins involved in membrane remodeling processes (Ren et al. 2006). An attractive hypothesis is that FAM92A and 92B facilitate ciliary vesicle formation by promoting vesicle fusion at the basal body after small vesicle docking to the distal appendage. Furthermore, as FAM92A and 92B remain at the basal body during and after axonemal extension (unpublished data), they are well-positioned to potentially regulate ciliary membrane formation after the ciliary vesicle is established.

Despite clear similarities between primary and multicilia, few studies have analyzed the differences. Two well-established distinctions between the two systems are the mode of centriole generation as well as the transcriptional control of multiciliogenesis

(Bettencourt-Dias and Glover 2007; Brooks and Wallingford 2014; Meunier and Spassky 2016). This work highlights though specific unique roles for CEP164 in primary versus multicilia. While CEP164 is necessary for IFT88 recruitment to the basal body in primary cilia (Schmidt et al. 2012; Cajanek and Nigg 2014), both IFT88 and IFT20 localize to the basal body despite CEP164 removal in differentiating airway ciliated cells (Figure 4.7). Furthermore, CEP164 interacts with TTBK2 to promote CP110 removal and initiate primary ciliogenesis (Cajanek and Nigg 2014; Oda et al. 2014). However, CP110 recruitment to basal bodies during airway ciliated cell differentiation is maintained in a CEP164-independent manner (Figure 4.8). These data are consistent with prior studies that localize CP110 adjacent to basal bodies and suggest that CP110 may have unique functions in basal body apical transport and ciliary adhesion complex formation during multiciliated cell differentiation (Walentek et al. 2016). Hence, it will be important to define in the future the similar and distinct mechanisms by which proteins act to promote or inhibit primary versus multiciliogenesis.

A particularly surprising finding was the differential regulation of ciliary membrane proteins. I uncovered decreases in both the ciliary localization of Rab8 and Rab11 (Figure 4.9). Previously, CEP164 has been shown to interact with the Rab8 GEF Rabin8 and recruit Rab8 to primary cilia (Schmidt et al. 2012). My data supports a parallel role in multicilia for CEP164 in Rab8 ciliary recruitment. However, it was noted that CEP164 had no effect on Rab11 (Schmidt et al. 2012). Here, I not only observe novel Rab11 localization to the proximal portion of multicilia, but also show that this localization is dependent on CEP164. I speculate that this Rab11 domain in multicilia may act similarly to the pericentrosomal material where ciliary proteins are often first recruited in primary

cilia. On the other hand, I observed overt increases in ciliary Arl13b and INPP5E (Figure 4.10). CEP164 has been shown to be important for Arl13b and INPP5E trafficking to primary cilia (Humbert et al. 2012). Additionally, INPP5E has been shown to physically interact with both CEP164 and Arl13b; however, an interaction between CEP164 and Arl13b has not been tested. Hence, it is unclear whether CEP164 interacts with INPP5E to recruit Arl13b or *vice versa*. Though, based on these data, I propose that CEP164 can recognize and control access of distinct vesicle types carrying unique cargos to the cilium in multiciliated cells. In so doing, CEP164 recruits Rab-positive vesicles/membranes and limits the proportion of Arl13b- and INPP5E-containing vesicles/membranes, which I view as trafficking in tandem. This idea is also consistent with the notion that the transition fiber acts as a ciliary gate that regulates entry and exist of proteins into the cilium (Reiter et al. 2012; Wei et al. 2015). Recently, another distal appendage/transition fiber protein FBF1 has been shown to regulate the entry of IFT particles into the cilium (Wei et al. 2013). Hence, CEP164 may be functioning in an analogous manner to FBF1 for ciliary membranes and ciliary membrane proteins. In support of this idea, the mislocalization of the transition zone protein NPHP1 to the short ciliary axonemes in CEP164-KO ciliated cells suggests a defective ciliary gate apparatus (Figure 4.11). An alternative, but not mutually exclusive, possibility is that CEP164 maintains proper Arl13b and INPP5E levels at basal bodies during airway ciliated cell differentiation to regulate ciliary membrane phosphoinositide levels (Chavez et al. 2015; Garcia-Gonzalo et al. 2015; Nakatsu 2015). The Arf4 GAP ASAP1 is a BAR-domain containing protein that acts as a scaffold for the Rab11-Rabin8-Rab8 complex and is activated, in part, by PtdIns(4,5)P2 (Deretic 2013). Hence, normal distribution of INPP5E along cilia may be necessary for proper

PtdIns(4,5)P2 levels at the basal body to recruit and activate ASAP1 and the Rab11-Rabin8-Rab8 protein cascade. Furthermore, PtdIns(4)P has been suggested to regulate the CEP164-TTBK2 interaction, implying that CEP164 may be the central hub, coordinating multiple steps during ciliogenesis (Xu et al. 2016).

Overall, my data supports a critical role of CEP164 in multiciliogenesis. In my model for CEP164 function in multiciliogenesis, CEP164 first recruits both the Rab11-Rab8 protein axis along with Cby1, FAM92A, and FAM92B to the basal body to allow for ciliary vesicle formation and subsequent basal body docking. Small Rab8-positive vesicles destined to become ciliary membrane continue to be recruited by CEP164 to the proximal Rab11 portion of the nascent cilium. However, CEP164 tightly controls the amount of Arl13b- and INPP5E-positive membranes that are brought to the cilium, most likely to control ciliary membrane lipid composition in multicilia. While several unanswered questions about CEP164 function in primary and multicilia remain, I anticipate that this mouse model will provide the basis for future investigations into the mechanisms of multiciliogenesis as well as for the ability to probe CEP164 function in other physiological contexts.

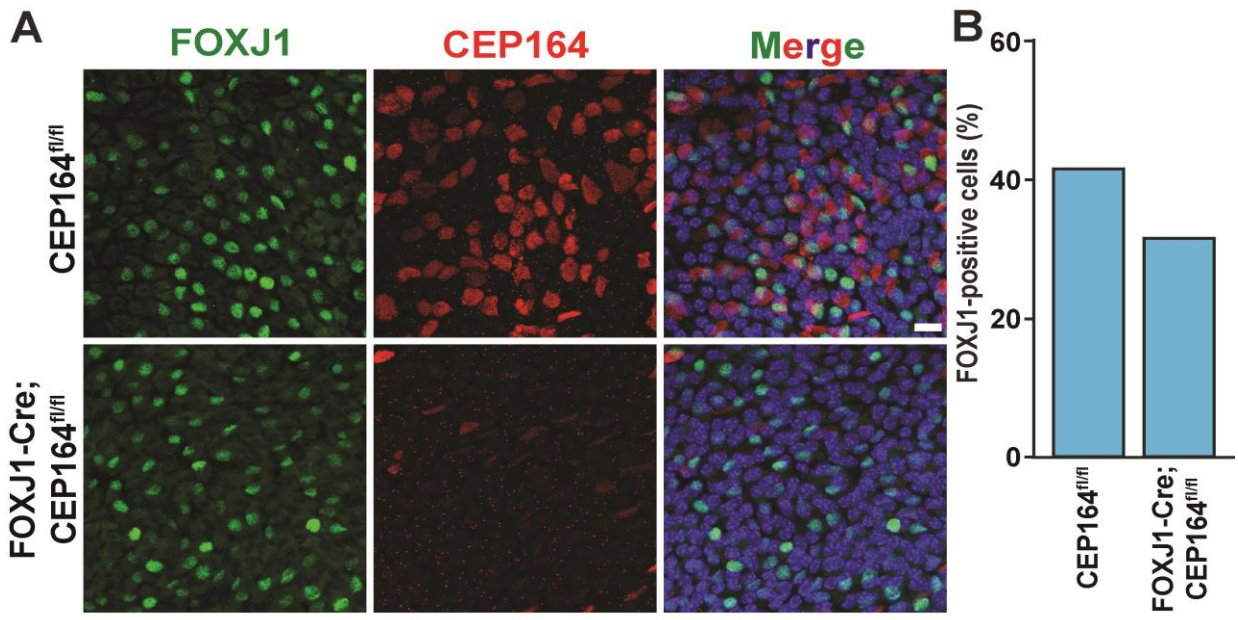

Figure 4.1: Efficient removal of CEP164 by FOXJ1-Cre-mediated recombination in ciliated cells in MTEC cultures.
(A) MTECs were prepared from CEP164$^{fl/fl}$ and FOXJ1-Cre;CEP164$^{fl/fl}$ mice, fixed at ALId14, and immunostained for FOXJ1 (green) and CEP164 (red). Nuclei were stained using DAPI (blue). ~90% of ciliated cells in MTEC cultures from FOXJ1-Cre;CEP164$^{fl/fl}$ mice lost CEP164 expression after Cre-mediated recombination. Scale bar, 25 μm. (B) Quantification of FOXJ1-positive ciliated cells. The percent of FOXJ1-positive cells in FOXJ1-Cre;CEP164$^{fl/fl}$ MTECs was moderately reduced (~10%) in comparison to CEP164$^{fl/fl}$ MTECs. >800 cells were counted per genotype.

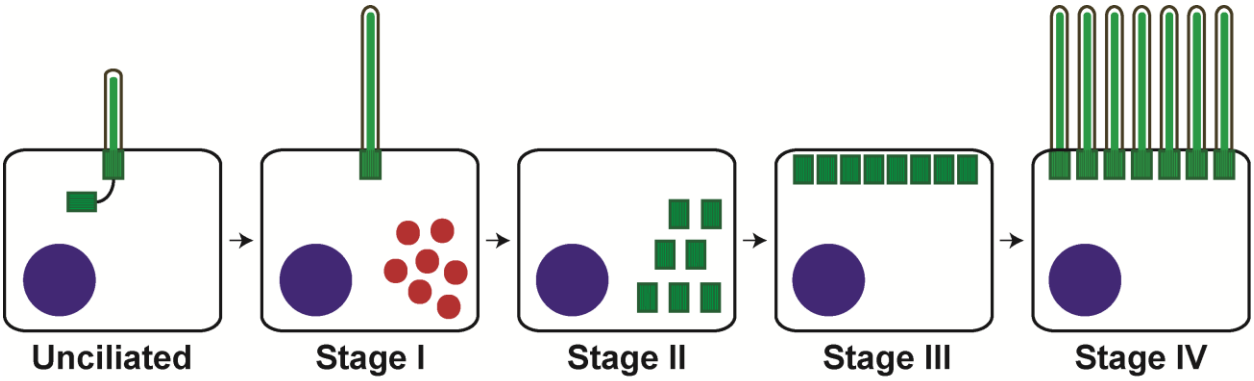

Figure 4.2: Stages of multiciliated cell differentiation.
Prior to initating multiciliogenesis, unciliated cells have a primary cilium that extends from the mother, or mature, centriole. After multiciliogenesis begins, an elongated primary cilium is observed as well as multiple foci of centriolar proteins in the cell cytoplasm (Stage I). Centriole duplication then begins as newly made centrioles cluster to one side of the cell (Stage II). Following centriolar amplification, centrioles disperse evenly in the cytoplasm and apically migrate (Stage III). Finally, after basal bodies dock to the apical cell surface, axonemal extension occurs (Stage IV).

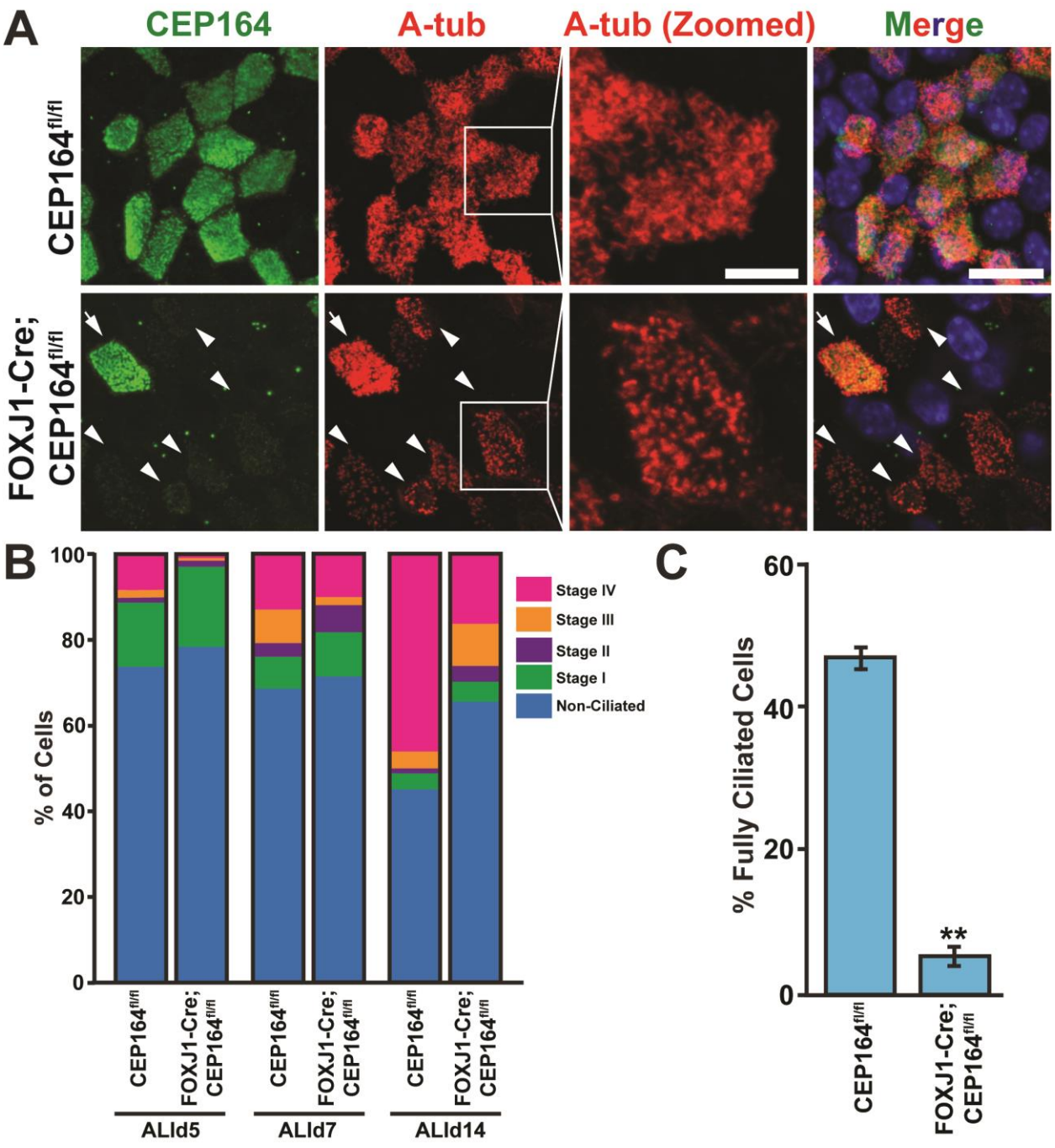

Figure 4.3: CEP164 deletion results in defective airway multiciliogenesis.
(A) ALId14 MTECs were stained for CEP164 (green) and A-tub (red). Nuclei were stained with DAPI (blue). Arrowheads denote CEP164-KO ciliated cells with sparse, stubby cilia. Zoomed views of cilia are shown for the squared areas. Arrows indicate a ciliated cell with CEP164 expression that escaped Cre-mediated recombination in FOXJ1-Cre;CEP164$^{fl/fl}$ MTEC cultures. Scale bars, 10 μm and 5 μm for zoomed images. (B) Quantification of ciliated cells at different stages (I-IV) of ciliogenesis. MTECs from CEP164$^{fl/fl}$ and FOXJ1-Cre;CEP164$^{fl/fl}$ were fixed at ALId5, d7, and d14 and immunostained for A-tub. >225 cells were counted per genotype per ALI day. (C)

Quantification of fully ciliated cells. MTECs from CEP164$^{fl/fl}$ and FOXJ1-Cre;CEP164$^{fl/fl}$ were fixed at ALId14 and immunostained for A-tub. Percentages were calculated by dividing the number of fully ciliated cells with abundant cilia by total cell number. >250 total cells per genotype were counted. n=3. Error bars represent ±SEM. **, $p<0.005$.

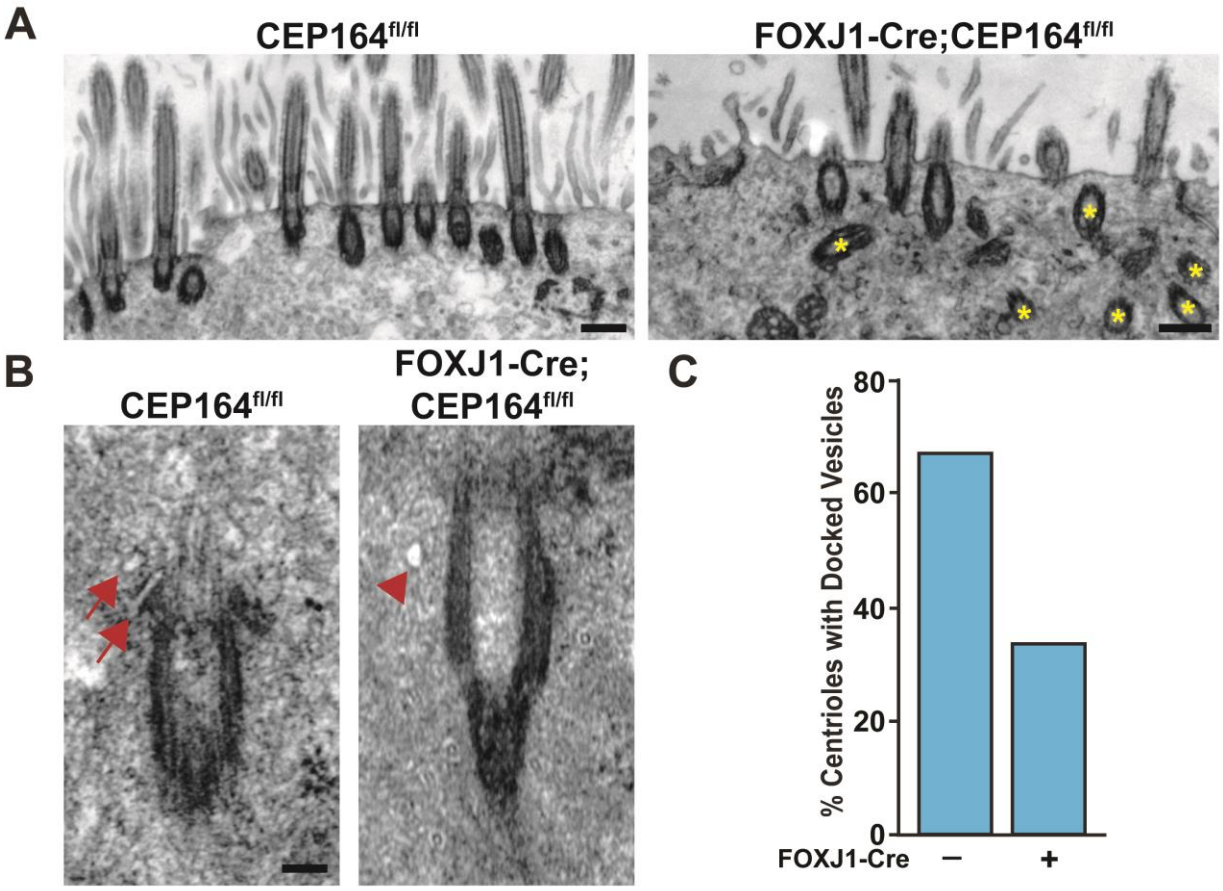

Figure 4.4: CEP164 regulates basal body docking and ciliary vesicle formation.
(A) Electron micrographs of ciliated cells from CEP164$^{fl/fl}$ and FOXJ1-Cre;CEP164$^{fl/fl}$ adult tracheas. Asterisks depict multiple cytoplasmic basal bodies in FOXJ1-Cre; CEP164$^{fl/fl}$ trachea. Scale bars, 500 nm. (B) Electron micrographs of CEP164$^{fl/fl}$ and FOXJ1-Cre;CEP164$^{fl/fl}$ P8 tracheas subjected to *ex vivo* culture in the presence of taxol to block apical migration of basal bodies and permit visualization of vesicle docking events. Arrows denote ciliary vesicle attached to the distal end of the cytoplasmic centriole, whereas the arrowhead signifies an undocked vesicle. (C) Quantification of the percent of centrioles with docked vesicles in taxol-treated P8 tracheas. >30 cytoplasmic centrioles were counted per condition.

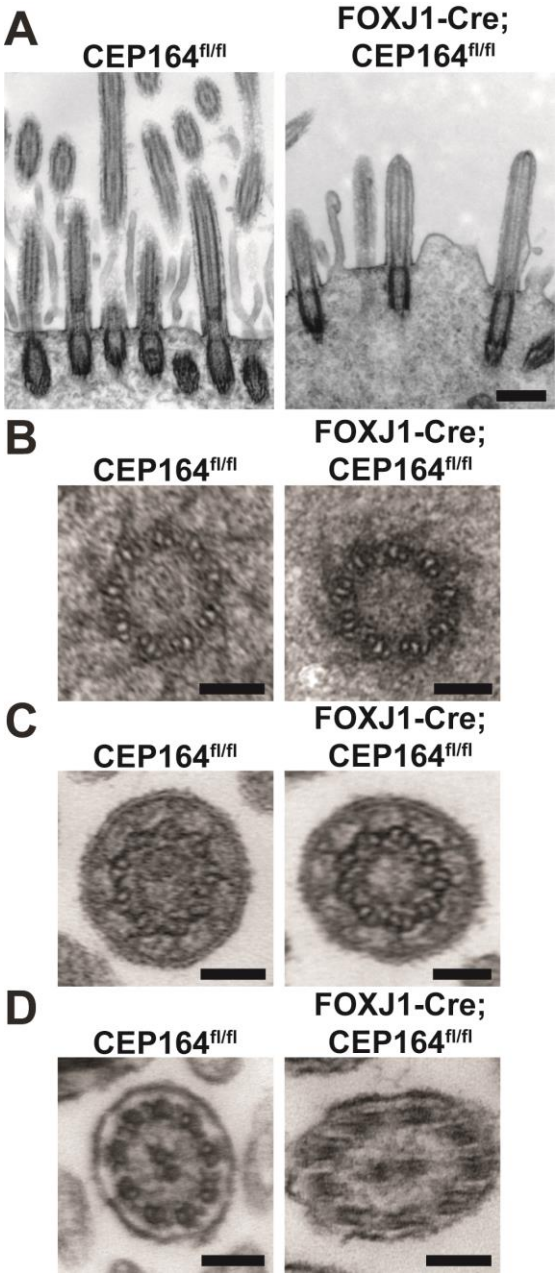

Figure 4.5: Transmission electron microscopy reveals short cilia as well as intact transition fibers and transition zone in the absence of CEP164.
(A) Elongated cilia were abundant in cross-sections of tracheas from CEP164$^{fl/fl}$ adult mice while short cilia were frequently found in tracheas from FOXJ1;CEP164$^{fl/fl}$ adult mice. Scale bar, 500 nm. (B) Nine transition fibers emanating from the microtubule triplets of the basal body were present in cross-sections of cilia in ALId14 MTEC cultures from both CEP164$^{fl/fl}$ and FOXJ1-Cre;CEP164$^{fl/fl}$ mice. Scale bars, 100 nm. (C) Y-linkers within the transition zone were visible in cross-sections of cilia in ALId14 MTEC cultures from both CEP164$^{fl/fl}$ and FOXJ1-Cre;CEP164$^{fl/fl}$ mice. Scale bars, 100 nm. (D) Axonemal cross-sections display a 9+2 microtubule arrangement in ALId14 MTEC cultures from both CEP164$^{fl/fl}$ and FOXJ1-Cre;CEP164$^{fl/fl}$ mice. Scale bars, 100 nm.

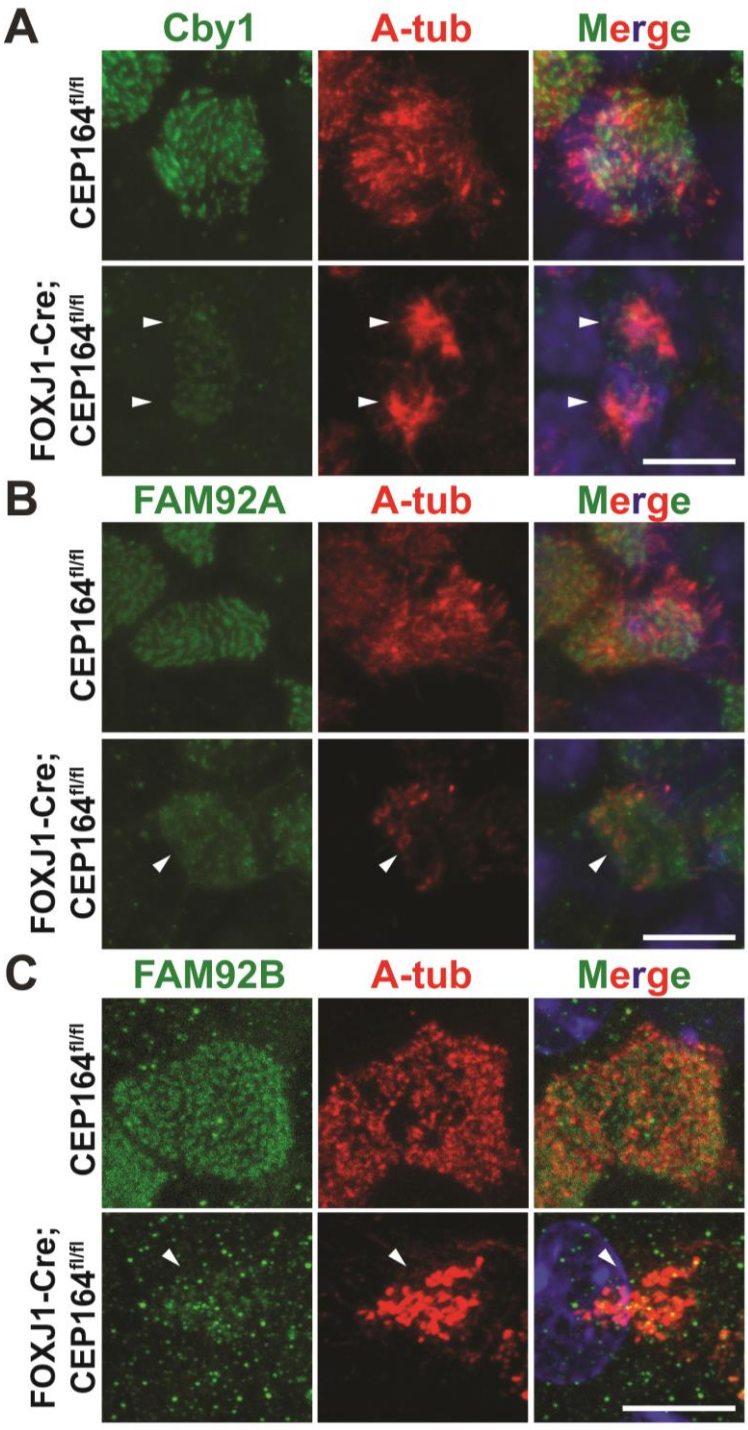

Figure 4.6: CEP164 recruits Cby1 and FAM92 proteins to basal bodies in ciliated cells.
ALId14 MTECs from CEP164$^{fl/fl}$ or FOXJ1-Cre;CEP164$^{fl/fl}$ mice were immunostained for Cby1 (A), FAM92A (B), or FAM92B (C) (green) and A-tub (red). DAPI staining (blue) marks nuclei in merged images. Arrowheads indicate individual CEP164-KO ciliated cells. Scale bars, 10 μm.

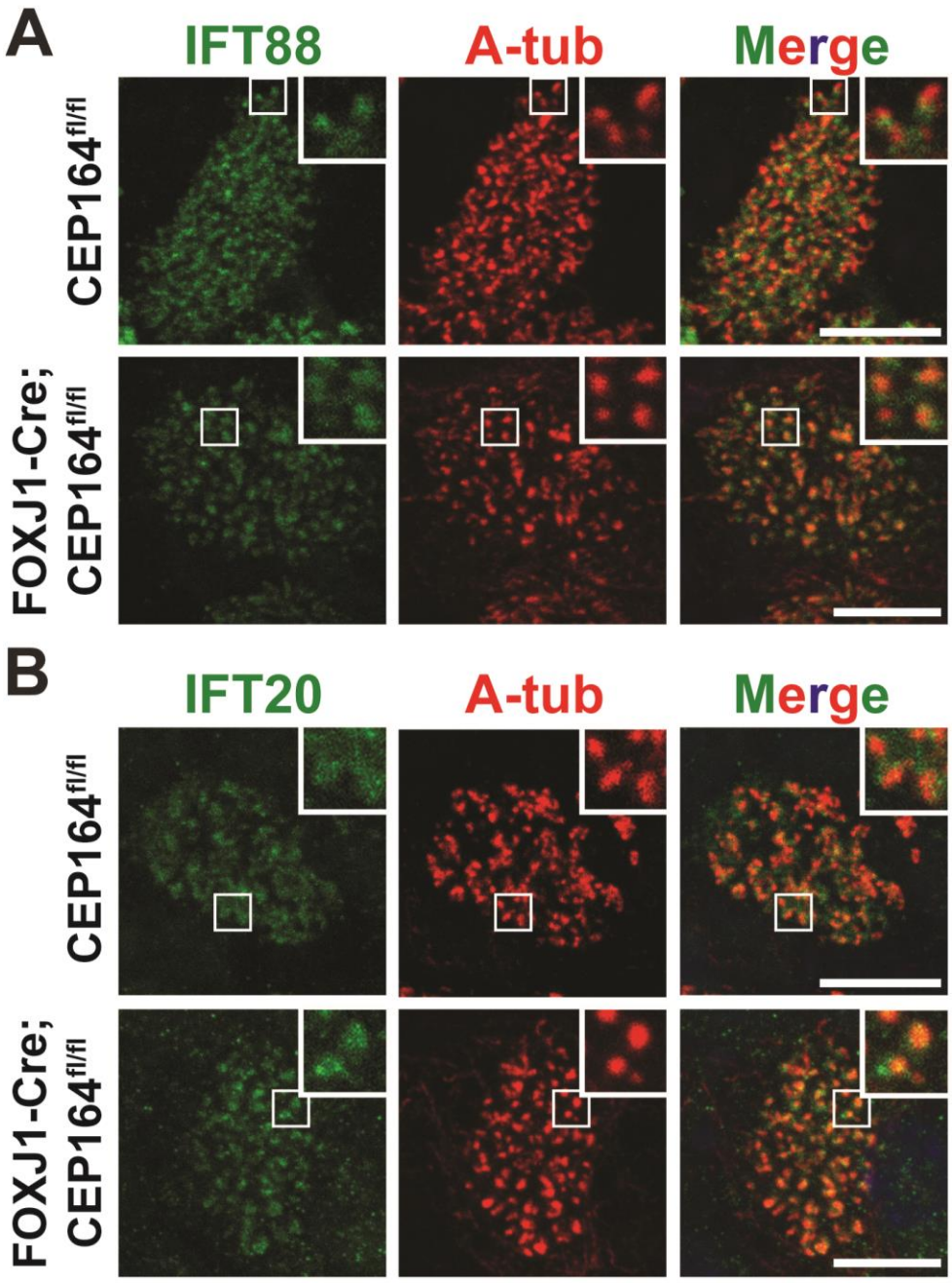

Figure 4.7: CEP164 is dispensable for the basal body localization of IFT proteins IFT88 and IFT20 in ciliated cells.
ALId14 MTECs from CEP164$^{fl/fl}$ or FOXJ1-Cre;CEP164$^{fl/fl}$ mice were immunostained for IFT88 (A) or IFT20 (B) (green) and A-tub (red). Nuclei were detected with DAPI (blue). All ciliated cells were at early stage IV. The insets show zoomed views of the squared areas. Scale bars, 10 μm.

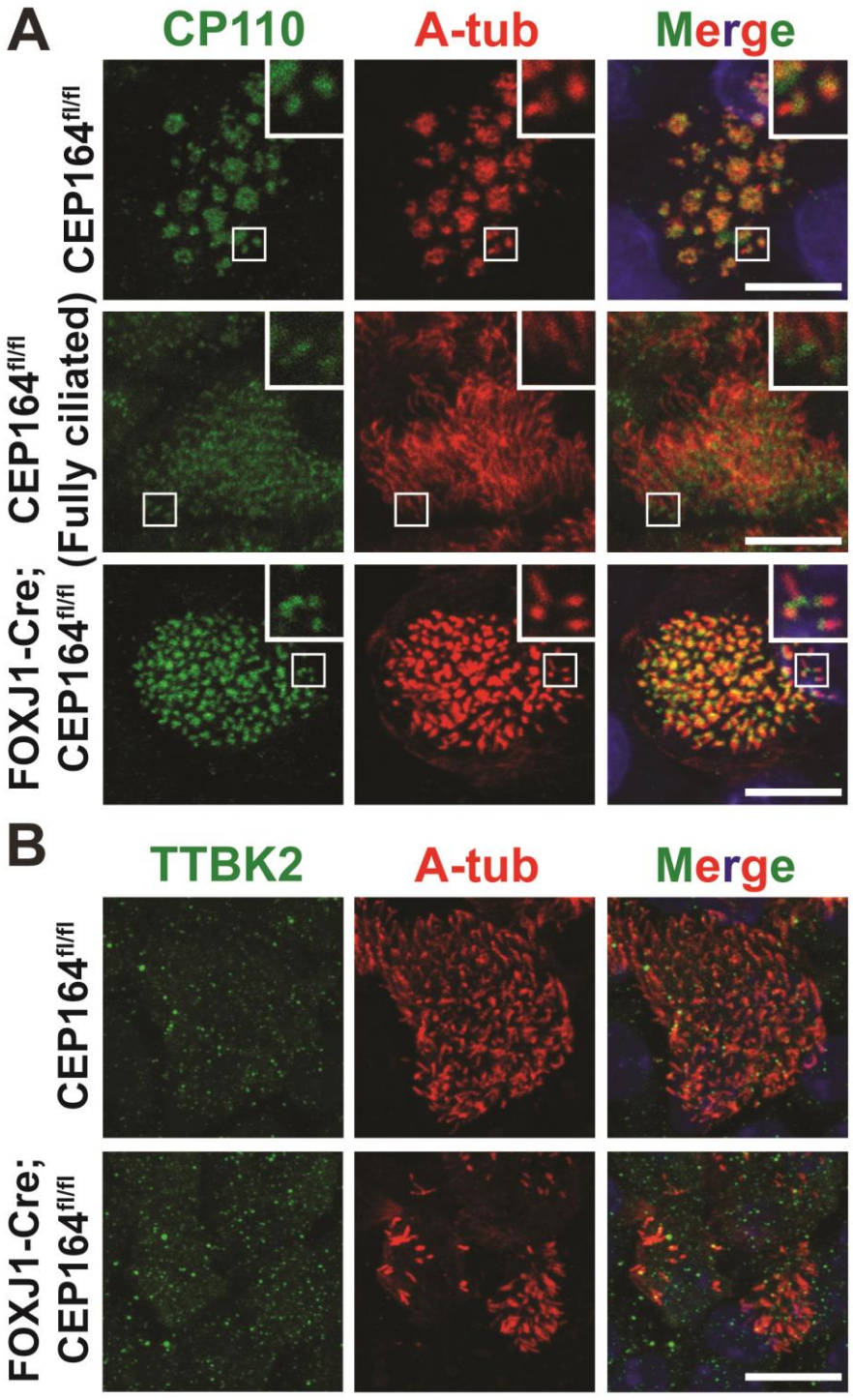

Figure 4.8: CEP164 is dispensable for the basal body localization of CP110 and TTBK2 in ciliated cells.
ALId14 MTECs from CEP164$^{fl/fl}$ or FOXJ1-Cre;CEP164$^{fl/fl}$ mice were immunostained for CP110 (A) or TTBK2 (B) (green) and A-tub (red). Nuclei were detected with DAPI (blue). All ciliated cells were at early stage IV except for the fully differentiated cell (Fully ciliated) imaged to show the clear basal body localization of CP110. The insets show zoomed views of the squared areas. Scale bars, 10 μm.

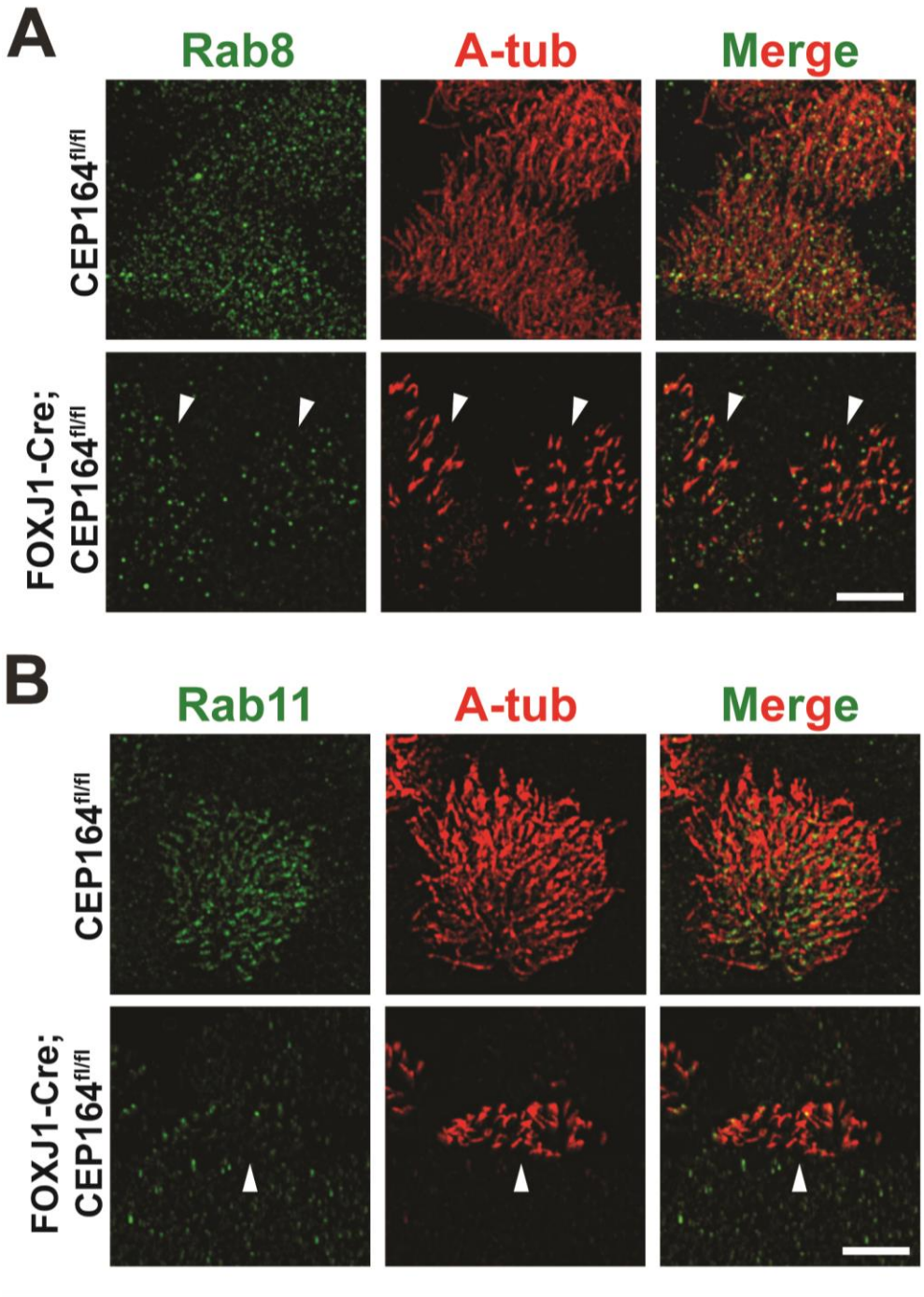

Figure 4.9: CEP164 is required for the proper targeting of Rab proteins in ciliated cells.
CEP164$^{fl/fl}$ and FOXJ1-Cre;CEP164$^{fl/fl}$ MTECs at ALId14 were immunostained for Rab8 (A) or Rab11 (B) (green) and A-tub (red) and subjected to super-resolution SIM imaging**.** Arrowheads point to individual CEP164-KO ciliated cells. Scale bar, 5 μm.

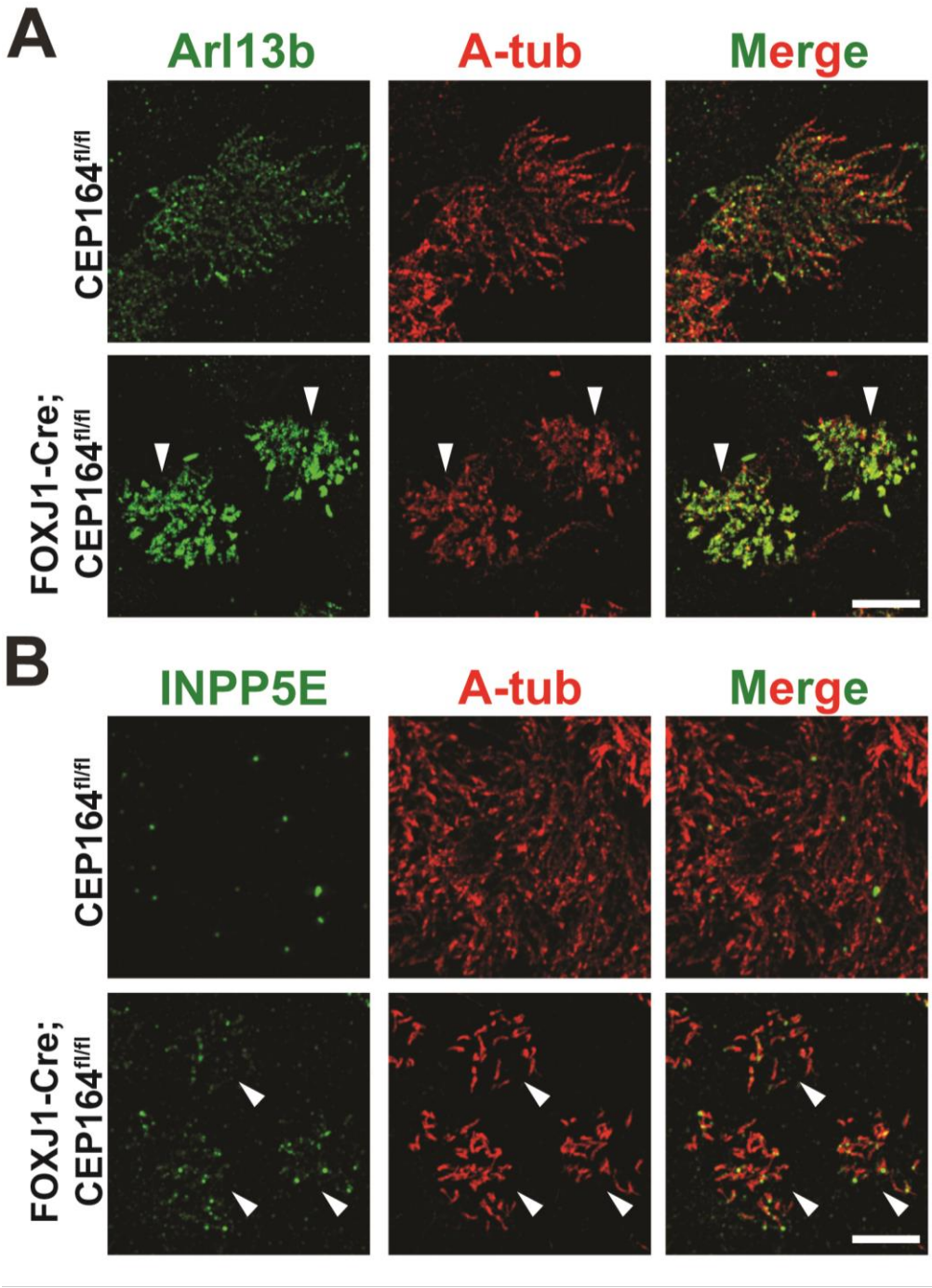

Figure 4.10: CEP164 is required for the proper ciliary targeting of Arl13b and INNP5E in ciliated cells.
ALId14 MTECs from CEP164$^{fl/fl}$ and FOXJ1-Cre;CEP164$^{fl/fl}$ mice were immunostained for Arl13b or INPP5E (green) and A-tub (red) and imaged by SIM. Arrowheads indicate individual CEP164-KO ciliated cells. Scale bar, 5 μm.

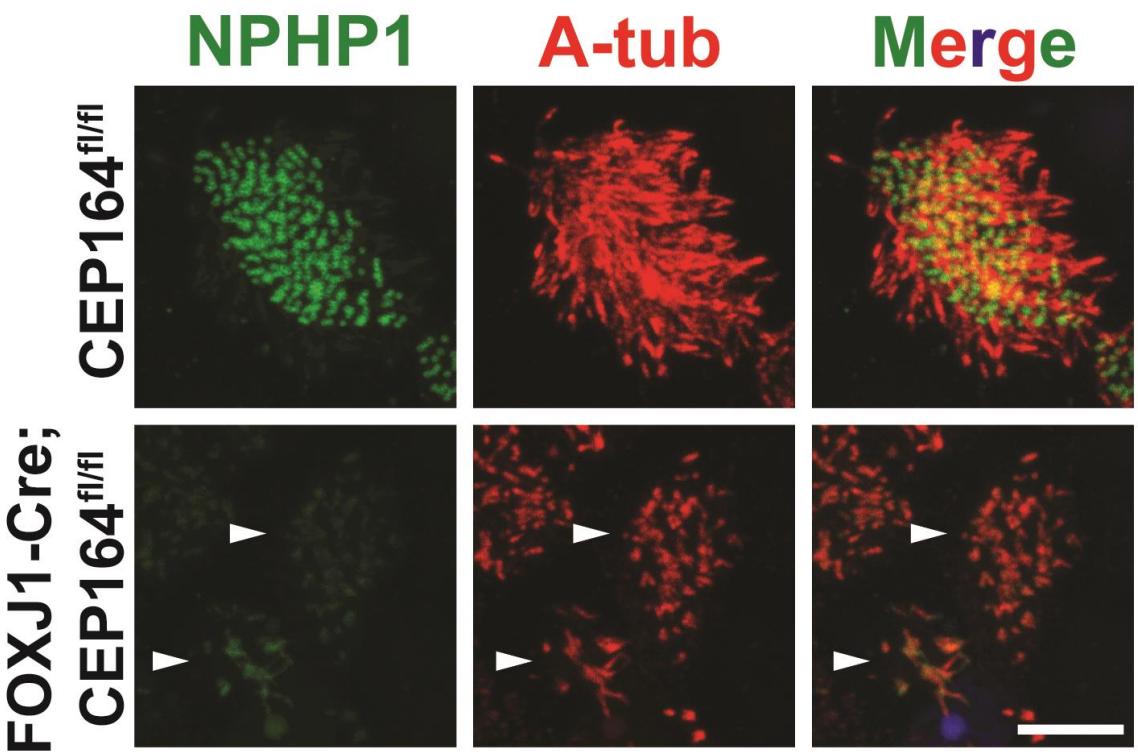

Figure 4.11: CEP164 is necessary for normal localization of the transition zone protein NPHP1.
ALId14 MTECs from CEP164$^{fl/fl}$ or FOXJ1-Cre;CEP164$^{fl/fl}$ mice were immunostained for NPHP1 (green) and A-tub (red). DAPI staining (blue) marks nuclei in merged images. Arrowheads point to CEP164-KO individual ciliated cells. Scale bars, 10 μm.

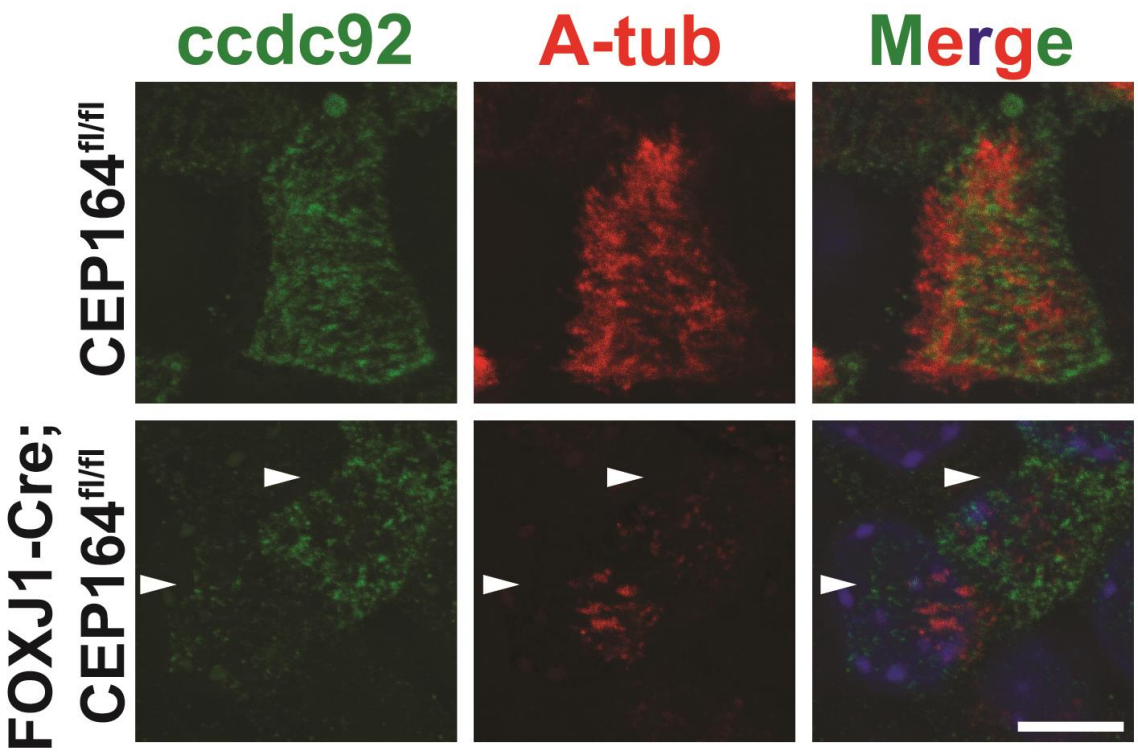

Figure 4.12: CEP164 is important for the centriolar localization of ccdc92.
ALId14 MTECs from CEP164$^{fl/fl}$ or FOXJ1-Cre;CEP164$^{fl/fl}$ mice were immunostained for ccdc92 (green) and A-tub (red). DAPI staining (blue) marks nuclei in merged images. Arrowheads indicate individual CEP164-KO ciliated cells. Scale bars, 10 μm.

Chapter 5: General Discussion

Cilia play a diverse set of functions in eukaryotic, and, in particular, mammalian, development and homeostasis (Eggenschwiler and Anderson 2007), as exemplified by the wide range of clinical phenotypes observed in patients with ciliopathies (Fliegauf et al. 2007). Motile multicilia are specifically responsible for the clearing of mucus and debris from the airway, circulating cerebrospinal fluid, and transporting the ovum through the oviduct (Ibanez-Tallon et al. 2003). Unfortunately, genetic, such as PCD and CF, and non-genetic, such as COPD and asthma, disorders that affect multicilia have an enormous impact on human health (Tilley et al. 2014); though, our knowledge of and tools to study multicilia are limited.

Essential structures for ciliogenesis to proceed normally are the distal appendages, or transition fibers, as referred at the base of cilia (Reiter et al. 2012; Wei et al. 2015). In primary cilia formation, they are signatures of a mature centriole, regulate the initiation of primary ciliogenesis, coordinate multiple vesicular docking events and the formation of the ciliary membrane, and are sites of entry and exit of the privileged ciliary compartment. To achieve all this, a core unit of proteins composes the distal appendage (Tanos et al. 2013); however, several upstream effectors modulate their function while many downstream effectors facilitate this function (Wei et al. 2015). Highlighting the importance of the distal appendages and their associated protein network, multiple disease mutations are found in a host of genes that encode for distal appendage or distal appendage-associated proteins (van Reeuwijk et al. 2011). Despite their vast consequence on human health and biology, very little is known about these proteins

physiological function. Furthermore, even less is known about their roles in multicilia formation.

In this dissertation, I interrogate the functions of a core distal appendage protein CEP164 and a downstream distal appendage effector Cby1 in multicilia. First, I identify a novel role for Cby1 in regulating ciliary morphology and the IFT processes that are responsible for transporting cargos along the cilium. Then, I establish and characterize a novel conditional KO mouse model where CEP164 is deleted in multiciliated cells and the testis. In so doing, I elucidate a clear requirement for CEP164 in multiliogenesis. These mice have hydrocephalus and male infertility along with a dramatic loss of airway, ependymal, and oviduct cilia. Furthermore, CEP164 promotes vesicular docking, ciliary vesicle formation, and basal body docking in airway ciliated cells, similar to that seen in primary ciliogenesis. However, the present study emphasizes important differences between primary and multicilia formation, which should shape interpretation of data generated in these two systems going forward. My data also suggests that CEP164 engages the Rab11-Rabin8-Rab8 protein cascade as well as a Cby1-FAM92 protein axis to facilitate ciliary membrane biogenesis while tightly controlling the amount of Arl13b and INPP5E in the cilium. Importantly, this is the first report of differential regulation of ciliary membrane protein trafficking as seen with these two sets of membrane proteins in airway ciliated cells, which should be therefore the subject of future investigations.

Based on these findings, I propose a model (Figure 5.1) for CEP164 and Cby1 function in airway ciliated cells where CEP164, working in concert with Cby1, promotes Rab-positive vesicular membranes to dock to the distal appendage. Additionally, CEP164 either directly recruits to the centriole or adjusts the amount at the centriole of Arl13b- and

INPP5E-positive membranes. Then, through remodeling events, these vesicular membranes fuse to create the ciliary vesicle and promote basal body docking. At this point, Cby1, potentially with another distal appendage protein FBF1 (Wei et al. 2013), engages IFT processes to build the cilium. In parallel, CEP164 continues to recruit Rab-positive membranes and modulate the amount of Arl13b- and INPP5E-positive membrane that enters the ciliary compartment. This additionally provides tight control over the lipid composition of the ciliary membrane. Finally, working in concert, CEP164 and Cby1 form and maintain the airway cilia.

While speculative, this model leaves many unanswered questions. For example, after vesicular recruitment, how do the membrane remodeling processes occur to form the ciliary vesicle and to incorporate new membrane into the growing cilium? This is a critical point for the airway ciliated cell that must traffic a substantial amount of membrane to hundreds of growing cilia. Obvious targets are the BAR-domain containing proteins FAM92A and 92B, which are effectors of Cby1 that localize to the ciliary base (Li et al. 2016b). BAR-domain containing proteins are known to function in membrane deforming and remodeling events (Ren et al. 2006). Thus, these are likely candidates for this role; however, no KO mice for either protein exist in order to test this hypothesis in airway ciliated cells. In addition, both FAM92A and 92B persist at the ciliary base of mature airway cilia. Thus, it is tempting to think that these two proteins may either play a similar role to Cby1 in the maintenance of cilia or, on the other hand, might possibly be important for the incorporation of new membrane that is trafficked to maintain ciliary membrane integrity. Very little is known about the latter process; however, as multicilia play a vital role in chronic respiratory diseases, this should be a focus of future work.

The Rab11-Rabin8-Rab8 protein network is clearly a critical nexus of ciliary membrane trafficking for both primary and multicilia formation that is highly regulated, in particular, by CEP164 (Schmidt et al. 2012; Deretic 2013). Of great interest, several proteins that are linked to this protein cascade also regulate each other, including Ahi1, CEP290, Cby1, CEP164, FAM92A, FAM92B, EHD1, and EHD3 (Kim et al. 2008; Hsiao et al. 2009; Burke et al. 2014; Lu et al. 2015b; Li et al. 2016b). These regulatory relationships suggest the presence of a larger protein network whose function is to regulate the Rab11-Rabin8-Rab8 cascade. Additionally, as the BBSome has been shown to be a coatomer complex and to regulate the Rab11-Rabin8-Rab8 cascade, this provides additional interesting links to IFT processes (Jin et al. 2010). While we have some glimpses into how this large network interacts, it should be of the utmost importance to tease apart these relationships. This is of particular importance as, despite the importance of Rab8 to ciliary membrane formation, it appears to be dispensable for ciliogenesis, implying that the Rab11-Rabin8-Rab8 cascade working together with its larger associated protein module properly regulates ciliogenesis.

Finally, CEP164 and Cby1 are only two proteins of the several that are contained within or associated with the distal appendage (Reiter et al. 2012; Tanos et al. 2013; Tony Yang et al. 2015; Wei et al. 2015). While it is clear from my studies that complex regulatory processes occur at these appendage structures, further work is needed to interrogate the mechanisms, for example, of how CEP164 differentially regulates two different pools of ciliary membrane proteins. Moreover, the actions of the other distal appendage or distal appendage-associated proteins must be elucidated through more detailed animal studies. This is hopefully only the first of many reports on

mouse models of distal appendage proteins. Only through other studies, such as this, can we fully grasp the functions of the distal appendage in health and disease.

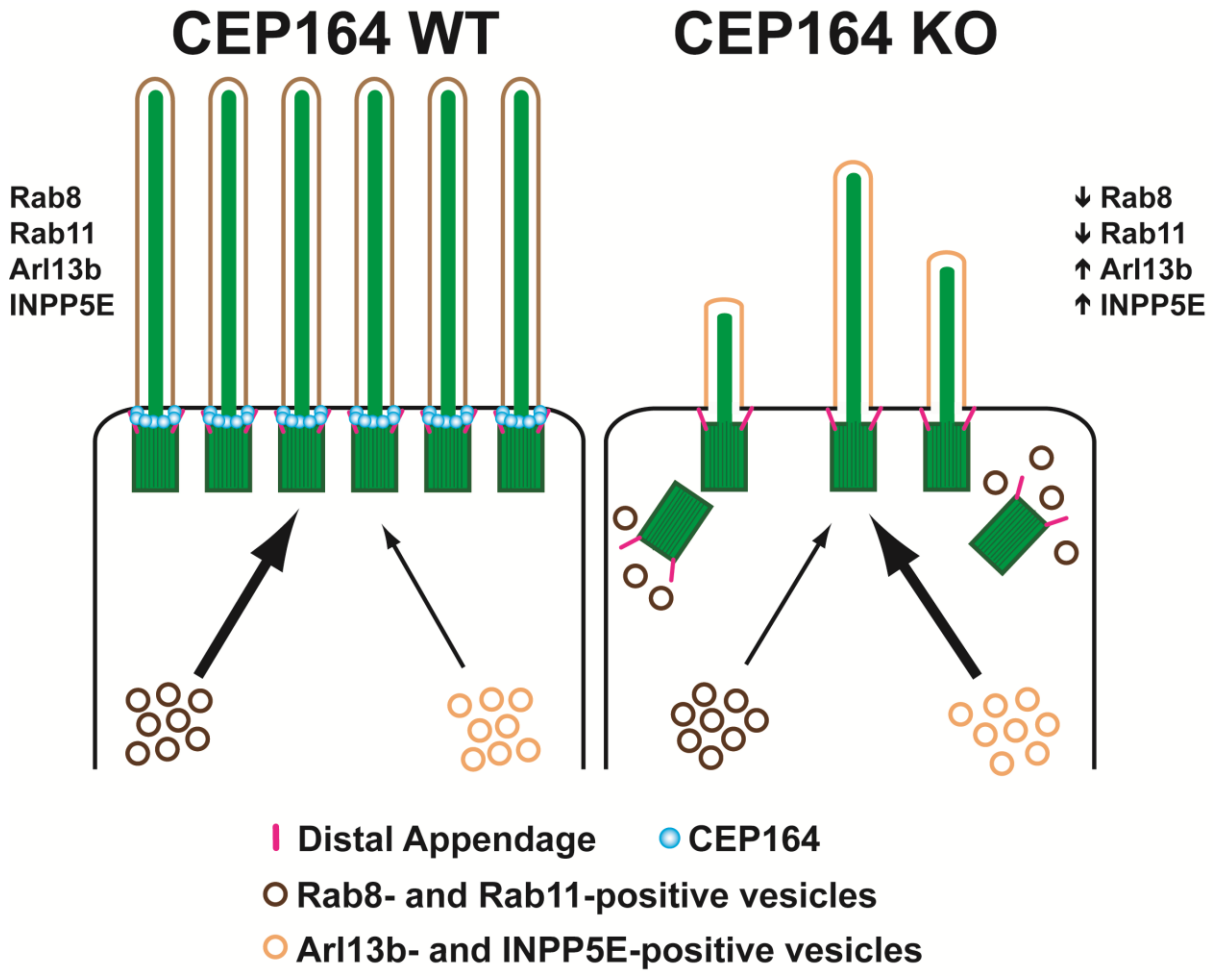

Figure 5.1: A model for CEP164 function in multiciliogenesis.
In CEP164 WT ciliated cells, pools of Rab8- and Rab11-positive vesicles and Arl13b- and INPP5E-positive vesicles are captured by CEP164 for docking with the distal appendage to form the ciliary vesicle and for integration into the ciliary membrane at specified levels. Greater amounts of Rab8- and Rab11-positive vesicles are recruited by CEP164. In the absence of CEP164, basal bodies cannot recruit small vesicles to dock at centrioles, causing cytoplasmic basal bodies, and increased levels of Arl13b- and INPP5E-positive vesicles are recruited, leading to changes in ciliary membrane composition and short cilia.

References

Adeva M, El-Youssef M, Rossetti S, Kamath PS, Kubly V, Consugar MB, Milliner DM, King BF, Torres VE, Harris PC. 2006. Clinical and molecular characterization defines a broadened spectrum of autosomal recessive polycystic kidney disease (ARPKD). *Medicine (Baltimore)* **85**: 1-21.

Afzelius BA. 1976. A human syndrome caused by immotile cilia. *Science* **193**: 317-319.

Andersen JS, Wilkinson CJ, Mayor T, Mortensen P, Nigg EA, Mann M. 2003. Proteomic characterization of the human centrosome by protein correlation profiling. *Nature* **426**: 570-574.

Ansley SJ, Badano JL, Blacque OE, Hill J, Hoskins BE, Leitch CC, Kim JC, Ross AJ, Eichers ER, Teslovich TM et al. 2003. Basal body dysfunction is a likely cause of pleiotropic Bardet-Biedl syndrome. *Nature* **425**: 628-633.

Arbi M, Pefani DE, Kyrousi C, Lalioti ME, Kalogeropoulou A, Papanastasiou AD, Taraviras S, Lygerou Z. 2016. GemC1 controls multiciliogenesis in the airway epithelium. *EMBO Rep* **17**: 400-413.

Archer FL, Wheatley DN. 1971. Cilia in cell-cultured fibroblasts. II. Incidence in mitotic and post-mitotic BHK 21-C13 fibroblasts. *Journal of anatomy* **109**: 277-292.

Bachmann-Gagescu R, Dona M, Hetterschijt L, Tonnaer E, Peters T, de Vrieze E, Mans DA, van Beersum SE, Phelps IG, Arts HH et al. 2015. The Ciliopathy Protein CC2D2A Associates with NINL and Functions in RAB8-MICAL3-Regulated Vesicle Trafficking. *PLoS Genet* **11**: e1005575.

Banizs B, Pike MM, Millican CL, Ferguson WB, Komlosi P, Sheetz J, Bell PD, Schwiebert EM, Yoder BK. 2005. Dysfunctional cilia lead to altered ependyma and choroid plexus function, and result in the formation of hydrocephalus. *Development* **132**: 5329-5339.

Bettencourt-Dias M, Glover DM. 2007. Centrosome biogenesis and function: centrosomics brings new understanding. *Nat Rev Mol Cell Biol* **8**: 451-463.

Bettencourt-Dias M, Hildebrandt F, Pellman D, Woods G, Godinho SA. 2011. Centrosomes and cilia in human disease. *Trends in genetics : TIG* **27**: 307-315.

Bhogaraju S, Engel BD, Lorentzen E. 2013. Intraflagellar transport complex structure and cargo interactions. *Cilia* **2**: 10.

Bielas SL, Silhavy JL, Brancati F, Kisseleva MV, Al-Gazali L, Sztriha L, Bayoumi RA, Zaki MS, Abdel-Aleem A, Rosti RO et al. 2009. Mutations in INPP5E, encoding inositol polyphosphate-5-phosphatase E, link phosphatidyl inositol signaling to the ciliopathies. *Nat Genet* **41**: 1032-1036.

Bisgrove BW, Yost HJ. 2006. The roles of cilia in developmental disorders and disease. *Development* **133**: 4131-4143.

Blatt EN, Yan XH, Wuerffel MK, Hamilos DL, Brody SL. 1999. Forkhead transcription factor HFH-4 expression is temporally related to ciliogenesis. *Am J Respir Cell Mol Biol* **21**: 168-176.

Boehlke C, Bashkurov M, Buescher A, Krick T, John AK, Nitschke R, Walz G, Kuehn EW. 2010. Differential role of Rab proteins in ciliary trafficking: Rab23 regulates smoothened levels. *J Cell Sci* **123**: 1460-1467.

Boisvieux-Ulrich E, Laine MC, Sandoz D. 1989. In vitro effects of taxol on ciliogenesis in quail oviduct. *J Cell Sci* **92 (Pt 1)**: 9-20.

Boon M, Jorissen M, Proesmans M, De Boeck K. 2013. Primary ciliary dyskinesia, an orphan disease. *European journal of pediatrics* **172**: 151-162.

Boucher RC. 2004. New concepts of the pathogenesis of cystic fibrosis lung disease. *Eur Respir J* **23**: 146-158.

Boucher RC. 2007. Cystic fibrosis: a disease of vulnerability to airway surface dehydration. *Trends Mol Med* **13**: 231-240.

Bradley A, Anastassiadis K, Ayadi A, Battey JF, Bell C, Birling MC, Bottomley J, Brown SD, Burger A, Bult CJ et al. 2012. The mammalian gene function resource: the International Knockout Mouse Consortium. *Mamm Genome* **23**: 580-586.

Brody SL, Yan XH, Wuerffel MK, Song SK, Shapiro SD. 2000. Ciliogenesis and left-right axis defects in forkhead factor HFH-4-null mice. *Am J Respir Cell Mol Biol* **23**: 45-51.

Brooks ER, Wallingford JB. 2014. Multiciliated Cells. *Curr Biol* **24**: R973-R982.

Burke MC, Li FQ, Cyge B, Arashiro T, Brechbuhl HM, Chen X, Siller SS, Weiss MA, O'Connell CB, Love D et al. 2014. Chibby promotes ciliary vesicle formation and basal body docking during airway cell differentiation. *The Journal of cell biology* **207**: 123-137.

Cajanek L, Nigg EA. 2014. Cep164 triggers ciliogenesis by recruiting Tau tubulin kinase 2 to the mother centriole. *Proceedings of the National Academy of Sciences of the United States of America*.

Calderon-Garciduenas L, Rodriguez-Alcaraz A, Villarreal-Calderon A, Lyght O, Janszen D, Morgan KT. 1998. Nasal epithelium as a sentinel for airborne environmental pollution. *Toxicol Sci* **46**: 352-364.

Camner P, Mossberg B, Philipson K. 1973. Tracheobronchial clearance and chronic obstructive lung disease. *Scand J Respir Dis* **54**: 272-281.

Cantagrel V, Silhavy JL, Bielas SL, Swistun D, Marsh SE, Bertrand JY, Audollent S, Attie-Bitach T, Holden KR, Dobyns WB et al. 2008. Mutations in the cilia gene ARL13B lead to the classical form of Joubert syndrome. *Am J Hum Genet* **83**: 170-179.

Carson JL, Collier AM, Fernald GW, Hu SC. 1994. Microtubular discontinuities as acquired ciliary defects in airway epithelium of patients with chronic respiratory diseases. *Ultrastruct Pathol* **18**: 327-332.

Carvalho-Santos Z, Azimzadeh J, Pereira-Leal JB, Bettencourt-Dias M. 2011. Evolution: Tracing the origins of centrioles, cilia, and flagella. *The Journal of cell biology* **194**: 165-175.

Caspary T, Larkins CE, Anderson KV. 2007. The graded response to Sonic Hedgehog depends on cilia architecture. *Developmental cell* **12**: 767-778.

Cevik S, Hori Y, Kaplan OI, Kida K, Toivenon T, Foley-Fisher C, Cottell D, Katada T, Kontani K, Blacque OE. 2010. Joubert syndrome Arl13b functions at ciliary membranes and stabilizes protein transport in Caenorhabditis elegans. *The Journal of cell biology* **188**: 953-969.

Cevik S, Sanders AA, Van Wijk E, Boldt K, Clarke L, van Reeuwijk J, Hori Y, Horn N, Hetterschijt L, Wdowicz A et al. 2013. Active transport and diffusion barriers restrict Joubert Syndrome-associated ARL13B/ARL-13 to an Inv-like ciliary membrane subdomain. *PLoS Genet* **9**: e1003977.

Chaki M, Airik R, Ghosh AK, Giles RH, Chen R, Slaats GG, Wang H, Hurd TW, Zhou W, Cluckey A et al. 2012. Exome capture reveals ZNF423 and CEP164 mutations, linking renal ciliopathies to DNA damage response signaling. *Cell* **150**: 533-548.

Chavez M, Ena S, Van Sande J, de Kerchove d'Exaerde A, Schurmans S, Schiffmann SN. 2015. Modulation of Ciliary Phosphoinositide Content Regulates Trafficking and Sonic Hedgehog Signaling Output. *Developmental cell* **34**: 338-350.
Chodhari R, Mitchison HM, Meeks M. 2004. Cilia, primary ciliary dyskinesia and molecular genetics. *Paediatric respiratory reviews* **5**: 69-76.
Choksi SP, Lauter G, Swoboda P, Roy S. 2014. Switching on cilia: transcriptional networks regulating ciliogenesis. *Development* **141**: 1427-1441.
Chung MI, Kwon T, Tu F, Brooks ER, Gupta R, Meyer M, Baker JC, Marcotte EM, Wallingford JB. 2014. Coordinated genomic control of ciliogenesis and cell movement by RFX2. *eLife* **3**: e01439.
Cloonan SM, Lam HC, Ryter SW, Choi AM. 2014. "Ciliophagy": The consumption of cilia components by autophagy. *Autophagy* **10**: 532-534.
Cole DG. 2003. The intraflagellar transport machinery of Chlamydomonas reinhardtii. *Traffic* **4**: 435-442.
Corbit KC, Aanstad P, Singla V, Norman AR, Stainier DY, Reiter JF. 2005. Vertebrate Smoothened functions at the primary cilium. *Nature* **437**: 1018-1021.
Cyge B, Fischer V, Takemaru K, Li FQ. 2011. Generation and characterization of monoclonal antibodies against human Chibby protein. *Hybridoma (Larchmt)* **30**: 163-168.
Czarnecki PG, Shah JV. 2012. The ciliary transition zone: from morphology and molecules to medicine. *Trends Cell Biol* **22**: 201-210.
Daly OM, Gaboriau D, Karakaya K, King S, Dantas TJ, Lalor P, Dockery P, Kramer A, Morrison CG. 2016. Gene-targeted CEP164-deficient cells show a ciliation defect with intact DNA repair capacity. *J Cell Sci* **129**: 1769-1774.
Dammermann A, Merdes A. 2002. Assembly of centrosomal proteins and microtubule organization depends on PCM-1. *The Journal of cell biology* **159**: 255-266.
Das A, Guo W. 2011. Rabs and the exocyst in ciliogenesis, tubulogenesis and beyond. *Trends Cell Biol* **21**: 383-386.
Deane JA, Cole DG, Seeley ES, Diener DR, Rosenbaum JL. 2001. Localization of intraflagellar transport protein IFT52 identifies basal body transitional fibers as the docking site for IFT particles. *Curr Biol* **11**: 1586-1590.
Delgehyr N, Sillibourne J, Bornens M. 2005. Microtubule nucleation and anchoring at the centrosome are independent processes linked by ninein function. *J Cell Sci* **118**: 1565-1575.
Delling M, Indzhykulian AA, Liu X, Li Y, Xie T, Corey DP, Clapham DE. 2016. Primary cilia are not calcium-responsive mechanosensors. *Nature* **531**: 656-60.
Dentler WL. 1980. Structures linking the tips of ciliary and flagellar microtubules to the membrane. *J Cell Sci* **42**: 207-220.
Dentler WL. 1984. Attachment of the cap to the central microtubules of Tetrahymena cilia. *J Cell Sci* **66**: 167-173.
Dentler WL, LeCluyse EL. 1982. Microtubule capping structures at the tips of tracheal cilia: evidence for their firm attachment during ciliary bend formation and the restriction of microtubule sliding. *Cell Motil* **2**: 549-572.
Dentler WL, Rosenbaum JL. 1977. Flagellar elongation and shortening in Chlamydomonas. III. structures attached to the tips of flagellar microtubules and their

relationship to the directionality of flagellar microtubule assembly. *The Journal of cell biology* **74**: 747-759.
Deretic D. 2013. Crosstalk of Arf and Rab GTPases en route to cilia. *Small GTPases* **4**: 70-77.
Didon L, Zwick RK, Chao IW, Walters MS, Wang R, Hackett NR, Crystal RG. 2013. RFX3 modulation of FOXJ1 regulation of cilia genes in the human airway epithelium. *Respir Res* **14**: 70.
Dunnill MS. 1960. The pathology of asthma, with special reference to changes in the bronchial mucosa. *J Clin Pathol* **13**: 27-33.
Dyson JM, Conduit SE, Feeney SJ, Hakim S, DiTommaso T, Fulcher AJ, Sriratana A, Ramm G, Horan KA, Gurung R et al. 2017. INPP5E regulates phosphoinositide-dependent cilia transition zone function. *The Journal of cell biology* **216**: 247-263.
Eggenschwiler JT, Anderson KV. 2007. Cilia and developmental signaling. *Annual review of cell and developmental biology* **23**: 345-373.
Ehre C, Ridley C, Thornton DJ. 2014. Cystic fibrosis: an inherited disease affecting mucin-producing organs. *Int J Biochem Cell Biol* **52**: 136-145.
Eliasson R, Mossberg B, Camner P, Afzelius BA. 1977. The immotile-cilia syndrome. A congenital ciliary abnormality as an etiologic factor in chronic airway infections and male sterility. *The New England journal of medicine* **297**: 1-6.
Enjolras C, Thomas J, Chhin B, Cortier E, Duteyrat JL, Soulavie F, Kernan MJ, Laurencon A, Durand B. 2012. Drosophila chibby is required for basal body formation and ciliogenesis but not for Wg signaling. *The Journal of cell biology* **197**: 313-325.
Erle DJ, Sheppard D. 2014. The cell biology of asthma. *The Journal of cell biology* **205**: 621-631.
Escudier E, Duquesnoy P, Papon JF, Amselem S. 2009. Ciliary defects and genetics of primary ciliary dyskinesia. *Paediatric respiratory reviews* **10**: 51-54.
Fawcett DW, Porter KR. 1954. A Study of the Fine Structure of Ciliated Epithelia. *J Morphol* **94**: 221-282.
Feng S, Knodler A, Ren J, Zhang J, Zhang X, Hong Y, Huang S, Peranen J, Guo W. 2012. A Rab8 guanine nucleotide exchange factor-effector interaction network regulates primary ciliogenesis. *J Biol Chem* **287**: 15602-15609.
Firat-Karalar EN, Stearns T. 2014. The centriole duplication cycle. *Philosophical transactions of the Royal Society of London Series B, Biological sciences* **369**.
Fisch C, Dupuis-Williams P. 2011. Ultrastructure of cilia and flagella - back to the future! *Biology of the cell / under the auspices of the European Cell Biology Organization* **103**: 249-270.
Fliegauf M, Benzing T, Omran H. 2007. When cilia go bad: cilia defects and ciliopathies. *Nature reviews Molecular cell biology* **8**: 880-893.
Fliegauf M, Olbrich H, Horvath J, Wildhaber JH, Zariwala MA, Kennedy M, Knowles MR, Omran H. 2005. Mislocalization of DNAH5 and DNAH9 in respiratory cells from patients with primary ciliary dyskinesia. *American journal of respiratory and critical care medicine* **171**: 1343-1349.
Follit JA, Tuft RA, Fogarty KE, Pazour GJ. 2006. The intraflagellar transport protein IFT20 is associated with the Golgi complex and is required for cilia assembly. *Mol Biol Cell* **17**: 3781-3792.

Funk MC, Bera AN, Menchen T, Kuales G, Thriene K, Lienkamp SS, Dengjel J, Omran H, Frank M, Arnold SJ. 2015. Cyclin O (Ccno) functions during deuterosome-mediated centriole amplification of multiciliated cells. *The EMBO journal* **34**: 1078-1089.

Gao X, Bali AS, Randell SH, Hogan BL. 2015. GRHL2 coordinates regeneration of a polarized mucociliary epithelium from basal stem cells. *The Journal of cell biology* **211**: 669-682.

Garcia-Gonzalo FR, Phua SC, Roberson EC, Garcia G, 3rd, Abedin M, Schurmans S, Inoue T, Reiter JF. 2015. Phosphoinositides Regulate Ciliary Protein Trafficking to Modulate Hedgehog Signaling. *Developmental cell* **34**: 400-409.

Gibbs BC, Rao Damerla R, Vladar EK, Chatterjee B, Wan Y, Liu X, Cui C, Gabriel GC, Zahid M, Yagi H et al. 2016. Prickle1 mutation causes planar cell polarity and directional cell migration defects associated with cardiac outflow tract anomalies and other structural birth defects. *Biol Open* **5**: 323-335.

Gilula NB, Satir P. 1972. The ciliary necklace. A ciliary membrane specialization. *The Journal of cell biology* **53**: 494-509.

Gleeson JG, Keeler LC, Parisi MA, Marsh SE, Chance PF, Glass IA, Graham Jr JM, Maria BL, Barkovich AJ, Dobyns WB. 2004. Molar tooth sign of the midbrain-hindbrain junction: occurrence in multiple distinct syndromes. *Am J Med Genet A* **125A**: 125-134; discussion 117.

Goetz SC, Anderson KV. 2010. The primary cilium: a signalling centre during vertebrate development. *Nature reviews Genetics* **11**: 331-344.

Goetz SC, Liem KF, Jr., Anderson KV. 2012. The spinocerebellar ataxia-associated gene Tau tubulin kinase 2 controls the initiation of ciliogenesis. *Cell* **151**: 847-858.

Gonczy P. 2012. Towards a molecular architecture of centriole assembly. *Nature reviews Molecular cell biology* **13**: 425-435.

Gonzalez-Cano L, Fuertes-Alvarez S, Robledinos-Anton N, Bizy A, Villena-Cortes A, Farinas I, Marques MM, Marin MC. 2016. p73 is required for ependymal cell maturation and neurogenic SVZ cytoarchitecture. *Dev Neurobiol* **76**: 730-747.

Graser S, Stierhof YD, Lavoie SB, Gassner OS, Lamla S, Le Clech M, Nigg EA. 2007. Cep164, a novel centriole appendage protein required for primary cilium formation. *The Journal of cell biology* **179**: 321-330.

Grosshans BL, Ortiz D, Novick P. 2006. Rabs and their effectors: achieving specificity in membrane traffic. *Proceedings of the National Academy of Sciences of the United States of America* **103**: 11821-11827.

Guarguaglini G, Duncan PI, Stierhof YD, Holmstrom T, Duensing S, Nigg EA. 2005. The forkhead-associated domain protein Cep170 interacts with Polo-like kinase 1 and serves as a marker for mature centrioles. *Mol Biol Cell* **16**: 1095-1107.

Haimo LT, Rosenbaum JL. 1981. Cilia, flagella, and microtubules. *The Journal of cell biology* **91**: 125s-130s.

Hehnly H, Chen CT, Powers CM, Liu HL, Doxsey S. 2012. The centrosome regulates the Rab11- dependent recycling endosome pathway at appendages of the mother centriole. *Curr Biol* **22**: 1944-1950.

Hessel J, Heldrich J, Fuller J, Staudt MR, Radisch S, Hollmann C, Harvey BG, Kaner RJ, Salit J, Yee-Levin J et al. 2014. Intraflagellar transport gene expression associated with short cilia in smoking and COPD. *PLoS One* **9**: e85453.

Hildebrandt F, Attanasio M, Otto E. 2009. Nephronophthisis: disease mechanisms of a ciliopathy. *Journal of the American Society of Nephrology : JASN* **20**: 23-35.
Hildebrandt F, Benzing T, Katsanis N. 2011. Ciliopathies. *The New England journal of medicine* **364**: 1533-1543.
Hirokawa N, Tanaka Y, Okada Y. 2009. Left-right determination: involvement of molecular motor KIF3, cilia, and nodal flow. *Cold Spring Harb Perspect Biol* **1**: a000802.
Hoh RA, Stowe TR, Turk E, Stearns T. 2012. Transcriptional program of ciliated epithelial cells reveals new cilium and centrosome components and links to human disease. *PLoS One* **7**: e52166.
Holembowski L, Kramer D, Riedel D, Sordella R, Nemajerova A, Dobbelstein M, Moll UM. 2014. TAp73 is essential for germ cell adhesion and maturation in testis. *The Journal of cell biology* **204**: 1173-1190.
Hosie P, Fitzgerald DA, Jaffe A, Birman CS, Morgan L. 2014. Primary ciliary dyskinesia: Overlooked and undertreated in children. *Journal of paediatrics and child health* **50**: 952-958.
Hsiao YC, Tong ZJ, Westfall JE, Ault JG, Page-McCaw PS, Ferland RJ. 2009. Ahi1, whose human ortholog is mutated in Joubert syndrome, is required for Rab8a localization, ciliogenesis and vesicle trafficking. *Hum Mol Genet* **18**: 3926-3941.
Huangfu D, Anderson KV. 2005. Cilia and Hedgehog responsiveness in the mouse. *Proceedings of the National Academy of Sciences of the United States of America* **102**: 11325-11330.
Huber LA, Pimplikar S, Parton RG, Virta H, Zerial M, Simons K. 1993. Rab8, a small GTPase involved in vesicular traffic between the TGN and the basolateral plasma membrane. *The Journal of cell biology* **123**: 35-45.
Humbert MC, Weihbrecht K, Searby CC, Li Y, Pope RM, Sheffield VC, Seo S. 2012. ARL13B, PDE6D, and CEP164 form a functional network for INPP5E ciliary targeting. *Proceedings of the National Academy of Sciences of the United States of America* **109**: 19691-19696.
Humke EW, Dorn KV, Milenkovic L, Scott MP, Rohatgi R. 2010. The output of Hedgehog signaling is controlled by the dynamic association between Suppressor of Fused and the Gli proteins. *Genes Dev* **24**: 670-682.
Ibanez-Tallon I, Heintz N, Omran H. 2003. To beat or not to beat: roles of cilia in development and disease. *Hum Mol Genet* **12 Spec No 1**: R27-35.
Igarashi P, Somlo S. 2002. Genetics and pathogenesis of polycystic kidney disease. *Journal of the American Society of Nephrology : JASN* **13**: 2384-2398.
Ingham PW, Nakano Y, Seger C. 2011. Mechanisms and functions of Hedgehog signalling across the metazoa. *Nature reviews Genetics* **12**: 393-406.
Iomini C, Li L, Esparza JM, Dutcher SK. 2009. Retrograde intraflagellar transport mutants identify complex A proteins with multiple genetic interactions in Chlamydomonas reinhardtii. *Genetics* **183**: 885-896.
Ishikawa H, Kubo A, Tsukita S. 2005. Odf2-deficient mother centrioles lack distal/subdistal appendages and the ability to generate primary cilia. *Nature cell biology* **7**: 517-524.
Jackson PK, Attardi LD. 2016. p73 and FoxJ1: Programming Multiciliated Epithelia. *Trends Cell Biol* **26**: 239-240.

Jacoby M, Cox JJ, Gayral S, Hampshire DJ, Ayub M, Blockmans M, Pernot E, Kisseleva MV, Compere P, Schiffmann SN et al. 2009. INPP5E mutations cause primary cilium signaling defects, ciliary instability and ciliopathies in human and mouse. *Nat Genet* **41**: 1027-1031.

Jensen VL, Carter S, Sanders AA, Li C, Kennedy J, Timbers TA, Cai J, Scheidel N, Kennedy BN, Morin RD et al. 2016. Whole-Organism Developmental Expression Profiling Identifies RAB-28 as a Novel Ciliary GTPase Associated with the BBSome and Intraflagellar Transport. *PLoS Genet* **12**: e1006469.

Jensen VL, Li C, Bowie RV, Clarke L, Mohan S, Blacque OE, Leroux MR. 2015. Formation of the transition zone by Mks5/Rpgrip1L establishes a ciliary zone of exclusion (CIZE) that compartmentalises ciliary signalling proteins and controls PIP2 ciliary abundance. *The EMBO journal* **20**:2537-2556.

Jin H, Nachury MV. 2009. The BBSome. *Curr Biol* **19**: R472-473.

Jin H, White SR, Shida T, Schulz S, Aguiar M, Gygi SP, Bazan JF, Nachury MV. 2010. The conserved Bardet-Biedl syndrome proteins assemble a coat that traffics membrane proteins to cilia. *Cell* **141**: 1208-1219.

Joo K, Kim CG, Lee MS, Moon HY, Lee SH, Kim MJ, Kweon HS, Park WY, Kim CH, Gleeson JG et al. 2013. CCDC41 is required for ciliary vesicle docking to the mother centriole. *Proceedings of the National Academy of Sciences of the United States of America* **110**: 5987-5992.

Jord AA, Lemaitre AI, Delgehyr N, Faucourt M, Spassky N, Meunier A. 2014. Centriole amplification by mother and daughter centrioles differs in multiciliated cells. *Nature*.

Katz SM, Holsclaw DS, Jr. 1980. Ultrastructural features of respiratory cilia in cystic fibrosis. *Am J Clin Pathol* **73**: 682-685.

Killoran RC, Fan J, Yang D, Shilton BH, Choy WY. 2015. Structural Analysis of the 14-3-3zeta/Chibby Interaction Involved in Wnt/beta-Catenin Signaling. *PLoS One* **10**: e0123934.

Kim E, Walz G. 2007. Sensitive cilia set up the kidney. *Nat Med* **13**: 1409-1411.

Kim J, Krishnaswami SR, Gleeson JG. 2008. CEP290 interacts with the centriolar satellite component PCM-1 and is required for Rab8 localization to the primary cilium. *Hum Mol Genet* **17**: 3796-3805.

King SM. 2016. Axonemal Dynein Arms. *Cold Spring Harb Perspect Biol* **8**.

Kistler WS, Baas D, Lemeille S, Paschaki M, Seguin-Estevez Q, Barras E, Ma W, Duteyrat JL, Morle L, Durand B et al. 2015. RFX2 Is a Major Transcriptional Regulator of Spermiogenesis. *PLoS Genet* **11**: e1005368.

Klos Dehring DA, Vladar EK, Werner ME, Mitchell JW, Hwang P, Mitchell BJ. 2013. Deuterosome-mediated centriole biogenesis. *Developmental cell* **27**: 103-112.

Knodler A, Feng S, Zhang J, Zhang X, Das A, Peranen J, Guo W. 2010. Coordination of Rab8 and Rab11 in primary ciliogenesis. *Proceedings of the National Academy of Sciences of the United States of America* **107**: 6346-6351.

Knowles MR, Daniels LA, Davis SD, Zariwala MA, Leigh MW. 2013. Primary Ciliary Dyskinesia: Recent Advances in Diagnostics, Genetics, and Characterization of Clinical Disease. *American journal of respiratory and critical care medicine* **188**: 913-922.

Kozminski KG, Johnson KA, Forscher P, Rosenbaum JL. 1993. A motility in the eukaryotic flagellum unrelated to flagellar beating. *Proceedings of the National Academy of Sciences of the United States of America* **90**: 5519-5523.

Kunimoto K, Yamazaki Y, Nishida T, Shinohara K, Ishikawa H, Hasegawa T, Okanoue T, Hamada H, Noda T, Tamura A et al. 2012. Coordinated ciliary beating requires Odf2-mediated polarization of basal bodies via basal feet. *Cell* **148**: 189-200.

Kyrousi C, Arbi M, Pilz GA, Pefani DE, Lalioti ME, Ninkovic J, Gotz M, Lygerou Z, Taraviras S. 2015. Mcidas and GemC1 are key regulators for the generation of multiciliated ependymal cells in the adult neurogenic niche. *Development* **142**: 3661-3674.

Kyrousi C, Lygerou Z, Taraviras S. 2017. How a radial glial cell decides to become a multiciliated ependymal cell. *Glia* **65**: 1032-1042.

Lam HC, Cloonan SM, Bhashyam AR, Haspel JA, Singh A, Sathirapongsasuti JF, Cervo M, Yao H, Chung AL, Mizumura K et al. 2013. Histone deacetylase 6-mediated selective autophagy regulates COPD-associated cilia dysfunction. *J Clin Invest* **123**: 5212-5230.

Langousis G, Hill KL. 2014. Motility and more: the flagellum of Trypanosoma brucei. *Nat Rev Microbiol* **12**: 505-518.

Larkins CE, Aviles GD, East MP, Kahn RA, Caspary T. 2011. Arl13b regulates ciliogenesis and the dynamic localization of Shh signaling proteins. *Mol Biol Cell* **22**: 4694-4703.

Lee JD, Anderson KV. 2008. Morphogenesis of the node and notochord: the cellular basis for the establishment and maintenance of left-right asymmetry in the mouse. *Dev Dyn* **237**: 3464-3476.

Lee YL, Sante J, Comerci CJ, Cyge B, Menezes LF, Li FQ, Germino GG, Moerner WE, Takemaru K, Stearns T. 2014. Cby1 promotes Ahi1 recruitment to a ring-shaped domain at the centriole-cilium interface and facilitates proper cilium formation and function. *Mol Biol Cell* **25**: 2919-2933.

Leigh MW, Pittman JE, Carson JL, Ferkol TW, Dell SD, Davis SD, Knowles MR, Zariwala MA. 2009a. Clinical and genetic aspects of primary ciliary dyskinesia/Kartagener syndrome. *Genetics in medicine : official journal of the American College of Medical Genetics* **11**: 473-487.

Leigh MW, Zariwala MA, Knowles MR. 2009b. Primary ciliary dyskinesia: improving the diagnostic approach. *Current opinion in pediatrics* **21**: 320-325.

Leopold PL, O'Mahony MJ, Lian XJ, Tilley AE, Harvey BG, Crystal RG. 2009. Smoking is associated with shortened airway cilia. *PLoS One* **4**: e8157.

Li C, Jensen VL, Park K, Kennedy J, Garcia-Gonzalo FR, Romani M, De Mori R, Bruel AL, Gaillard D, Doray B et al. 2016a. MKS5 and CEP290 Dependent Assembly Pathway of the Ciliary Transition Zone. *PLoS Biol* **14**: e1002416.

Li FQ, Chen X, Fisher C, Siller SS, Zelikman K, Kuriyama R, Takemaru KI. 2016b. BAR Domain-Containing FAM92 Proteins Interact with Chibby1 To Facilitate Ciliogenesis. *Mol Cell Biol* **36**: 2668-2680.

Li FQ, Mofunanya A, Fischer V, Hall J, Takemaru K. 2010. Nuclear-cytoplasmic shuttling of Chibby controls beta-catenin signaling. *Mol Biol Cell* **21**: 311-322.

Li FQ, Mofunanya A, Harris K, Takemaru K. 2008. Chibby cooperates with 14-3-3 to regulate beta-catenin subcellular distribution and signaling activity. *The Journal of cell biology* **181**: 1141-1154.

Li FQ, Siller SS, Takemaru KI. 2015a. Basal body docking in airway ciliated cells. *Oncotarget* **6**: 19944-19945.

Li FQ, Singh AM, Mofunanya A, Love D, Terada N, Moon RT, Takemaru K. 2007. Chibby promotes adipocyte differentiation through inhibition of beta-catenin signaling. *Mol Cell Biol* **27**: 4347-4354.

Li W, Mukherjee A, Wu J, Zhang L, Teves ME, Li H, Nambiar S, Henderson SC, Horwitz AR, Strauss Iii JF et al. 2015b. Sperm Associated Antigen 6 (SPAG6) Regulates Fibroblast Cell Growth, Morphology, Migration and Ciliogenesis. *Sci Rep* **5**: 16506.

Li Y, Ling K, Hu J. 2012. The emerging role of Arf/Arl small GTPases in cilia and ciliopathies. *J Cell Biochem* **113**: 2201-2207.

Liem KF, Jr., Ashe A, He M, Satir P, Moran J, Beier D, Wicking C, Anderson KV. 2012. The IFT-A complex regulates Shh signaling through cilia structure and membrane protein trafficking. *The Journal of cell biology* **197**: 789-800.

Liew GM, Ye F, Nager AR, Murphy JP, Lee JS, Aguiar M, Breslow DK, Gygi SP, Nachury MV. 2014. The Intraflagellar Transport Protein IFT27 Promotes BBSome Exit from Cilia through the GTPase ARL6/BBS3. *Developmental cell* **31**: 265-278.

Lim L, Zhou H, Costa RH. 1997. The winged helix transcription factor HFH-4 is expressed during choroid plexus epithelial development in the mouse embryo. *Proceedings of the National Academy of Sciences of the United States of America* **94**: 3094-3099.

Lin J, Tritschler D, Song K, Barber CF, Cobb JS, Porter ME, Nicastro D. 2011. Building blocks of the nexin-dynein regulatory complex in Chlamydomonas flagella. *J Biol Chem* **286**: 29175-29191.

Linck RW, Chemes H, Albertini DF. 2016. The axoneme: the propulsive engine of spermatozoa and cilia and associated ciliopathies leading to infertility. *J Assist Reprod Genet* **33**: 141-156.

Love D, Li FQ, Burke MC, Cyge B, Ohmitsu M, Cabello J, Larson JE, Brody SL, Cohen JC, Takemaru K. 2010. Altered lung morphogenesis, epithelial cell differentiation and mechanics in mice deficient in the Wnt/beta-catenin antagonist Chibby. *PLoS One* **5**: e13600.

Lu H, Toh MT, Narasimhan V, Thamilselvam SK, Choksi SP, Roy S. 2015a. A function for the Joubert syndrome protein Arl13b in ciliary membrane extension and ciliary length regulation. *Developmental biology* **397**: 225-236.

Lu Q, Insinna C, Ott C, Stauffer J, Pintado PA, Rahajeng J, Baxa U, Walia V, Cuenca A, Hwang YS et al. 2015b. Early steps in primary cilium assembly require EHD1/EHD3-dependent ciliary vesicle formation. *Nature cell biology* **17**: 228-240.

Luo N, Lu J, Sun Y. 2012. Evidence of a role of inositol polyphosphate 5-phosphatase INPP5E in cilia formation in zebrafish. *Vision research* **75**: 98-107.

Ma L, Quigley I, Omran H, Kintner C. 2014. Multicilin drives centriole biogenesis via E2f proteins. *Genes & development* **28**: 1461-1471.

Mahjoub MR. 2013. The importance of a single primary cilium. *Organogenesis* **9**: 61-69.

Mahoney JE, Mori M, Szymaniak AD, Varelas X, Cardoso WV. 2014. The hippo pathway effector Yap controls patterning and differentiation of airway epithelial progenitors. *Developmental cell* **30**: 137-150.

Maria M, Lamers IJ, Schmidts M, Ajmal M, Jaffar S, Ullah E, Mustafa B, Ahmad S, Nazmutdinova K, Hoskins B et al. 2016. Genetic and clinical characterization of Pakistani families with Bardet-Biedl syndrome extends the genetic and phenotypic spectrum. *Sci Rep* **6**: 34764.

Marshall CB, Mays DJ, Beeler JS, Rosenbluth JM, Boyd KL, Santos Guasch GL, Shaver TM, Tang LJ, Liu Q, Shyr Y et al. 2016. p73 Is Required for Multiciliogenesis and Regulates the Foxj1-Associated Gene Network. *Cell Rep* **14**: 2289-2300.

Marszalek JR, Ruiz-Lozano P, Roberts E, Chien KR, Goldstein LS. 1999. Situs inversus and embryonic ciliary morphogenesis defects in mouse mutants lacking the KIF3A subunit of kinesin-II. *Proceedings of the National Academy of Sciences of the United States of America* **96**: 5043-5048.

Mazelova J, Astuto-Gribble L, Inoue H, Tam BM, Schonteich E, Prekeris R, Moritz OL, Randazzo PA, Deretic D. 2009. Ciliary targeting motif VxPx directs assembly of a trafficking module through Arf4. *The EMBO journal* **28**: 183-192.

Mazo G, Soplop N, Wang WJ, Uryu K, Tsou MB. 2016. Spatial Control of Primary Ciliogenesis by Subdistal Appendages Alters Sensation-Associated Properties of Cilia. *Developmental cell* **39**: 424-437.

McClenahan FK, Sharma H, Shan X, Eyermann C, Colognato H. 2016. Dystroglycan Suppresses Notch to Regulate Stem Cell Niche Structure and Function in the Developing Postnatal Subventricular Zone. *Developmental cell* **38**: 548-566.

Meunier A, Spassky N. 2016. Centriole continuity: out with the new, in with the old. *Curr Opin Cell Biol* **38**: 60-67.

Mitchell B, Stubbs JL, Huisman F, Taborek P, Yu C, Kintner C. 2009. The PCP pathway instructs the planar orientation of ciliated cells in the Xenopus larval skin. *Curr Biol* **19**: 924-929.

Mitchison HM, Schmidts M, Loges NT, Freshour J, Dritsoula A, Hirst RA, O'Callaghan C, Blau H, Al Dabbagh M, Olbrich H et al. 2012. Mutations in axonemal dynein assembly factor DNAAF3 cause primary ciliary dyskinesia. *Nat Genet* **44**: 381-389, S381-382.

Mogensen MM, Malik A, Piel M, Bouckson-Castaing V, Bornens M. 2000. Microtubule minus-end anchorage at centrosomal and non-centrosomal sites: the role of ninein. *J Cell Sci* **113 (Pt 17)**: 3013-3023.

Murcia NS, Richards WG, Yoder BK, Mucenski ML, Dunlap JR, Woychik RP. 2000. The Oak Ridge Polycystic Kidney (orpk) disease gene is required for left-right axis determination. *Development* **127**: 2347-2355.

Nachury MV. 2008. Tandem affinity purification of the BBSome, a critical regulator of Rab8 in ciliogenesis. *Methods in enzymology* **439**: 501-513.

Nachury MV, Loktev AV, Zhang Q, Westlake CJ, Peranen J, Merdes A, Slusarski DC, Scheller RH, Bazan JF, Sheffield VC et al. 2007. A core complex of BBS proteins cooperates with the GTPase Rab8 to promote ciliary membrane biogenesis. *Cell* **129**: 1201-1213.

Nachury MV, Seeley ES, Jin H. 2010. Trafficking to the ciliary membrane: how to get across the periciliary diffusion barrier? *Annual review of cell and developmental biology* **26**: 59-87.

Nakatsu F. 2015. A Phosphoinositide Code for Primary Cilia. *Developmental cell* **34**: 379-380.

Nemajerova A, Kramer D, Siller SS, Herr C, Shomroni O, Pena T, Gallinas Suazo C, Glaser K, Wildung M, Steffen H et al. 2016. TAp73 is a central transcriptional regulator of airway multiciliogenesis. *Genes & development* **30**: 1300-1312.

Nigg EA, Raff JW. 2009. Centrioles, centrosomes, and cilia in health and disease. *Cell* **139**: 663-678.

Nigg EA, Stearns T. 2011. The centrosome cycle: Centriole biogenesis, duplication and inherent asymmetries. *Nature cell biology* **13**: 1154-1160.

Nonaka S, Tanaka Y, Okada Y, Takeda S, Harada A, Kanai Y, Kido M, Hirokawa N. 1998. Randomization of left-right asymmetry due to loss of nodal cilia generating leftward flow of extraembryonic fluid in mice lacking KIF3B motor protein. *Cell* **95**: 829-837.

Norris DP, Jackson PK. 2016. Cell biology: Calcium contradictions in cilia. *Nature* **531**: 582-583.

Ocbina PJ, Anderson KV. 2008. Intraflagellar transport, cilia, and mammalian Hedgehog signaling: analysis in mouse embryonic fibroblasts. *Dev Dyn* **237**: 2030-2038.

Oda T, Chiba S, Nagai T, Mizuno K. 2014. Binding to Cep164, but not EB1, is essential for centriolar localization of TTBK2 and its function in ciliogenesis. *Genes to cells : devoted to molecular & cellular mechanisms* **19**: 927-940.

Ohata S, Nakatani J, Herranz-Perez V, Cheng J, Belinson H, Inubushi T, Snider WD, Garcia-Verdugo JM, Wynshaw-Boris A, Alvarez-Buylla A. 2014. Loss of Dishevelleds disrupts planar polarity in ependymal motile cilia and results in hydrocephalus. *Neuron* **83**: 558-571.

Olcese C, Patel MP, Shoemark A, Kiviluoto S, Legendre M, Williams HJ, Vaughan CK, Hayward J, Goldenberg A, Emes RD et al. 2017. X-linked primary ciliary dyskinesia due to mutations in the cytoplasmic axonemal dynein assembly factor PIH1D3. *Nat Commun* **8**: 14279.

Onoufriadis A, Paff T, Antony D, Shoemark A, Micha D, Kuyt B, Schmidts M, Petridi S, Dankert-Roelse JE, Haarman EG et al. 2013. Splice-site mutations in the axonemal outer dynein arm docking complex gene CCDC114 cause primary ciliary dyskinesia. *Am J Hum Genet* **92**: 88-98.

Paavola P, Salonen R, Baumer A, Schinzel A, Boyd PA, Gould S, Meusburger H, Tenconi R, Barnicoat A, Winter R et al. 1997. Clinical and genetic heterogeneity in Meckel syndrome. *Hum Genet* **101**: 88-92.

Park TJ, Haigo SL, Wallingford JB. 2006. Ciliogenesis defects in embryos lacking inturned or fuzzy function are associated with failure of planar cell polarity and Hedgehog signaling. *Nat Genet* **38**: 303-311.

Park TJ, Mitchell BJ, Abitua PB, Kintner C, Wallingford JB. 2008. Dishevelled controls apical docking and planar polarization of basal bodies in ciliated epithelial cells. *Nat Genet* **40**: 871-879.

Pazour GJ, Baker SA, Deane JA, Cole DG, Dickert BL, Rosenbaum JL, Witman GB, Besharse JC. 2002a. The intraflagellar transport protein, IFT88, is essential for vertebrate photoreceptor assembly and maintenance. *The Journal of cell biology* **157**: 103-113.

Pazour GJ, San Agustin JT, Follit JA, Rosenbaum JL, Witman GB. 2002b. Polycystin-2 localizes to kidney cilia and the ciliary level is elevated in orpk mice with polycystic kidney disease. *Curr Biol* **12**: R378-380.

Pazour GJ, Wilkerson CG, Witman GB. 1998. A dynein light chain is essential for the retrograde particle movement of intraflagellar transport (IFT). *The Journal of cell biology* **141**: 979-992.
Pedersen LB, Veland IR, Schroder JM, Christensen ST. 2008. Assembly of primary cilia. *Dev Dyn* **237**: 1993-2006.
Pedersen M. 1990. Ciliary activity and pollution. *Lung* **168 Suppl**: 368-376.
Pigino G, Ishikawa T. 2012. Axonemal radial spokes: 3D structure, function and assembly. *Bioarchitecture* **2**: 50-58.
Piperno G, Siuda E, Henderson S, Segil M, Vaananen H, Sassaroli M. 1998. Distinct mutants of retrograde intraflagellar transport (IFT) share similar morphological and molecular defects. *The Journal of cell biology* **143**: 1591-1601.
Porter ME, Bower R, Knott JA, Byrd P, Dentler W. 1999. Cytoplasmic dynein heavy chain 1b is required for flagellar assembly in Chlamydomonas. *Mol Biol Cell* **10**: 693-712.
Porter ME, Sale WS. 2000. The 9 + 2 axoneme anchors multiple inner arm dyneins and a network of kinases and phosphatases that control motility. *The Journal of cell biology* **151**: F37-42.
Praetorius HA, Leipziger J. 2013. Primary cilium-dependent sensing of urinary flow and paracrine purinergic signaling. *Semin Cell Dev Biol* **24**: 3-10.
Qin H, Diener DR, Geimer S, Cole DG, Rosenbaum JL. 2004. Intraflagellar transport (IFT) cargo: IFT transports flagellar precursors to the tip and turnover products to the cell body. *The Journal of cell biology* **164**: 255-266.
Qin J, Lin Y, Norman RX, Ko HW, Eggenschwiler JT. 2011. Intraflagellar transport protein 122 antagonizes Sonic Hedgehog signaling and controls ciliary localization of pathway components. *Proceedings of the National Academy of Sciences of the United States of America* **108**: 1456-1461.
Quigley IK, Kintner C. 2017. Rfx2 Stabilizes Foxj1 Binding at Chromatin Loops to Enable Multiciliated Cell Gene Expression. *PLoS Genet* **13**: e1006538.
Quintyne NJ, Gill SR, Eckley DM, Crego CL, Compton DA, Schroer TA. 1999. Dynactin is required for microtubule anchoring at centrosomes. *The Journal of cell biology* **147**: 321-334.
Reiter JF, Blacque OE, Leroux MR. 2012. The base of the cilium: roles for transition fibres and the transition zone in ciliary formation, maintenance and compartmentalization. *EMBO Rep* **13**: 608-618.
Ren G, Vajjhala P, Lee JS, Winsor B, Munn AL. 2006. The BAR domain proteins: molding membranes in fission, fusion, and phagy. *Microbiol Mol Biol Rev* **70**: 37-120.
Riechelmann H, Kienast K, Schellenberg J, Mann WJ. 1994. An in vitro model to study effects of airborne pollutants on human ciliary activity. *Rhinology* **32**: 105-108.
Riordan JR, Rommens JM, Kerem B, Alon N, Rozmahel R, Grzelczak Z, Zielenski J, Lok S, Plavsic N, Chou JL et al. 1989. Identification of the cystic fibrosis gene: cloning and characterization of complementary DNA. *Science* **245**: 1066-1073.
Rodriguez CI, Buchholz F, Galloway J, Sequerra R, Kasper J, Ayala R, Stewart AF, Dymecki SM. 2000. High-efficiency deleter mice show that FLPe is an alternative to Cre-loxP. *Nat Genet* **25**: 139-140.
Rohatgi R, Milenkovic L, Scott MP. 2007. Patched1 regulates hedgehog signaling at the primary cilium. *Science* **317**: 372-376.
Rohatgi R, Snell WJ. 2010. The ciliary membrane. *Curr Opin Cell Biol* **22**: 541-546.

Rosenbaum JL, Witman GB. 2002. Intraflagellar transport. *Nature reviews Molecular cell biology* **3**: 813-825.
Rubin BK. 2007. Mucus structure and properties in cystic fibrosis. *Paediatric respiratory reviews* **8**: 4-7.
Rugina AL, Dimitriu AG, Nistor N, Mihaila D. 2014. Primary ciliary dyskinesia diagnosed by electron microscopy in one case of Kartagener syndrome. *Romanian journal of morphology and embryology = Revue roumaine de morphologie et embryologie* **55**: 697-701.
Sale WS, Satir P. 1976. Splayed Tetrahymena cilia. A system for analyzing sliding and axonemal spoke arrangements. *The Journal of cell biology* **71**: 589-605.
Sale WS, Satir P. 1977. The termination of the central microtubules from the cilia of Tetrahymena pyriformis. *Cell Biol Int Rep* **1**: 45-49.
Salonen R. 1984. The Meckel syndrome: clinicopathological findings in 67 patients. *Am J Med Genet* **18**: 671-689.
Salonen R, Paavola P. 1998. Meckel syndrome. *J Med Genet* **35**: 497-501.
Sang L, Miller JJ, Corbit KC, Giles RH, Brauer MJ, Otto EA, Baye LM, Wen X, Scales SJ, Kwong M et al. 2011. Mapping the NPHP-JBTS-MKS protein network reveals ciliopathy disease genes and pathways. *Cell* **145**: 513-528.
Satir P. 1968. Studies on cilia. 3. Further studies on the cilium tip and a "sliding filament" model of ciliary motility. *The Journal of cell biology* **39**: 77-94.
Schmidt KN, Kuhns S, Neuner A, Hub B, Zentgraf H, Pereira G. 2012. Cep164 mediates vesicular docking to the mother centriole during early steps of ciliogenesis. *The Journal of cell biology* **199**: 1083-1101.
Scholey JM. 2003. Intraflagellar transport. *Annual review of cell and developmental biology* **19**: 423-443.
-. 2008. Intraflagellar transport motors in cilia: moving along the cell's antenna. *The Journal of cell biology* **180**: 23-29.
Sedmak T, Wolfrum U. 2010. Intraflagellar transport molecules in ciliary and nonciliary cells of the retina. *The Journal of cell biology* **189**: 171-186.
Seixas C, Choi SY, Polgar N, Umberger NL, East MP, Zuo X, Moreiras H, Ghossoub R, Benmerah A, Kahn RA et al. 2016. Arl13b and the exocyst interact synergistically in ciliogenesis. *Mol Biol Cell* **27**: 308-320.
Shah AS, Farmen SL, Moninger TO, Businga TR, Andrews MP, Bugge K, Searby CC, Nishimura D, Brogden KA, Kline JN et al. 2008. Loss of Bardet-Biedl syndrome proteins alters the morphology and function of motile cilia in airway epithelia. *Proceedings of the National Academy of Sciences of the United States of America* **105**: 3380-3385.
Shawlot W, Vazquez-Chantada M, Wallingford JB, Finnell RH. 2015. Rfx2 is required for spermatogenesis in the mouse. *Genesis*.
Shi J, Zhao Y, Galati D, Winey M, Klymkowsky MW. 2014. Chibby functions in Xenopus ciliary assembly, embryonic development, and the regulation of gene expression. *Developmental biology* **395**: 287-298.
Siller SS, Burke MC, Li FQ, Takemaru K. 2015. Chibby functions to preserve normal ciliary morphology through the regulation of intraflagellar transport in airway ciliated cells. *Cell Cycle* **14**: 3163-3172.

Sillibourne JE, Hurbain I, Grand-Perret T, Goud B, Tran P, Bornens M. 2013. Primary ciliogenesis requires the distal appendage component Cep123. *Biol Open* **2**: 535-545.
Sivasubramaniam S, Sun X, Pan YR, Wang S, Lee EY. 2008. Cep164 is a mediator protein required for the maintenance of genomic stability through modulation of MDC1, RPA, and CHK1. *Genes & development* **22**: 587-600.
Skarnes WC, Rosen B, West AP, Koutsourakis M, Bushell W, Iyer V, Mujica AO, Thomas M, Harrow J, Cox T et al. 2011. A conditional knockout resource for the genome-wide study of mouse gene function. *Nature* **474**: 337-342.
Slaats GG, Ghosh AK, Falke LL, Le Corre S, Shaltiel IA, van de Hoek G, Klasson TD, Stokman MF, Logister I, Verhaar MC et al. 2014. Nephronophthisis-Associated CEP164 Regulates Cell Cycle Progression, Apoptosis and Epithelial-to-Mesenchymal Transition. *PLoS Genet* **10**: e1004594.
Sorokin S. 1962. Centrioles and the formation of rudimentary cilia by fibroblasts and smooth muscle cells. *The Journal of cell biology* **15**: 363-377.
Sorokin SP. 1968. Reconstructions of centriole formation and ciliogenesis in mammalian lungs. *J Cell Sci* **3**: 207-230.
Spassky N, Meunier A. 2017. The development and functions of multiciliated epithelia. *Nature reviews Molecular cell biology*.
Steere N, Chae V, Burke M, Li FQ, Takemaru K, Kuriyama R. 2012. A Wnt/beta-catenin pathway antagonist Chibby binds Cenexin at the distal end of mother centrioles and functions in primary cilia formation. *PLoS One* **7**: e41077.
Stenmark H. 2009. Rab GTPases as coordinators of vesicle traffic. *Nature reviews Molecular cell biology* **10**: 513-525.
Stepanek L, Pigino G. 2016. Microtubule doublets are double-track railways for intraflagellar transport trains. *Science* **352**: 721-724.
Stubbs JL, Vladar EK, Axelrod JD, Kintner C. 2012. Multicilin promotes centriole assembly and ciliogenesis during multiciliate cell differentiation. *Nature cell biology* **14**: 140-147.
Sung CH, Leroux MR. 2013. The roles of evolutionarily conserved functional modules in cilia-related trafficking. *Nature cell biology* **15**: 1387-1397.
Swoboda P, Adler HT, Thomas JH. 2000. The RFX-type transcription factor DAF-19 regulates sensory neuron cilium formation in C. elegans. *Mol Cell* **5**: 411-421.
Takeda S, Yonekawa Y, Tanaka Y, Okada Y, Nonaka S, Hirokawa N. 1999. Left-right asymmetry and kinesin superfamily protein KIF3A: new insights in determination of laterality and mesoderm induction by kif3A-/- mice analysis. *The Journal of cell biology* **145**: 825-836.
Takemaru K, Fischer V, Li FQ. 2009. Fine-tuning of nuclear-catenin by Chibby and 14-3-3. *Cell Cycle* **8**: 210-213.
Takemaru K, Yamaguchi S, Lee YS, Zhang Y, Carthew RW, Moon RT. 2003. Chibby, a nuclear beta-catenin-associated antagonist of the Wnt/Wingless pathway. *Nature* **422**: 905-909.
Tan FE, Vladar EK, Ma L, Fuentealba LC, Hoh R, Espinoza FH, Axelrod JD, Alvarez-Buylla A, Stearns T, Kintner C et al. 2013. Myb promotes centriole amplification and later steps of the multiciliogenesis program. *Development* **140**: 4277-4286.

Tanos BE, Yang HJ, Soni R, Wang WJ, Macaluso FP, Asara JM, Tsou MF. 2013. Centriole distal appendages promote membrane docking, leading to cilia initiation. *Genes & development* **27**: 163-168.

Taschner M, Bhogaraju S, Lorentzen E. 2012. Architecture and function of IFT complex proteins in ciliogenesis. *Differentiation; research in biological diversity* **83**: S12-22.

Tilley AE, Walters MS, Shaykhiev R, Crystal RG. 2014. Cilia Dysfunction in Lung Disease. *Annual review of physiology* **77**: 379-406.

Tissir F, Qu Y, Montcouquiol M, Zhou L, Komatsu K, Shi D, Fujimori T, Labeau J, Tyteca D, Courtoy P et al. 2010. Lack of cadherins Celsr2 and Celsr3 impairs ependymal ciliogenesis, leading to fatal hydrocephalus. *Nat Neurosci* **13**: 700-707.

Tony Yang T, Su J, Wang WJ, Craige B, Witman GB, Bryan Tsou MF, Liao JC. 2015. Superresolution Pattern Recognition Reveals the Architectural Map of the Ciliary Transition Zone. *Sci Rep* **5**: 14096.

Torres VE, Harris PC. 2007. Polycystic kidney disease: genes, proteins, animal models, disease mechanisms and therapeutic opportunities. *J Intern Med* **261**: 17-31.

Torres VE, Harris PC, Pirson Y. 2007. Autosomal dominant polycystic kidney disease. *Lancet* **369**: 1287-1301.

Tsang WY, Bossard C, Khanna H, Peranen J, Swaroop A, Malhotra V, Dynlacht BD. 2008. CP110 suppresses primary cilia formation through its interaction with CEP290, a protein deficient in human ciliary disease. *Developmental cell* **15**: 187-197.

Tsao CC, Gorovsky MA. 2008. Tetrahymena IFT122A is not essential for cilia assembly but plays a role in returning IFT proteins from the ciliary tip to the cell body. *J Cell Sci* **121**: 428-436.

Tukachinsky H, Lopez LV, Salic A. 2010. A mechanism for vertebrate Hedgehog signaling: recruitment to cilia and dissociation of SuFu-Gli protein complexes. *The Journal of cell biology* **191**: 415-428.

Valente EM, Marsh SE, Castori M, Dixon-Salazar T, Bertini E, Al-Gazali L, Messer J, Barbot C, Woods CG, Boltshauser E et al. 2005. Distinguishing the four genetic causes of Jouberts syndrome-related disorders. *Ann Neurol* **57**: 513-519.

van Reeuwijk J, Arts HH, Roepman R. 2011. Scrutinizing ciliopathies by unraveling ciliary interaction networks. *Hum Mol Genet* **20**: R149-157.

Vetter M, Stehle R, Basquin C, Lorentzen E. 2015. Structure of Rab11-FIP3-Rabin8 reveals simultaneous binding of FIP3 and Rabin8 effectors to Rab11. *Nat Struct Mol Biol* **22**: 695-702.

Vladar EK, Antic D, Axelrod JD. 2009. Planar cell polarity signaling: the developing cell's compass. *Cold Spring Harb Perspect Biol* **1**: a002964.

Vladar EK, Brody SL. 2013. Analysis of ciliogenesis in primary culture mouse tracheal epithelial cells. *Methods in enzymology* **525**: 285-309.

Vladar EK, Stearns T. 2007. Molecular characterization of centriole assembly in ciliated epithelial cells. *The Journal of cell biology* **178**: 31-42.

Voronina VA, Takemaru K, Treuting P, Love D, Grubb BR, Hajjar AM, Adams A, Li FQ, Moon RT. 2009. Inactivation of Chibby affects function of motile airway cilia. *The Journal of cell biology* **185**: 225-233.

Walentek P, Quigley IK. 2017. What we can learn from a tadpole about ciliopathies and airway diseases: Using systems biology in Xenopus to study cilia and mucociliary epithelia. *Genesis* **55**.

Walentek P, Quigley IK, Sun DI, Sajjan UK, Kintner C, Harland RM. 2016. Ciliary transcription factors and miRNAs precisely regulate Cp110 levels required for ciliary adhesions and ciliogenesis. *eLife* **5**.

Wallingford JB, Mitchell B. 2011. Strange as it may seem: the many links between Wnt signaling, planar cell polarity, and cilia. *Genes & development* **25**: 201-213.

Wang J, Morita Y, Mazelova J, Deretic D. 2012. The Arf GAP ASAP1 provides a platform to regulate Arf4- and Rab11-Rab8-mediated ciliary receptor targeting. *The EMBO journal* **31**: 4057-4071.

Wang X, Zhou Y, Wang J, Tseng IC, Huang T, Zhao Y, Zheng Q, Gao Y, Luo H, Zhang X et al. 2016. SNX27 Deletion Causes Hydrocephalus by Impairing Ependymal Cell Differentiation and Ciliogenesis. *J Neurosci* **36**: 12586-12597.

Warner FD, Satir P. 1974. The structural basis of ciliary bend formation. Radial spoke positional changes accompanying microtubule sliding. *The Journal of cell biology* **63**: 35-63.

Waters AM, Beales PL. 2011. Ciliopathies: an expanding disease spectrum. *Pediatric nephrology* **26**: 1039-1056.

Watnick T, Germino G. 2003. From cilia to cyst. *Nat Genet* **34**: 355-356.

Wei Q, Ling K, Hu J. 2015. The essential roles of transition fibers in the context of cilia. *Curr Opin Cell Biol* **35**: 98-105.

Wei Q, Xu Q, Zhang Y, Li Y, Zhang Q, Hu Z, Harris PC, Torres VE, Ling K, Hu J. 2013. Transition fibre protein FBF1 is required for the ciliary entry of assembled intraflagellar transport complexes. *Nat Commun* **4**: 2750.

Wei Q, Zhang Y, Li Y, Zhang Q, Ling K, Hu J. 2012. The BBSome controls IFT assembly and turnaround in cilia. *Nature cell biology* **14**: 950-957.

Westlake CJ, Baye LM, Nachury MV, Wright KJ, Ervin KE, Phu L, Chalouni C, Beck JS, Kirkpatrick DS, Slusarski DC et al. 2011. Primary cilia membrane assembly is initiated by Rab11 and transport protein particle II (TRAPPII) complex-dependent trafficking of Rabin8 to the centrosome. *Proceedings of the National Academy of Sciences of the United States of America* **108**: 2759-2764.

Williams CL, Li C, Kida K, Inglis PN, Mohan S, Semenec L, Bialas NJ, Stupay RM, Chen N, Blacque OE et al. 2011. MKS and NPHP modules cooperate to establish basal body/transition zone membrane associations and ciliary gate function during ciliogenesis. *The Journal of cell biology* **192**: 1023-1041.

Williams CL, McIntyre JC, Norris SR, Jenkins PM, Zhang L, Pei Q, Verhey K, Martens JR. 2014. Direct evidence for BBSome-associated intraflagellar transport reveals distinct properties of native mammalian cilia. *Nat Commun* **5**: 5813.

Wu S, Mehta SQ, Pichaud F, Bellen HJ, Quiocho FA. 2005. Sec15 interacts with Rab11 via a novel domain and affects Rab11 localization in vivo. *Nat Struct Mol Biol* **12**: 879-885.

Wu Y, Hu X, Li Z, Wang M, Li S, Wang X, Lin X, Liao S, Zhang Z, Feng X et al. 2016. Transcription Factor RFX2 Is a Key Regulator of Mouse Spermiogenesis. *Sci Rep* **6**: 20435.

Xu Q, Zhang Y, Wei Q, Huang Y, Hu J, Ling K. 2016. Phosphatidylinositol phosphate kinase PIPKIgamma and phosphatase INPP5E coordinate initiation of ciliogenesis. *Nat Commun* **7**: 10777.

Yadav SP, Sharma NK, Liu C, Dong L, Li T, Swaroop A. 2016. Centrosomal protein CP110 controls maturation of mother centriole during cilia biogenesis. *Development* **143**: 1491-1501.

Yang TT, Hampilos PJ, Nathwani B, Miller CH, Sutaria ND, Liao JC. 2013. Superresolution STED microscopy reveals differential localization in primary cilia. *Cytoskeleton* **70**: 54-65.

Ye X, Zeng H, Ning G, Reiter JF, Liu A. 2014. C2cd3 is critical for centriolar distal appendage assembly and ciliary vesicle docking in mammals. *Proceedings of the National Academy of Sciences of the United States of America* **111**: 2164-2169.

Yee LE, Reiter JF. 2015. Ciliary vesicle formation: a prelude to ciliogenesis. *Developmental cell* **32**: 665-666.

Yoder BK, Hou X, Guay-Woodford LM. 2002. The polycystic kidney disease proteins, polycystin-1, polycystin-2, polaris, and cystin, are co-localized in renal cilia. *Journal of the American Society of Nephrology : JASN* **13**: 2508-2516.

Yoshimura S, Egerer J, Fuchs E, Haas AK, Barr FA. 2007. Functional dissection of Rab GTPases involved in primary cilium formation. *The Journal of cell biology* **178**: 363-369.

You Y, Richer EJ, Huang T, Brody SL. 2002. Growth and differentiation of mouse tracheal epithelial cells: selection of a proliferative population. *Am J Physiol Lung Cell Mol Physiol* **283**: L1315-1321.

Zaghloul NA, Katsanis N. 2009. Mechanistic insights into Bardet-Biedl syndrome, a model ciliopathy. *J Clin Invest* **119**: 428-437.

Zeng H, Jia J, Liu A. 2010. Coordinated translocation of mammalian Gli proteins and suppressor of fused to the primary cilium. *PLoS One* **5**: e15900.

Zerial M, McBride H. 2001. Rab proteins as membrane organizers. *Nature reviews Molecular cell biology* **2**: 107-117.

Zhang J, Guan L, Wen W, Lu Y, Zhu Q, Yuan H, Chen Y, Wang H, Zhang J, Li H. 2014. A novel mutation of DNAH5 in chronic rhinosinusitis and primary ciliary dyskinesia in a Chinese family. *European archives of oto-rhino-laryngology : official journal of the European Federation of Oto-Rhino-Laryngological Societies* **271**: 1589-1594.

Zhang Q, Seo S, Bugge K, Stone EM, Sheffield VC. 2012. BBS proteins interact genetically with the IFT pathway to influence SHH-related phenotypes. *Hum Mol Genet* **21**: 1945-1953.

Zhang Y, Huang G, Shornick LP, Roswit WT, Shipley JM, Brody SL, Holtzman MJ. 2007. A transgenic FOXJ1-Cre system for gene inactivation in ciliated epithelial cells. *Am J Respir Cell Mol Biol* **36**: 515-519.

Zhang Z, Li W, Zhang Y, Zhang L, Teves ME, Liu H, Strauss JF, 3rd, Pazour GJ, Foster JA, Hess RA et al. 2016. Intraflagellar transport protein IFT20 is essential for male fertility and spermiogenesis in mice. *Mol Biol Cell* **27**: 3705-3716.

Zhao H, Zhu L, Zhu Y, Cao J, Li S, Huang Q, Xu T, Huang X, Yan X, Zhu X. 2013. The Cep63 paralogue Deup1 enables massive de novo centriole biogenesis for vertebrate multiciliogenesis. *Nature cell biology* **15**: 1434-1444.

Zhou F, Narasimhan V, Shboul M, Chong YL, Reversade B, Roy S. 2015. Gmnc Is a Master Regulator of the Multiciliated Cell Differentiation Program. *Curr Biol* **25**: 3267-3273.